

RESEARCH ARTICLE

OPEN ACCESS Check for updates



Observations on the skull of the type specimen of Tyrannosaurus rex Osborn, 1905

Thomas D. Carr

Department of Biology, Carthage College, Kenosha, WI, USA

ABSTRACT

The skull bones of the type specimen of Tyrannosaurus rex have been undescribed since the early 20th Century. The objectives were to provide a description of the type skull, assess the homology of characters seen in adults and juveniles, and test the taxonomic informativeness of the size difference between the second and third dentary teeth. This work is based on published data and first-hand observations of fossils and casts. Comparative descriptions of each skull bone, and details of the dentition of the type were written. Several retained 'juvenile' characters are not homologous with the juvenile condition. The difference in size between the second and third dentary teeth are taxonomically uninformative. Inferences were made regarding the complementary joint surfaces of the skull bones that were attached to those found in CM 9380. Both dental characters suggested to differentiate species in the hypodigm of *T. rex* were seen in the left and right dentaries of the type; therefore, the characters are taxonomically uninformative. The subocular process seen in the lacrimal in T. rex and other large theropods was hypothesised to mark the limit of the eyeball-containing region of the orbital fenestra.

ARTICLE HISTORY

Received 3 January 2025 Accepted 22 July 2025

KEYWORDS

Tyrannosaurus rex; variation; ontogeny; Tyrannosauridae; Cretaceous

1. Introduction

Scientific descriptions of the skull of the type specimen (then AMNH 973) of Tyrannosaurus rex were published early in the 20th century (Osborn, 1905, 1906, 1912). The type has an unusual history among namebearing specimens, having been transferred from one museum to another. A brief summary of the purchase of the type specimen by the Carnegie Museum (CM) from the American Museum of Natural History (AMNH), based on written correspondence between the institutions, is given in Appendix 1.

Since its transfer to the CM, the type remained a mainstay in the literature on tyrannosaurid palaeobiology, including studies of variation and morphology (Allain & Chure, 2002; Brochu, 2003; Brusatte et al., 2012; Carpenter, 1990; Molnar, 1991; Carr, 2022; Gold et al., 2013; Hendrickx et al., 2014; Hurum & Sabath, 2003; Kawabe & Hattori, 2022; Porter & Witmer, 2020; Smith, 2005), functional morphology (Claessens, 2004; Dececchi et al., 2020; Holtz, 1995; Hutchinson et al., 2011; Usami & Kinugasa, 2017), ontogeny (Carr, 1999; Carr & Sues, 2010, 2020), taxonomy (Carr et al., 2022; Paul, 2025; Paul et al., 2022; Urban & Lamanna, 2006), palaeopathology (Wolff et al., 2009), mass estimation (Campione et al., 2014; Hurrell, 2019; Paul, 1998; Persons et al., 2019), and sexual dimorphism (Tereshchenko, 2020).

1.1. Rationale & goals

Of concern here is that recent work has focused on variation in the T. rex hypodigm (Carr, 2020; Carr et al., 2022; Paul, 2025; Paul et al., 2022), which has renewed interest in the type specimen and the definition of the species. Although CM 9380 in many ways is comparable with other adult specimens (Carr, 2020), the skull bones do show some important differences that help us to understand the extremes in variation of the taxon. Although many aspects of the osteology of T. rex have been published, the type specimen has not been revisited in detail since the early Twentieth Century (Carr 1999, 2020; Brochu 2003; Currie 2003). The goal of this work is to fill in that gap in knowledge based on a comparative description of the skull bones and

dentition of CM 9380 with other T. rex specimens. Until this writing, Osborn's (1906) brief three-page summary of the skull bones of the type constituted the most extensive published description of the type specimen.

This work begins with a chronological literature review of research done on the type skull, followed by a comparative description of the skull, and inferences regarding missing skull bones. Much of the comparative description is derived from the supplementary data 2 of Carr (2020), an extensive spreadsheet of specimens and their character states. That format does not make for straightforward reading, and so it was rewritten here to meet the goals of emphasising the morphology of the type in the context of variation in the species. The growth stages of Carr (2020) - small juvenile, large juvenile, subadult, young adult, adult – are used here. The directional conventions of rostral and caudal are used instead of anterior and posterior (Sampson & Witmer, 2007). Tyrannosaurid taxonomy used here follows that in Carr (2022).

1.2. A note on the taxonomy of late Maastrichtian tyrannosaurids of North America

Several new taxa have been proposed based on the hypodigm of T. rex (Dalman et al., 2024; Paul, 2025; Paul et al., 2022). The hypothesis of Paul et al. (2022) was challenged by Carr et al. (2022), who showed that the hypodigm could not be parsed into three statistically distinct groups. It is the opinion of this author that the characters proposed by Dalman et al. (2024) to distinguish a novel taxon from New Mexico are seen throughout the hypodigm of T. rex and so the evidence for a new taxon is not persuasive. The goal of this article is to provide a straightforward comparative description of the type specimen, and assumes the hypodigm represents one taxon.

1.3. Materials and methods

The description is based on first-hand observations of CM 9380, and observations of high-resolution casts of the skull bones (MOR-CAST-318) held in the collections of the Museum of the Rockies. The casts are used here to illustrate the specimen, given that their uniform colour helps to emphasise the features discussed here; all photos were taken by the author. Single exemplars (specimens) of character states are given here; see the supplementary file 2 of Carr (2020) for the complete account of specimens and their character states.

1.4. Institutional abbreviations

AMNH FARB, American Museum of Natural History, Fossil Amphibians, Reptiles, and Birds, New York, NY; BMRP, Burpee Natural History Museum, Rockford, IL; CM, Carnegie Museum, Pittsburgh, PA; CMNH, Cleveland Museum of Natural History, Cleveland, OH; DDM, Dinosaur Discovery Museum, Kenosha, WI; FMNH, Field Museum, Chicago, IL; MOR, Museum of the Rockies, Bozeman, MT; LACM, Los Angeles County Museum of Natural History, Los Angeles, CA; NHMUK, Natural History Museum, London, UK; NMMNH, New Mexico Museum of Natural History and Science, Albuquerque, NM; PIN, Palaeontological Institute, Moscow, RU; RSM, Royal Saskatchewan Museum, Eastend, SK; TMM, Texas Memorial Museum, Austin, TX; TMP, Royal Tyrrell Museum of Palaeontology, Drumheller, AB; UCMP, University of California Museum of Palaeontology, Berkeley, CA; UWBM, University of Washington Burke Museum, Seattle, WA; **UWGM**, Geology Museum, University of Wisconsin-Madison, Madison, WI.

1.5. Chronological literature review

1.5.1. (Osborn, 1905)

The first description of the skull bones of CM 9380 appeared on 4 October 1905, following a review of tyrannosaurid nomenclature (Osborn, 1905). In the brief section on the type - six paragraph long - Osborn listed the skull bones that were known at the time: the lacrimal, surangular, and dentaries, which were shown in the figure of the skeleton (1905, Figure 1, p. 262). Osborn noted that the skull bones were not yet prepared at the time of publication. Osborn noted the presence of the frontal, but based on his description that is 'extremely rugose, constituting a horn above the orbit', this must have been the lacrimal given the texture and since the frontals are missing from the

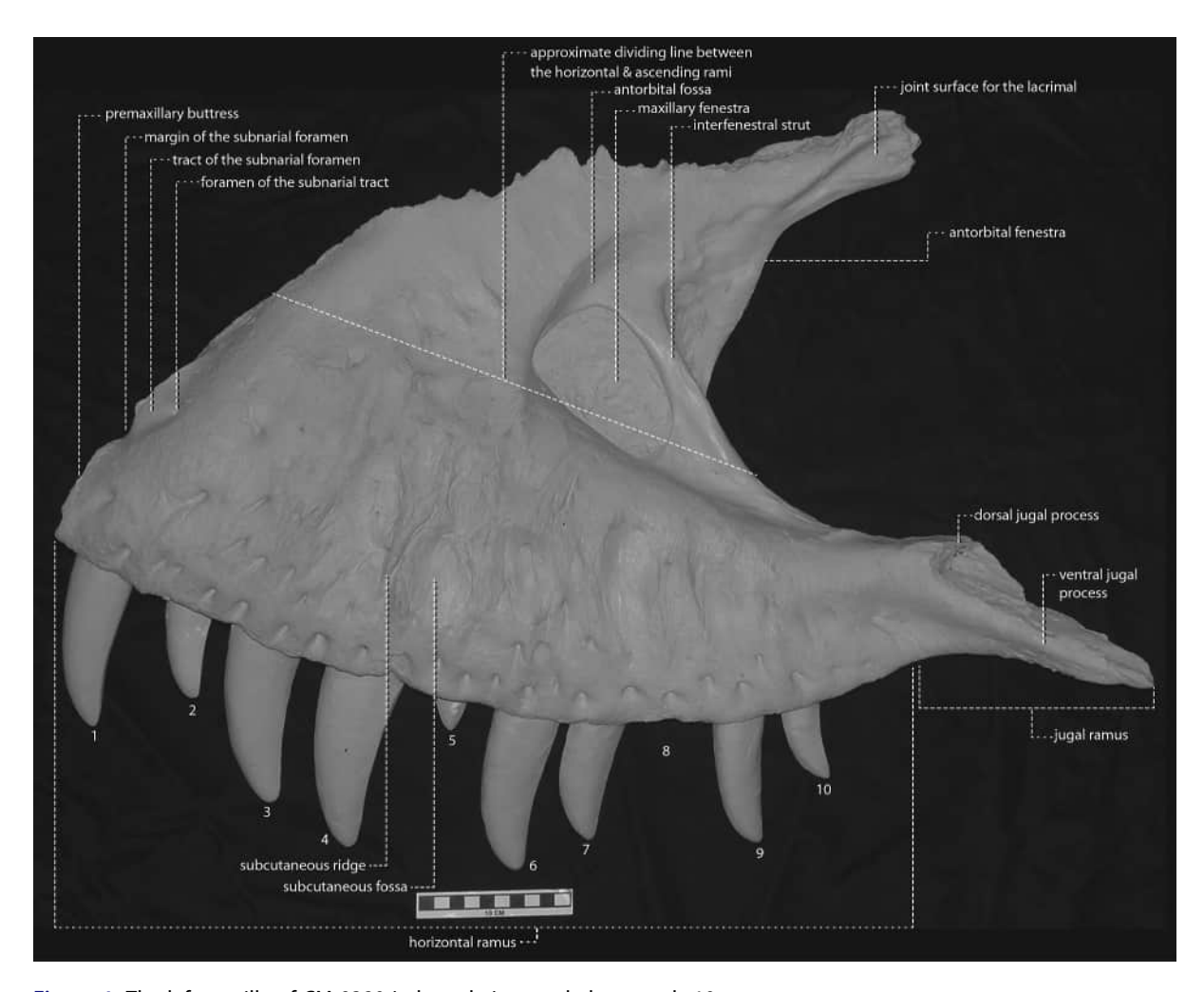


Figure 1. The left maxilla of CM 9380 in lateral view, scale bar equals 10 cm.

specimen (Osborn, 1905, p. 263). Osborn also noted the presence of the angular and articular, but as those bones are also missing from the specimen, this must be in reference to the surangular (1905, p. 263).

Osborn included a figure of the partial skeleton to scale with a human skeleton, which was drafted by W. D. Matthew (Osborn, 1905, Figure 1, p. 262). The illustration shows the bones that were known to be collected shaded in, whereas the missing bones are in a lighter shade. Although Osborn wrote that the frontals are present, he shows the lacrimal shaded in, and, despite his identification of three jaw bones in the text, only the dentary and the caudal portion of the surangular (= articular? = of Osborn) are shaded as present (1905, Figure 1, p. 262).

1.5.2. (Osborn, 1906)

A year after T. rex was named, Osborn (1906) published an updated account of the type specimen, alongside two referred fossils; among the nontyrannosaurid fossils available at the time, he made comparisons with Allosaurus. Osborn (1906) identified in the type several skull bones, including the left maxilla, the lacrimals (= prefrontal of Osborn), left squamosal, ectopterygoid (= transverse of Osborn), the dentaries, and the left surangular. Aside from the nomenclatural differences, these are the skull bones that are recognised today as belonging to the type. Also, he included an updated and detailed figure of the skeleton of the type that was drafted by L. M. Sterling (Osborn, 1906, Plate 39).

In a summary preceding the description, Osborn (1906) emphasised several features of the skull of T. rex that were based on the type: a rostrocaudally short skull; the presence of the subnarial foramen, maxillary fenestra, and the antorbital fenestra; thirteen (miscount) teeth in the maxilla, twelve (miscount) to thirteen in

the dentaries; long and rostrally-extending quadratojugal process of the squamosal; incisiform mesial-most dentary tooth; denticulate teeth that are oval in cross section and wider than long.

The reconstructed skull was illustrated in left lateral view by L. M. Sterling; the proportions of the skull were almost certainly based on Allosaurus, where the premaxilla is shown as unnaturally long and the quadratojugal process of the squamosal is shown extending medial to the postorbital bar (Osborn, 1906, Figure 1, p. 285). In the figure, as in the text, the lacrimal is identified as the prefrontal (Osborn, 1906, Figure 1, p. 285).

In the description, Osborn corrected his identification of frontals (1905) to lacrimals (= his prefrontals). He also corrected his identification of the articular and angular (1905) to the surangular. Although it is identified in his table that shows the parts found in the type, no mention is made of the ectopterygoid (= his transverse) in the description (Osborn, 1906). Brief paragraph-length descriptions of each bone are given, with the most text (two paragraphs) given to the maxilla and dentary (Osborn, 1906).

1.5.3. (Osborn, 1912)

Although (Osborn's, 1912) monograph on T. rex was based primarily on AMNH FARB 5027 and AMNH FARB 5117, the type was a source of data and illustration. Among theropods, Osborn continued his convention of comparing T. rex with Allosaurus (Osborn, 1906, 1912). The type was illustrated, by E. M. Christman, in five instances: a medial view of the left dentary (halftone), a lingual view of three teeth and six alveoli from the right dentary (pen-and-ink), a lateral and medial view of the left maxilla (halftones), and a figure of an erupted dentary tooth and its replacement (pen-and-ink) (Osborn, 1912, Figures 20 - 24). In this article, Osborn abandoned the term 'transverse' for 'ectopterygoid' (Osborn, 1912, p. 5). Although the skull description was based primarily on the perfect skull of AMNH FARB 5027, data from the type was referred to when required. Osborn (1906) found that the type and AMNH FARB 5027 were almost the same size.

Osborn did not explicitly correct his earlier reconstructions (1905, 1906) of the skull showing the quadratojugal process of the squamosal extending medial to the postorbital bar, even though AMNH FARB 5027 showed these to be separate, nonoverlapping structures. Regardless, in this work he initially took a nuanced view of the skull proportions, where he considered the cranial region as abbreviate (i.e. short) and the facial region as elongated (Osborn, 1912). However, in the closing paragraphs of the monograph, Osborn reversed this characterisation - without explanation - and stated that both 'the face and jaws are shortened' (1912, p. 29).

Although Osborn did not extensively describe the type in the text, he did take care to point out several of its osteological details in the figures, including the interdental plates of the dentary (1912, Figure 20), the connections between the alveoli and associated neurovascular structures (1912, Figure 21), and the nine interdental plates of the maxilla (1912, Figure 23). His three-paragraph description of the dentary was primarily based on the type; the description of the dentition was based on the type and AMNH FARB 5027; the type was illustrated as an exemplar showing the replacement teeth, presumably at a break in the specimen (Osborn, 1912, Figure 24).

1.5.4. Osborn (1916)

Osborn's last article on T. rex osteology was also the last to mention the type (Osborn, 1916). This article emphasised the postcranial skeleton of the type and referred specimens, and no new information on the skull was given (Osborn, 1916).

1.5.5. Carpenter (1990)

Carpenter (1990) illustrated and compared the skull of CM 9380 with eight other specimens then known. He differentiated the skull of the type from the other specimens based on its oval maxillary fenestra, but otherwise he regarded the maxilla and dentary as within the range of variation for the species and made no further specific observations of the type's skull bones (Carpenter, 1990).

1.5.6. Molnar (1991)

The type featured in Molnar's (1991) monograph on the cranial osteology of *T. rex*. In particular, features of the maxilla were described alongside other specimens, but the type did not appear in the descriptions of other skull bones (Molnar, 1991).



1.5.7. Brochu (2003)

This monograph was focused on the complete skull of FMNH PR2081, and so the type was only mentioned in passing in the description of the maxilla (Brochu, 2003).

1.5.8. Larson (2008)

In his study of variation in T. rex, Larson figured the dentary of the type (2008: Figure 8.2). He focused on the size and form of the first dentary tooth, and he compared the sizes of the second and third dentary teeth (Larson, 2008). Larson's hypothesis was to demonstrate that the T. rex hypodigm actually includes two taxa, namely T. rex and 'T. x', which he did not name. Although the type was not specifically identified, Larson included tables of craniomandibular characters, including the maxilla, lacrimal, maxillary and dentary teeth, squamosal, and ectopterygoid, that he thought distinguished T. rex from other tyrannosaurid taxa (2008, tables 8.3, 8.4). Larson also included the type in a table of measurements and ratios of the second and third maxillary teeth (2008, table 8.2) and the maxilla and dentary that included data from the type (2008, table 8.6).

1.5.9. Carr (2020)

A summary assessment of the relative maturity of CM 9380, and of the diagnostic characters of T. rex identified by Osborn (1905), was given in the discussion section of this study of *T. rex* ontogeny (Carr, 2020).

1.5.10. Paul et al. (2022)

In their work that proposed to split the T. rex hypodigm into three species, a skeletal reconstruction of CM 9380 and the rostral end of its dentary in dorsal view were figured (Paul et al., 2022, Figure 1, 3). Measurements of the type were included in a table that included the length and height of the maxilla and dentary, and the length to height ratio for each bone, the diameter of the second and third dentary teeth, and the number of dentary incisors (Paul et al., 2022: Table 2). Although CM 9380 was not specifically discussed in the article, T. rex was characterised by the authors as a robust form with one dentary incisor that occurs high in the Hell Creek Formation (Paul et al., 2022).

1.5.11. Carr and Napoli et al. (2022)

In this test of Paul et al. (2022) the type was discussed and figured with regard to the morphology of the first three dentary teeth (Carr and Napoli et al., 2022, Figure 5). Owing to size variation, growth-related tooth loss, and small sample size, the authors regarded size variation among mesial dentary teeth as an unresolved foundation for distinguishing taxa and diagnosing species (Carr and Napoli et al., 2022). Also, they found evidence, based on the lengths of alveoli, for two incisiform teeth in CM 9380, contradicting the hypothesis of a single incisor (Paul et al., 2022).

1.5.12. Dalman et al. (2024)

The type was included in the inaugural study of a purported new tyrannosaurid taxon from New Mexico, and in the supplemental material it was treated as an exemplar of T. rex (Dalman et al., 2024, S1). Specifically, four features of the squamosal and two of the dentary were described and figured alongside other T. rex specimens (Dalman et al., 2024, S1: figure. S14, S15, S16).

2. Description

2.1. General form

Although incomplete, some conclusions can be drawn about the size and form of the skull of CM 9380. Skull length and femur length are isometric (Currie, 2003) and so the 1.3 metre length of the femur indicates that the skull, when complete, was approximately that length. The proximal end of the snout in the type, subadults (RSM 2990.1), young adults (MOR 1125), and other adults (AMNH FARB 5027) is expanded at the inflated lacrimals; in contrast, the proximal end is narrow in juveniles (FMNH PR2411) owing to uninflated lacrimals (Carr, 2020).

2.2. Orbital fenestra

Although only the lacrimals are preserved in CM 9380, the long ventral ramus of each bone indicates that the orbital fenestra was dorsoventrally taller than rostrocaudally long. This condition corresponds to the extremely tall condition that is seen in complete skulls of adult T. rex. Also, the subocular process of the postorbital is present in adult T. rex, indicating that this condition would have been present in the type. The absence of a distinct and massive process is only seen in shallow-skulled juveniles (CMNH 7541) (Carr, 2020).

In dorsal view, the wedge-shape dorsal ramus of the lacrimal (wide caudally, narrow rostrally) in the type indicates that the orbital fenestra had a rostrally-facing component. In juvenile T. rex (CMNH 7541) the fenestra faces more laterally than rostrally, whereas in all adults, the fenestra faces more rostrally than laterally (Carr, 2020). The shape of the lacrimal indicates that the opening in CM 9380 also faced more rostrally than laterally.

2.3. Antorbital fossa (= external antorbital fenestra)

In lateral view in CM 9380, the antorbital fossa is limited rostrodorsally and caudodorsally, whereas it extends caudoventrally. In other words, the fossa is narrowly exposed to lateral view on the expanded adjacent

Table 1. Measurements (in millimetres) of the left maxilla of the type specimen of Tyrannosaurus rex (CM 9380). All measurements were taken three times to the nearest hundredth, and the mean is documented here. Tilde (~) indicates measurement taken once.

Structure measured	Measurement
Antorbital fossa, rostrocaudal length	227.7
Maxilla, maximum length	694
Tooth row, length	554
Joint surface for the premaxilla, dorsoventral height	72.2
Maxillary fenestra, maximum length	105.3
Maxillary fenestra, dorsoventral height	65.3
Maxillary fenestra, caudodorsal margin, length	86.2~
Interfenestral strut, minimum length	18.5
Maxilla, dorsoventral height through rostral end of maxillary fenestra	364
Promaxillary fenestra, dorsoventral height	32~
Horizontal ramus, dorsoventral height at last alveolus	86.2
Ventral jugal process, length	151.9~
Ventral jugal process, base, dorsoventral height	72.2~
Horizontal ramus, length caudal to rostral margin of antorbital fenestra	333~
Bone, dorsoventral height through alveolus 1	141
Bone, dorsoventral height through alveolus 2	250
Bone, dorsoventral height through alveolus 3	297
Bone, dorsoventral height through alveolus 4	334.7
Bone, dorsoventral height through alveolus 5	366.3
Bone, dorsoventral height through alveolus 6	373.3
Bone, dorsoventral height through alveolus 7	369.3
Bone, dorsoventral height through alveolus 8	374.7
Bone, dorsoventral height through alveolus 9	371.2
Bone, dorsoventral height through alveolus 10	358.3
Bone, dorsoventral height through alveolus 11	-
Bone, dorsoventral height through alveolus 12	-
Horizontal ramus, height below antorbital fossa at alveolus 5	199.1
Horizontal ramus, height below antorbital fossa at alveolus 6	183
Horizontal ramus, height below antorbital fossa at alveolus 7	165.1
Horizontal ramus, height below antorbital fossa at alveolus 8	136.6
Horizontal ramus, height below antorbital fossa at alveolus 9	123.5
Horizontal ramus, height below antorbital fossa at alveolus 10	107
Horizontal ramus, height below antorbital fossa at alveolus 11	90.4
Horizontal ramus, height below antorbital fossa at alveolus 12	84.4
Horizontal ramus, height below antorbital fenestra at alveolus 9	152.1
Horizontal ramus, height below antorbital fenestra at alveolus 10	123.9
Horizontal ramus, height below antorbital fenestra at alveolus 11	95.4
Horizontal ramus, height below antorbital fenestra at alveolus 12	85.5
Maxillary tooth 10, mesiodistal length	25.1
Maxillary tooth 10, labiolingual width	19.4
Maxillary tooth 10, ratio width to length	77%

Table 2. Measurements (in millimetres) of the left and right lacrimals of the type specimen of *tyrannosaurus rex* (CM 9380). All measurements were taken three times to the nearest hundredth, and the mean is documented here. Tilde (~) indicates measurement taken once.

Structure measured	Left measurement	Right measurement
Total height of bone	333.7	332.3
Ventral ramus, height below pneumatic recess	248.3	242.2
Dorsal ramus, maximum mediolateral width	98.4	94.2
Lacrimal pneumatic recess, dorsoventral height	18.4	15.4
Lacrimal pneumatic recess, rostrocaudal length	14.8	17.8~
Dorsal ramus, dorsoventral height above recess	58.8	65.2
Ventral ramus, mediolateral width at midheight	-	74.2
Ventral ramus, length below dorsal ramus	103.4	104.7
Ventral ramus, length at midheight	81.8	87.8
Rostral ramus, length pillar ahead of recess	67.9	74.4
Rostral ramus, length accessory fossa	29.5	45.1
Ventral ramus, rostral jugal suture, length	61.2	65.9
Ventral ramus, caudal jugal suture, length	68.1	87.2

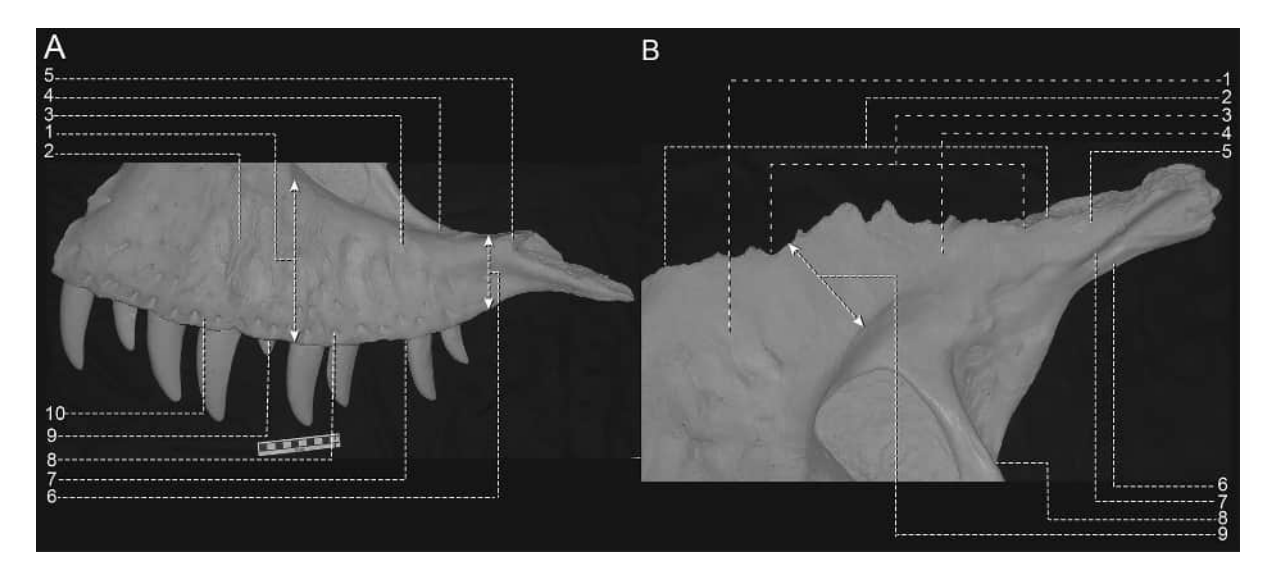


Figure 2. Detail of (A) the horizontal ramus of the left maxilla of CM 9380 in lateral view; the numbers correspond to the features: 1, horizontal ramus is deep; 2, subcutaneous surface is coarse; 3, ridge along the antorbital fossa is subtle; 4, antorbital fossa is significantly shallower than the horizontal ramus below it; 5, subcutaneous surface extends medial to the tip of the joint surface for the jugal; 6, continuous transition between the horizontal ramus and the jugal ramus; 7, distinct angulation towards the caudal end of the tooth row; 8, alveolar foramina are large; 9, alveolar skirts are absent; 10, subcutaneous surface extends medioventrally to the alveolar margin. (B) detail of the ascending ramus of the left maxilla of CM 9380 in lateral view; the numbers correspond to the features: 1, region rostrodorsal to the antorbital fenestra is inflated and convex; 2, joint surface for the nasal is serrate; 3, maxillary flange is distinct; 4, subcutaneous surface above the interfenestral strut is deep; 5, subcutaneous surface extends past rostral margin of the antorbital fenestra; 6, twist in the ascending ramus orients it ventromedially; 7, dorsal and ventral margins of the ascending ramus converge caudally; 8, rostralmost incursion of the antorbital fenestra is at the midheight of the maxillary fenestra; 9, antorbital fossa and the joint surface for the nasal are widely separated. Scale bar equals 10 cm.

regions of the maxilla and lacrimal, but the fossa extends caudoventrally onto the jugal (not preserved in the type) where it would be most widely exposed to lateral view (Carr, 2020). This limited dorsal exposure is seen in other adults, whereas in juveniles (BMRP 2002.4.1) the opposite is seen, a fossa that is widely exposed dorsally on the maxilla and lacrimal and only narrowly exposed on the jugal (Carr, 2020).

2.4. Antorbital fenestra (= internal antorbital fenestra)

In lateral view in CM 9380, the antorbital fenestra is as tall as long (Osborn, 1916, Figure 1), which is also seen in other adults (Carr, 2020). In some young adults (UWBM 99,000) and in juveniles (BMRP 2002.4.1), the fenestra is longer than tall (Carr, 2020).

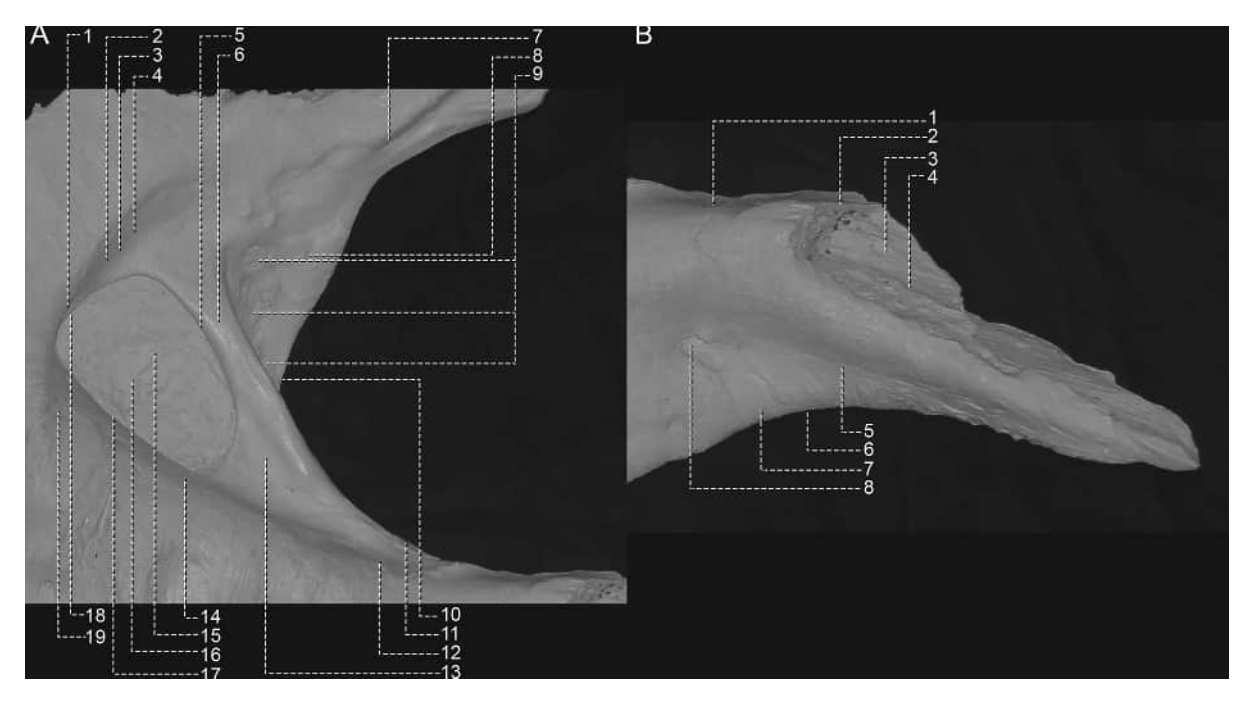


Figure 3. Detail of (A) the antorbital fossa of the left maxilla of CM 9380 in lateral view; the numbers correspond to the features: 1, promaxillary fenestra is concealed from view; 2, rostrodorsal region of the antorbital fossa is not obliterated by the maxillary fenestra; 3, rostrodorsal region of the antorbital fossa is most deeply inset; 4, rostrodorsal region of the antorbital fossa is not excavated by a subordinate fossa; 5, caudodorsal region of the maxillary fenestra is concave; 6, interfenestral strut is narrow; 7, antorbital fossa is deeply inset along the ascending ramus; 8, neurovascular foramen; 9, pneumatic foramina; 10. rostral margin of the antorbital fenestra is obtuse; 11. antorbital fossa forms a shallow rim below the antorbital fenestra; 12, antorbital fossa extends lateroventrally to the subcutaneous surface; 13, subordinate fossa in base of the interfenestral strut; 14, antorbital fossa is deeply inset below the maxillary and antorbital fenestra; 15, maxillary fenestra is large and extends past the rostral margin of the antorbital fossa; 16, maxillary fenestra closely approaches the ventral margin of the antorbital fossa; 17, ventral rim of maxillary fenestra is obliterated and formed by the antorbital fossa; 18, caudomedial margin of the promaxillary fenestra is formed by the maxillary fenestra; 19, rostroventral margin of the antorbital fossa grades into the horizontal ramus. (B) detail of the jugal ramus of the left maxilla of CM 9380 in lateral view; the numbers correspond to the features: 1, antorbital fossa is horizontally oriented ahead of the jugal ramus; 2, joint surface for the jugal does not reach the dorsal edge of the dorsal jugal process; 3, dorsal and ventral jugal processes are connected by a bony web; 4, joint surface for the jugal is coarse, deep, and wide; 5. ventral jugal process is deep and its dorsal half is strut-like; 6, jugal ramus extends at a distinct angle from the horizontal ramus; 7, the sulcus of the last foramen of the alveolar row breached the ventral margin of the jugal ramus; 8, the last foramen of the alveolar row is positioned below the midheight of the ventral jugal process.

3. Maxilla

3.1. General description

In CM 9380 only the left maxilla is preserved, which is complete except it is missing the tip of the ascending ramus, the rostral tip of the palatal process, and the medial wall of the maxillary sinus and promaxillary antrum (Figure 1). Measurements of the maxilla are given in Table 1. The tall triangular shape and specific features of the bone is typical for that of an adult tyrannosaurine: dorsoventrally deep horizontal ramus, the ascending ramus extends at a steep caudodorsal angle, inflated rostrodorsal to the antorbital fossa, serrate nasal joint surface, and a large maxillary fenestra (Figures 1, 2). Also, the rostral margin of the tall antorbital fenestra forms an obtuse angle, but this is partly obscured by the interfenestral strut (Figure 3A).

Although in lateral view it is highly excavated by the interdigitating joint surface for the nasal, the maxillary flange is distinct in CM 9380 (Figure 2B), large juveniles (BMRP 2002.4.1), subadults (LACM 23,845), young adults (MOR 1125), and other adults (AMNH FARB 5027), whereas it is vanishingly low in small juveniles (LACM 28,471) (Carr, 2020). In overall form, the maxilla in CM 9380 is tall, as is seen in other adults, in contrast to the shallow condition of juveniles (Figure 1; Carr, 2020).

Owing to the dorsoventral expansion of the bone, the rostrodorsal margin of the bone extends rostroventrally at a steep angle in CM 9380 (Figure 1), subadults (MOR 3044), young adults (MOR 1125), and other adults (AMNH FARB 5027); in contrast, the angle is low in juveniles (LACM 28,471) (Carr, 2020). In the type (Figure 1), young adults (MOR 1125), and other adults (AMNH FARB 5027), the region of the premaxillary buttress is dorsoventrally taller than the subnarial foramen, whereas in juveniles (LACM 28,471) they are the same height (Carr, 2020). The mediolateral width of the bone of the type, subadults (MOR 3044), young adults (MOR 1125), and other adults (AMNH FARB 5027) is wide, in contrast to the narrow condition of juveniles (LACM 28,471) (Carr, 1999, 2020). In part, the dorsoventral expansion of the bone is produced by inflation of the promaxillary antrum, which in lateral view expands the region rostrodorsal to the antorbital fossa; this expansion is seen in the type (Figures 2(B), 4(A)), subadults (MOR 3044), young adults (MOR 1125), and other adults (AMNH FARB 5027) (Carr, 2020). In contrast, the antrum and the external surface is not expanded in juveniles (LACM 28,471) (Carr, 2020).

In lateral view in CM 9380 (Figure 1), some juveniles (RSM 2347.1), subadults (MOR 3044), young adults (MOR 1125), and other adults (AMNH FARB 5027), the rostrodorsal margin of the bone between the maxillary flange and the joint surface for the premaxilla is convex, whereas in small juveniles (LACM 28,471), subadults (TMM 41,436-1), and one adult (UCMP 118,742) it is concave (Carr, 2020). In ventral view in CM 9380 and other adults, the bone is strongly sinuous in shape, where it curves rostromedially and caudolaterally (Carr, 2020). In contrast, in juveniles the bone is weakly sinusoidal (Carr, 2020).

3.2. Subcutaneous surface

In lateral view, the subcutaneous surface in CM 9380 (Figures 1, 2(A), 4(A)), juveniles (CMNH 7541), subadults (LACM 23,845), young adults (MOR 1125), and other adults (AMNH FARB 5027) is coarse rostral and ventral to the antorbital fossa, whereas it is smooth in the least mature juveniles (LACM 28,471) (Carr, 2020). The subcutaneous surface in the type (Figures 1, 2(A)), subadults (MOR 3044), young adults (LACM 150,167), and other adults (AMNH FARB 5027) is excavated by several shallow fossae along the horizontal ramus, whereas they are absent from juveniles (LACM 28,471) and some young adults (MOR 1125) (Carr, 2020). The fossae in the type (Figures 1, 2(A)), subadults (MOR 3044), young adults (LACM 150,167), and other adults (AMNH FARB 5027) are overlain by irregular, vertically trending ridges, whereas they are absent from juveniles (LACM 28,471) (Carr, 2020). In the type, the subcutaneous surface below the antorbital fossa is coarsely textured by irregular, dorsoventrally trending ridges and cusps (Figures 1, 2(A)).

In lateral view, a subtle ridge extends along the ventral edge of the antorbital fossa in CM 9380 (Figures 1, 2(A)), juveniles (LACM 28,471), young adults (MOR 1125), and some adults (CM 1400), whereas it is usually lost in adults (AMNH FARB 5027) (Carr, 2020). In the type (Figure 2(B)), juveniles (CMNH 7541), subadults (MOR 3044), young adults (MOR 1125), and other adults (AMNH FARB 5027) the subcutaneous surface extends caudodorsally along the ascending ramus caudal to the level of the rostral margin of the antorbital fenestra (Carr, 2020). In contrast, the subcutaneous surface stops ahead of the fenestra in the least mature juveniles (RSM 2347.1) (Carr, 2020). The subcutaneous surface above the interfenestral strut in the type (Figure 2(B)), subadults (MOR 3044), young adults (MOR 1125), and other adults (AMNH FARB 5027) is dorsoventrally deep, whereas it is shallow in juveniles (LACM 28,471) (Carr, 2020).

In CM 9380 (Figures 2(A), 4(A)), large juveniles (BMRP 2002.4.1), subadults (MOR 3044), young adults (MOR 1125), and other adults (AMNH FARB 5027) the subcutaneous surface extends medioventrally to the alveolar margin of the bone (Carr, 2020). In contrast, the surface is flat in small juveniles (RSM 2347.1) (Carr, 2020). In the type (Figure 3(B)), young adults (MOR 3044), and adults (AMNH FARB 5027), the surface at the rostral end of the joint surface for the jugal extends medially to separate the rostral end of the joint surface from the antorbital fossa (Carr, 2020). In contrast, the subcutaneous surface in juveniles (CMNH 7541) does not extend between the joint surface and the fossa (Carr, 2020).

3.3. Horizontal ramus (= body)

In lateral view, the horizontal ramus of the maxilla in CM 9380 (Figures 1, 2(A)) is dorsoventrally deep. This feature can be quantified by taking the ratio of the height of the subcutaneous surface below the antorbital fossa (199.1 mm) relative to the tooth row (554 mm), which is 36% in the type; in contrast, this ratio in

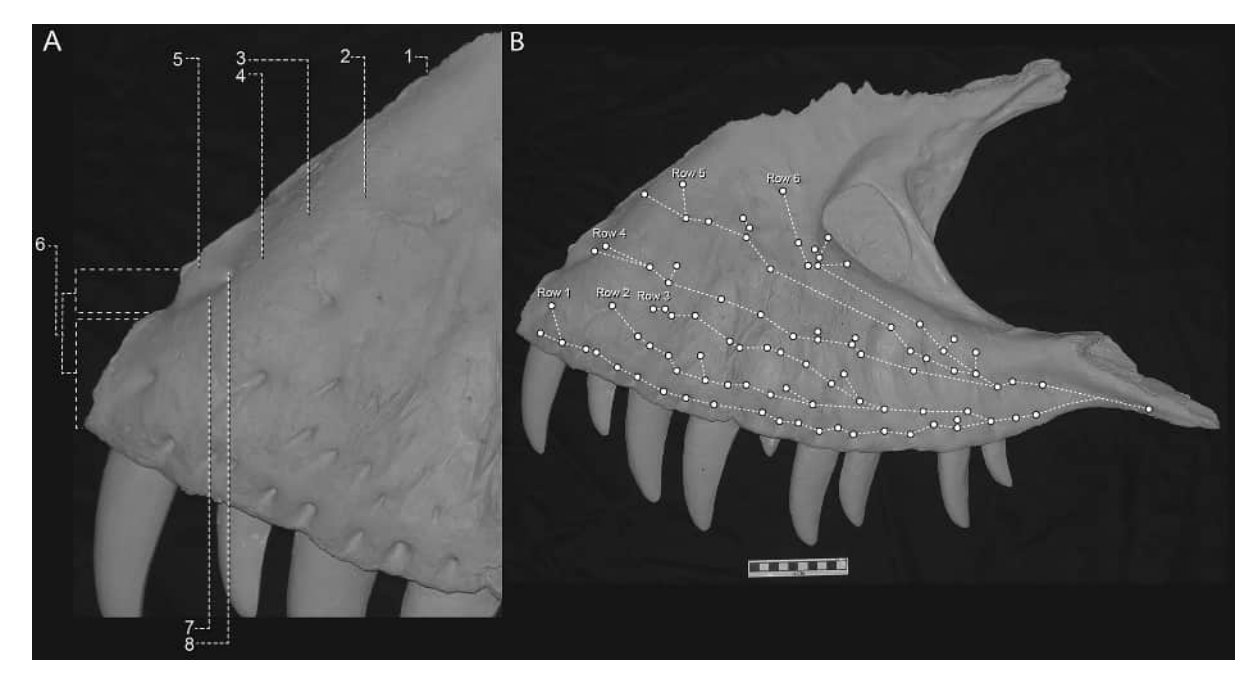


Figure 4. Detail of (A) the rostral end of the left maxilla of CM 9380 in lateral view; the numbers correspond to the features: 1, rostrodorsal margin is steep; 2, expanded region blocks the joint surface for the nasal from view; 3, narial fossa flattens the rostral surface of the maxilla; 4, the subnarial tract is bounded laterally by an indistinct ridge; 5, vestibular bulla is inflated; 6, premaxillary buttress is deeper than the subnarial foramen; 7, the subnarial tract is bounded laterally by an indistinct ridge; 8, dorsal foramen of the subnarial tract. (B) the six foramina rows of the left maxilla of CM 9380 in lateral view. Scale bar equals 10 cm.

a shallow-snouted juvenile (CMNH 7541) is 25%. The deep condition is also seen rostrally where the premaxillary buttress is taller than the subnarial foramen, whereas in juveniles those structures are the same height (Carr, 2020).

In lateral view in CM 9380 (Figures 2(A), 3(B)), subadults (MOR 3044), young adults (MOR 1125), and other adults (AMNH FARB 5027) the dentigerous region grades continuously into the jugal ramus; as such, the caudal region of the body subtly tapers in height as it extends caudally (Carr, 2020). In contrast, in juveniles (CMNH 7541) a distinct constriction (a 'waist') marks the transition between these regions and the alveolar region tapers distinctly as it extends caudally (Carr, 2020).

Alveolar skirts, flange-like extensions of bone lateral to alveoli, are absent from CM 9380 (Figure 2A), juveniles (LACM 28,471), subadults (MOR 3044), young adults (MOR 1125), and other adults (AMNH FARB 5027); in contrast, alveolar skirts are seen in some young adults (UWBM 99,000) and adults (MOR 980) (Carr, 2020). In the type (Figures 1, 2(A)), young adults (MOR 1125), and other adults (AMNH FARB 5027), the ventral margin of the tooth row has a distinct angulation between the horizontal rostral region and the steeply caudodorsally-extending caudal extent (Carr, 2020). This angulation is absent from juveniles (RSM 2347.1) and it is subtle in young adults (UWBM 99,000) and some adults (MOR 980) (Carr, 2020).

3.4. Lateral neurovascular foramina

In lateral view in CM 9380 (Figure 4B) there are, rostrally, six principal rows of foramina, whereas caudally, along the horizontal ramus, they converge into three rows. The marginal alveolar foramina in the type (Figures 2(A), 4(A)), subadults (LACM 23,845), and adults (AMNH FARB 5027) are large, whereas those of juveniles (LACM 28,471) and one subadult (TMM 41,436-1) are small (Carr, 2020). The caudal-most alveolar foramen in the type (Figures 2(A), 3(B)), subadults (MOR 3044), young adults (MOR 1125), and adults (AMNH FARB 5027) is positioned below the midheight of the ventral jugal process (Carr, 2020). In contrast, in juveniles (CMNH 7541) it is positioned at the midheight of the process (Carr, 2020). The sulcus that extends from the last alveolar foramen in the type (Figure 3B), young adults (UWBM 99,000), and other adults (AMNH

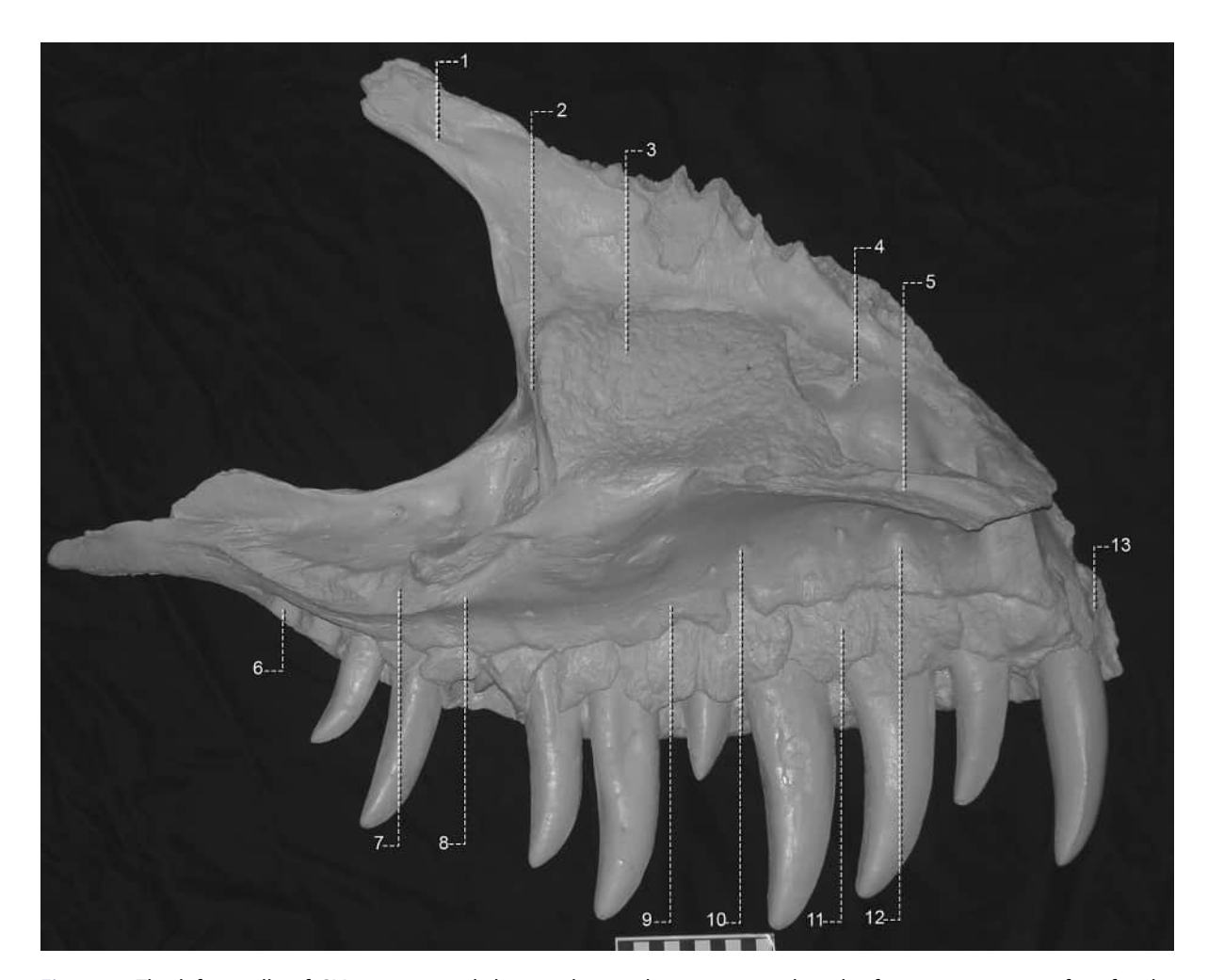


Figure 5. The left maxilla of CM 9380 in medial view; the numbers correspond to the features: 1, joint surface for the lacrimal; 2, medial interfenestral strut; 3, matrix-filled maxillary antrum and epiantral recess; 4, promaxillary sinus; 5, intermaxillary process; 6, alveolus #12; 7, joint surface for the palatine; 8, palatal process; 9, medial alveolar process; 10, medial alveolar foramen; 11, interdental plate; 12, dental pit; 13, joint surface for the premaxilla (= premaxillary buttress). Scale bar equals 10 cm.

FARB 5027), breaches the ventral margin of the jugal process, whereas in juveniles (CMNH 7541) and subadults (MOR 3044) the sulcus extends a short distance along the ventral margin (Carr, 2020).

3.5. Vestibular bulla

In lateral view in CM 9380, young adults (MOR 1125), and adults (AMNH FARB 5027) the vestibular bulla is inflated (Figure 4A), whereas it is not inflated in juveniles (LACM 28,471) (Carr, 2020).

3.6. Joint surface for the premaxilla

The joint surface for the premaxilla above the subnarial foramen in CM 9380 (Figure 4A) is braced by a laterally-everted lip, which extends to the joint surface for the maxillary process of the premaxilla.

3.7. Margin of the subnarial foramen

In lateral view in CM 9380 (Figures 1, 2(A), 4(A)), young adults (MOR 1125), and adults (AMNH FARB 5027) the subnarial foramen is a deep notch in the rostral margin of the bone, whereas in juveniles (LACM 28,471), young adults (UWBM 99,000), and some adults (LACM 23,844) and it is a shallow concavity (Carr, 2020).

3.8. Tract of the subnarial foramen

In lateral view in tyrannosaurids, the narial fossa extends from the premaxilla onto the maxilla as a shallow fossa that extends from the margin of the subnarial foramen. The fossa is usually penetrated by two neurovascular foramina, including a dorsal foramen and a ventral foramen. In CM 9380 (Figure 4A) and all other specimens, except for one large juvenile (BMRP 2002.4.1), it is penetrated by one foramen. In the type, large juveniles (BMRP 2002.4.1), young adults (UWBM 99,000), and other adults (AMNH FARB 5027) the tract is penetrated by the dorsal foramen; whereas the ventral foramen is seen in juveniles (LACM 28,471) and some adults (MOR 008) (Carr, 2020). The foramen in the type is round and a distinct sulcus extends from it into the subnarial foramen (Figure 4A); although the foramen is round, it is not enlarged as is seen in *T. bataar* (PIN 551–2).

The tract in CM 9380 (Figure 4A) is bounded laterally by a low and indistinct ridge whereas in young adults (UWBM 99,000), and most adults (AMNH FARB 5027) the fossa grades continuously into the coarse subcutaneous surface (Carr, 2020). In contrast, the fossa is bounded by a distinct and sharp ridge in juveniles (LACM 28,471) (Carr, 2020).

3.9. Narial fossa

In lateral view, the narial fossa in CM 9380 (Figure 4A), young adults (UWBM 99,000), and other adults (MOR) extends caudodorsally from the subnarial foramen onto the maxilla as a widely depressed region (Carr, 2020). In contrast, the region caudodorsal to the subnarial fossa is not widely depressed in juveniles (LACM 2871), young adults (MOR 1125), and other adults (RSM 2523.8) (Carr, 2020).

3.10. Ascending ramus

In lateral view in CM 9380 (Figure 2B), subadults (MOR 3044), young adults (MOR 1125), and other adults (AMNH FARB 5027) the region rostrodorsal to the antorbital fossa is expanded and convex, presumably an epiphenomenon of internal expansion of the promaxillary antrum (Carr, 2020). The expansion widely separates the rostrodorsal corner of the antorbital fossa from the nasal suture (Carr, 2020). In the type (Figure 2B), large juveniles (BMRP 2002.4.1), young adults (MOR 1125), and other adults (AMNH FARB 5027) this surface is convex, whereas it is concave in juveniles (RSM 2347.1), a young adult (UWBM 99,000), and in some adults (LACM 23,844) (Carr, 2020).

The dorsal and ventral margins of the ramus in CM 9380 (Figures 1, 2(B)), young adults (UWBM 99,000), and other adults (MOR 980) converge with each other as they extend caudally (excluding the joint surface for the nasal and lacrimal), whereas in juveniles (LACM 28,471), one young adult (MOR 1125), and an adult (AMNH FARB 5027) the margins are parallel (Carr, 2020). The region of the ramus above the antorbital fenestra in the type (Figure 2B), young adults (TMP 1981.006.0001), and other adults (AMNH FARB 5027) twists such that it extends ventromedially, whereas in juveniles (LACM 28,471) and a young adult (LACM 150,167) the ramus is flat and faces laterally, and in some young adults (MOR 1125) and adults (MOR 555) it extends ventromedially without the twist (Carr, 2020).

In lateral view in CM 9380 (Figures 1, 2(B)), large juveniles (BMRP 2002.4.1), subadults (MOR 3044), young adults (MOR 1125), and other adults (AMNH FARB 5027) the maxillary flange is distinct as in other adults, whereas it is low and indistinct in small juveniles (LACM 28,471) (Carr, 2020).

3.11. Joint surface for the lacrimal

In lateral view in CM 9380 (Figure 2B), small juveniles (RSM 2347.1), and a young adult (UWBM 99,000) the joint surface for the lacrimal has the form of a shallow groove, whereas in large juveniles (BMRP 2002.4.1), a young adult (UWBM 99,000) and other adults (MOR 980) it is a deep slot below the caudodorsolateral process (Carr, 2020).



3.12. Joint surface for the nasal

In lateral, medial, and dorsal views, the joint surface for the nasal in CM 9380 (Figures 1, 2(B), 5, 6(A,C)), subadults (LACM 23,845), young adults (MOR 1125), and other adults (AMNH FARB 5027) has a peg-in-socket form, whereas in juveniles (LACM 28,471) it has a tongue-in groove form (Carr, 2020). In lateral view in the type (Figure 4A), subadults (MOR 3044), young adults (MOR 1125), and other adults (MOR 980) the rostral end of the joint surface is blocked from view by the expanded rostrodorsal region, whereas in juveniles (BMRP 2002.4.1) the joint surface is exposed to view (Carr, 2020).

3.13. Antorbital fossa (= external antorbital fenestra)

In lateral view in CM 9380 (Figure 3A), juveniles (CMNH 7541), subadults (TMM 41,436-1), and adults (MOR 555) the antorbital fossa is not scoured rostrodorsally by a subordinate fossa or recess, whereas one is present in some juveniles (RSM 2347.1), a young adult (UWBM 99,000), and some adults (AMNH FARB 5027). In some young adults (MOR 1125) and adults (RSM 2523.8) the region is obliterated by the maxillary fenestra (Carr, 2020). The fossa in CM 9380 (Figure 3A), small juveniles (RSM 2347.1), subadults (MOR 3044), young adults (UWBM 99,000), and some adults (AMNH FARB 5027) forms an extremely shallow rim below the antorbital fenestra, whereas in some juveniles (CMNH 7541), young adults (MOR 1125), and one adult (FMNH PR2081) it forms a rim of uniform height (Carr, 2020). In the type (Figure 3A), small juveniles (RSM 2347.1), subadults (MOR 3044), young adults (LACM 150,167), and other adults AMNH FARB 5027) the fossa below the antorbital fenestra becomes shallow along its course.

In CM 9380 (Figure 3), subadults (MOR 3044), young adults (MOR 1125), and other adults (MOR 980) the fossa below the antorbital fenestra is extremely shallow, where the horizontal ramus is several times deeper than the fossa (Carr, 2020). In contrast, in juveniles (RSM 2347.1) and one subadult (TMM 41,436-1) the fossa is tall, and in some young adults (LACM 150,167) and adults (MOR 555) the rim is obliterated as it extends to the jugal ramus (Carr, 2020). In the type, the fossa is horizontally oriented (i.e. flat) ahead of the jugal ramus. The rostroventral margin of the fossa in the type (Figure 3A), large juveniles (BMRP 2002.4.1), subadults (MOR 3044), young adults (MOR 1125), and other adults (AMNH FARB 5027) is indistinct, whereas it is distinct in small juveniles (LACM 28,471) and one adult (FMNH PR2081) (Carr, 2020).

In CM 9380 (Figure 3A), large juveniles (BMRP 2002.4.1), subadults (MOR 3044), young adults (MOR 1125), and other adults (AMNH FARB 5027) the fossa is most deeply excavated along its rostrodorsal margin, whereas in small juveniles it is deepest along the rostral margin of the fossa, and in some young adults (LACM 150,167) and adults (MOR 555) it is deepest below the interfenestral strut (Carr, 2020). In the type (Figures 2 (B), 3(A)), the fossa is deeply inset above the antorbital fenestra, almost undercutting the subcutaneous surface. The fossa in the type (Figure 3A), subadults (MOR 3044), young adults (LACM 150,167), and other adults (AMNH FARB 5027) is deeply inset below the maxillary fenestra and the antorbital fenestra, whereas in juveniles (LACM 28,471), and one young adult (UWBM 99,000) it is shallowly inset (Carr, 2020).

In CM 9380 (Figure 3A), subadults (MOR 3044) and adults (MOR 008) accessory pneumatic fossae are present in the antorbital fossa, whereas these are absent from juveniles (CMNH 7541), young adults (MOR 1125), and some adults (AMNH FARB 5027) (Carr, 2020). In the type (Figure 3A), subadults (TMM 41,436–1), and some adults (AMNH FARB 5027), the fossa of the type is penetrated by lateromedially extending foramina, whereas they are absent from juveniles (RSM 2347.1), subadults (MOR 3044), young adults MOR 1125), and some adults (MOR 008) (Carr, 2020).

In the type (Figures 3(A), 6(C)), subadults (MOR 3044), young adults (MOR 1125), and other adults (AMNH FARB 5027) the fossa extends lateroventrally to the subcutaneous surface and the two are not separated by a crease (Carr, 2020). In contrast, a deep crease separates the fossa and subcutaneous surface in juveniles (CMNH 7541) and some young adults (UWBM 99,000); a subtle crease is seen in large juveniles (BMRP 2002.4.1) and in one adult (LACM 23,844) (Carr, 2020).

3.14. Promaxillary fenestra

In lateral view, the rostral margin of the antorbital fossa in CM 9380 (Figure 3A), subadults (MOR 3044), young adults (MOR 1125), and other adults (AMNH FARB 5027) is ridge-like and conceals the promaxillary fenestra, whereas in juveniles (LACM 28,471) the fenestra is not concealed from view (Carr, 2020). The fenestra in the type, young adults (MOR 1125), and other adults (AMNH FARB 5027) is situated at the same horizontal level as the ventral margin of the promaxillary fenestra, whereas a dorsalward position relative to the maxillary fenestra is seen in juveniles (CMNH 7541), subadults (MOR 3044), young adults (UWBM 99,000), and one adult (FMNH PR2081) (Carr, 2020). In caudolateral view in the type, subadults (TMM 41,436–1), young adults (MOR 1125), and other adults (AMNH FARB 5027) the fenestra is mediolaterally wide and round in shape, whereas in juveniles (LACM 28,471) it is a narrow slit (Carr, 2020). In the type (Figures 3(A), 4(B)), a neurovascular foramen penetrates the antorbital fossa caudolateral to the promaxillary fenestra.

In CM 9380 (Figure 3A), subadults (TMM 41,436–1), young adults (MOR 1125), and other adults (AMNH FARB 5027) the caudomedial edge of the promaxillary fenestra is formed by the rostral margin of the maxillary fenestra, whereas in juveniles (LACM 28,471) it is rostral to, and separate from, the maxillary fenestra (Carr, 2020). In caudolateral and medial views, the fenestra in the type, young adults (MOR 1125), and other adults (MOR 980) extends rostrally into the bone, whereas it extends rostromedially in juveniles (BMRP 2002.4.1) (Carr, 2020). Also when seen from behind, the lateral and medial margins of the fenestra, in the type, young adults (MOR 1125), and other adults (AMNH FARB 5027) converge at the dorsal margin of the maxillary fenestra, whereas in juveniles (BMRP 2002.4.1) and one young adult (UWBM 99,000) the margins converge at the rostral edge of the antorbital fossa, ahead of the maxillary fenestra (Carr, 2020). An intermediate condition is seen in one subadult (TMM 41,436–1) where the margins converge at the rostral margin of the maxillary fenestra (Carr, 2020).

3.15. Antorbital fenestra (= internal antorbital fenestra)

In lateral view the rostral margin of the antorbital fenestra in CM 9380 (Figure 3A) follows an obtuse angle, as in subadults (MOR 3044) and adults (AMNH FARB 5027), whereas the angle is acute in juveniles (RSM 2347.1) (Carr, 2020). The point of rostralmost incursion of the type (Figure 3A) is at the level of above the midheight of the maxillary fenestra, as in subadults (TMM 41,436–1) and adults (AMNH FARB 5027) (Carr, 2020). In contrast, the maximum incursion is below midheight in juveniles (BMRP 2002.4.1) and subadults (MOR 3044) (Carr, 2020). Relative to the teeth, the rostral margin of the fenestra in CM 9380 (Figures 1, 2(A)) is at the level of 4.5 tooth positions from the caudal end of the tooth row; in young adults (UWBM 99,000) and other adults (AMNH FARB 5027) the margin is at least five tooth positions or less ahead of the distal-most tooth (Carr, 2020). In contrast, the margin is rostrally positioned in juveniles (CMNH 7541), at six tooth positions (Carr, 2020). In the type (Figures 1, 2(A)) and other adults (MOR 980) there are four tooth positions ahead of the fenestra, in juveniles (CMNH 7541) there are seven teeth ahead of the fenestra (Carr, 2020). Some juvenile (BMRP 2002.4.1), subadults (MOR 3044), and young adults (UWBM 99,000) show an intermediate number between the extremes (Carr, 2020).

3.16. Maxillary fenestra

In lateral view, the maxillary fenestra of CM 9380 (Figure 3A), young adults (MOR 1125), and other adults (AMNH FARB 5027) reaches the rostral margin of the antorbital fossa, whereas it does not reach the margin in juveniles (LACM 28,471) (Carr, 2020). The fenestra in the type extends medially past the rostral margin of the fossa. The fenestra in CM 9380 (Figure 3A), one juvenile (RSM 2847.1), young adults (LACM 150,167), and other adults (AMNH FARB 5027) closely approaches the ventral margin of the fossa; in contrast, in some juveniles (CMNH 7541), young adults (MOR 1125), and some adults (MOR 980) it is situated above the ventral margin (Carr, 2020). The fenestra in the type (Figure 3A), young adults (MOR 1125), and other adults (AMNH FARB 5027) is massive, and occupies over half the length of the antorbital fossa; whereas in juveniles (BMRP 2002.4.1) it is less than half the length of the fenestra (Carr, 2020). Correspondingly, the interfenestral strut in the type (Figure 3A), young adults (LACM 150,167), and other adults (AMNH FARB 5027) is rostrocaudally narrow, whereas the strut is wide in juveniles (RSM 2347.1) and one young adult (MOR 1125) (Carr, 2020).

In lateral view, the rostrodorsal margin of the fenestra in CM 9380 (Figure 3A) and other adults (AMNH FARB 5027) closely approaches the edge of the antorbital fossa (Carr, 2020). This condition is not seen in juveniles, in which the structures are widely separated (BMRP 2002.4.1) (Carr, 2020). The

caudodorsal margin of the fenestra in the type (Figure 3A) and some other adults (AMNH FARB 5027) is concave; this margin is straight in young adults (TMP 1981.006.0001). This margin is convex in juveniles (BMRP 2002.4.1) and in young adults (UWBM 99,000) (Carr, 2020). The ventral margin of the fenestra in CM 9380 (Figure 3A) and other adults (UWBM 99,000) is obliterated and incorporated into the antorbital fossa (Carr, 2020); this is almost certainly an epiphenomenon of the expansion of the dental alveoli. In contrast, the margin in juveniles (BMRP 2002.4.1) and some adults (FMNH PR2081) is a low ridge (Carr, 2020).

3.17. Lateral interfenestral strut

In lateral view, the strut in CM 9380 (Figure 3A) is rostrocaudally narrow (w:h: < 65%; 28% in the type). In contrast, the subadult condition is a wide strut with a ratio that is 65% or greater (Carr, 2020). In the type (Figure 3A) and all other growth stages (aside from the perforated condition in the adult LACM 23,844), a fossa excavates the base (= ventral half) of the strut (Carr, 2020). Specifically in the type the base of the strut is deeply concave with a pair of subordinate fossae (Figure 3A). In the type, a small neurovascular foramen pierces the top of the strut (Figure 3A).

The proximal region of the strut in CM 9380 has a distinct twist (Figures 3(A), 6(C)), a condition that is not seen in other T. rex specimens, juvenile or adult, which is presumed here to represent individual variation. The condition in the type is different from other specimens in that the strut is a rostrodorsally extending rod, whereas its caudodorsal quadrant flares caudomedially, forming deep concavity next to the rostrodorsal corner of the antorbital fenestra (Figures 3(A), 6(C)). The rostrodorsal corner of the fossa is penetrated by large, presumably pneumatic, foramina (Figure 3A). A causal explanation for this morphology is difficult to explain, but it has the appearance that the caudodorsolateral region of the strut was absorbed by the antorbital air sac, exposing the chambers in its caudal wall. In contrast, in juveniles (BMRP 2002.4.1), subadults (MOR 3044), young adults (MOR 1125), and adults (AMNH FARB 5027) the differentiation between a rostrodorsal rod and a caudodorsal fossa is not seen, where instead the surface is flat and continuous with the rest of the ascending ramus that extends over the antorbital fenestra.

In medial view, the base of the strut in the type (Figures 5, 6(B), 7), young adults (MOR 1125), and other adults (MOR 555) is excavated by a deep fossa. In contrast, the fossa is absent from small juveniles (RSM 2347.1), and the fossa is shallow in large juveniles (BMRP 2002.4.1) and subadults (MOR 3044) (Carr, 2020).

3.18. Medial interfenestral strut

In medial view, the form of the strut in the type (Figures 5, 6(B), 7), subadults (MOR 3044), young adults (LACM 150,167), and other adults (MOR 980) is tall and thin, whereas in juveniles (BMRP 2002.4.1) and young adults (MOR 1125) it is stout (Carr, 2020). Also, in the type (Figures 5, 7), subadults (MOR 3044), young adults (LACM 150,167), and adults (MOR 980) the strut extends caudodorsally, whereas in variation is seen in one young adult (UWBM 99,000) where it extends vertically or rostrodorsally; the rostrodorsal condition is seen in one adult (MOR 980) (Carr, 2020).

The rostrocaudal position of the strut in the type (Figures 5, 7) and other adults (MOR 980) is at the midlength of the base of the lateral interfenestral strut, whereas in juveniles (BMRP 2002.4.1), subadults (MOR 3044), and one adult (RSM 2523.8) it is towards the caudal end of the lateral strut (Carr, 2020). In the type (Figure 6B), subadults, young adults, and adults, there are six or fewer teeth (five in CM 9380) caudal to the strut, whereas in juveniles (BMRP 2002.4.1) there are six or more (Carr, 2020). In the type (Figure 6A), two neurovascular foramina pierce the medial wall of the strut above the dorsal sinus, and caudodorsal to them a dorsoventrally deep foramen pierces the strut and opens as a deeper opening on the medial surface close to the caudal edge of the strut.

In medial view, the position of the dorsal half of the medial strut relative to the antorbital fenestra in CM 9380 (Figure 7), subadults (MOR 3044), young adults (MOR 1125), and adults (MOR 555) is ahead of the fenestra, such that the medial strut is concealed in lateral view (Figure 3A), whereas in juveniles (RSM 2347.1) and one young adult (LACM 150,167) it is positioned caudally such that it is seen in lateral view (Carr, 2020).

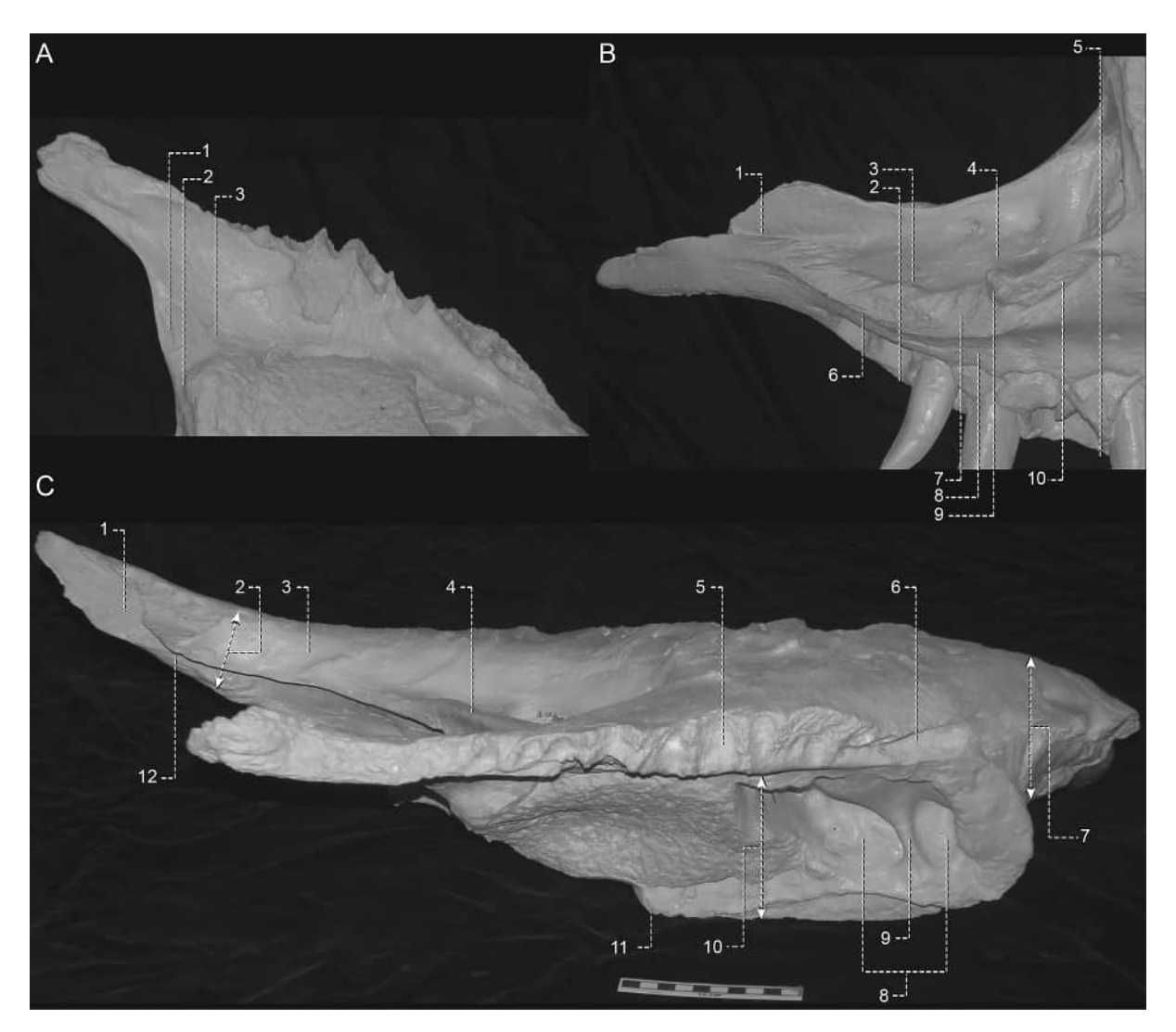


Figure 6. Detail of (A) the ascending ramus of the left maxilla of CM 9380 in medial view; the numbers correspond to the features: 1, large foramen; 2, small foramen; 3, large foramen. (B) detail of the jugal ramus of the left maxilla of CM 9380 in medial view; the numbers correspond to the features: 1, palatal shelf and dorsal jugal process are separated by a narrow slot; 2, joint surface for the jugal extends to the second last alveolus; 3, palatal shelf and sinus system are widened medially; 4, tooth root bulges are obscured by overgrowth of bone; 5, antorbital fenestra is at the level of the fifth alveolus; 6, palatal shelf positioned above ventral margin of medial alveolar process; 7, joint surface for the palatine is dorsoventrally deep; 8, last interdental pit is between alveoli 9 and 10; 9, joint surface for the palatine is notched rostrally; 10, joint surface for the palatine is flat caudally and rostrally is a ventrally-facing groove. (C) dorsal view of left maxilla; the numbers correspond to the features: 1, joint surface for the jugal is wide and coarse; 2, jugal ramus is mediolaterally wide; 3, antorbital fossa extends lateroventrally to the subcutaneous surface; 4, lateral interfenestral strut is rod-like; 5, peg-in-socket joint surface for the nasal; 6, rostral extent of the joint surface for the nasal is confined medially; 7, bone is mediolaterally wide; 8, floor of promaxillary sinus is excavated by deep recesses; 9, floor of sinus is crossed by a distinct strut; 10, maxillary sinus system doubles the width of the bone; 11, maxillary sinus abruptly widens the palatal process; 12, narrow slot between palatal process and dorsal jugal process. Scale bar equals 10 cm.

3.19. Maxillary sinus system

In dorsal view, the maxillary sinus system in CM 9380 (Figure 6C), subadults (MOR 3044), young adults (MOR 1125), and other adults (AMNH FARB 5027) is wide such that it extends far medial to the tooth root bulges, doubling the width of the bone (Carr, 2020). In contrast, this region is mediolaterally narrow in juveniles (BMRP 2002.4.1).

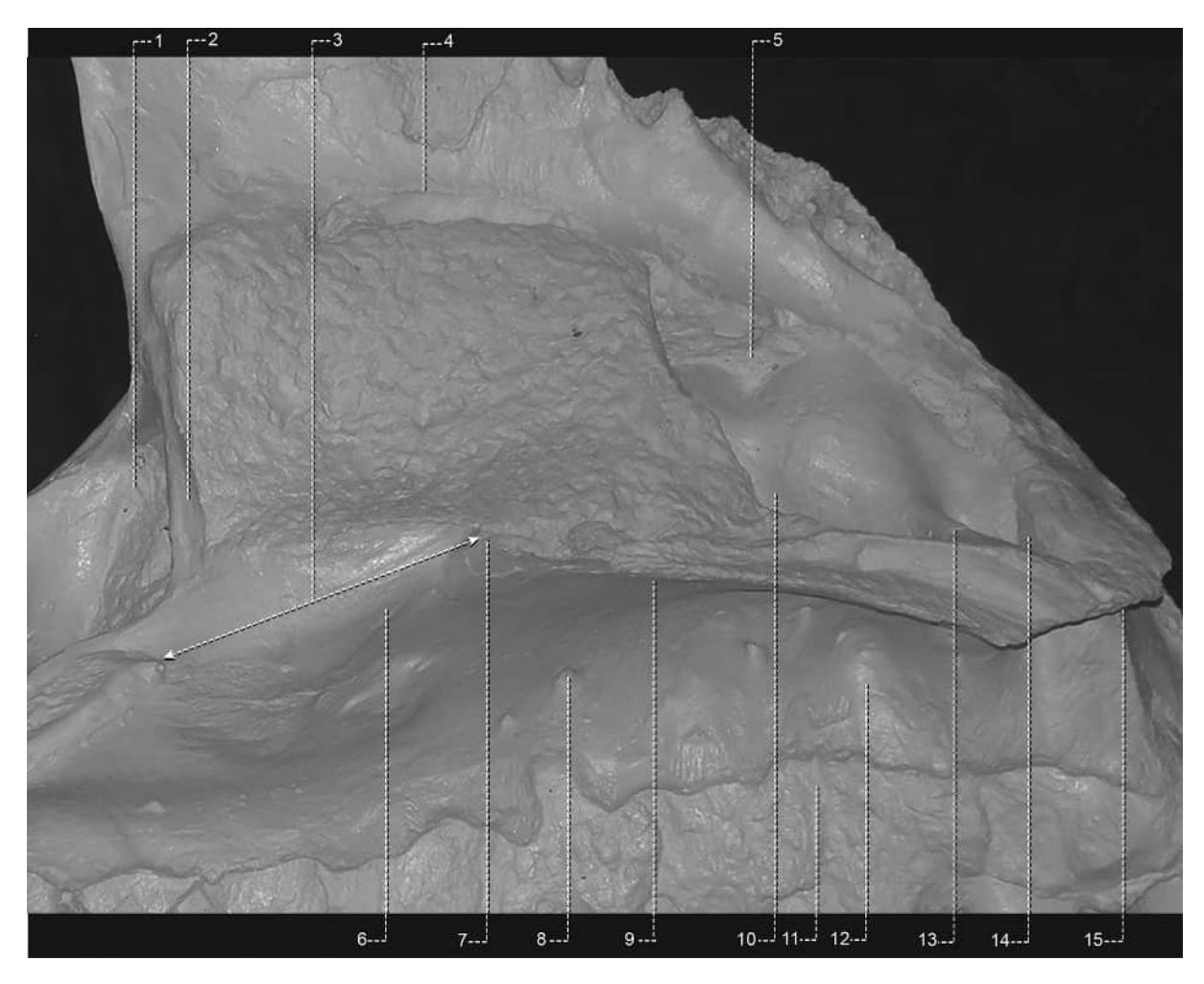


Figure 7. Detail of the maxillary sinus system of the left maxilla of CM 9380 in medial view; the numbers correspond to the features: 1, deep fossa in base of lateral interfenestral strut; 2, medial interfenestral strut is tall, thin, and extends caudodorsally; 3, bony choana is positioned rostrally; 4, dorsal margin of the maxillary antrum extends horizontally; 5, promaxillary sinus is dorsoventrally deep; 6, palatal and intermaxillary processes are continuous with each other; 7, joint surface for the maxilla reaches the level of the promaxillary fenestra; 8, medial alveolar process is penetrated by large foramina; 9, intermaxillary process extends dorsomedially; 10, floor of promaxillary sinus is deepened by recesses; 11, interdental plates are not separated by circular gaps; 12, rostral three interdental plates are the deepest of the row; 13, floor of promaxillary sinus is crossed by a strut; 14, promaxillary sinus extends rostrally to the second alveolus; 15, intermaxillary process extends to the first alveolus.

3.20. Promaxillary sinus

In medial view in CM 9380 (Figure 7) the promaxillary sinus extends rostrally, stopping above the second maxillary dental alveolus. This position is comparable to the rostral position in young adults (MOR 1125), and other adults (MOR 555) where the sinus extends as far forward as the first alveolus (Carr, 2020). In contrast, a caudal position is seen in juveniles (BMRP 2002.4.1) where the sinus stops at the septum between alveoli 2 and 3 (Carr, 2020).

The region of the promaxillary sinus in the type (Figure 7), subadults (MOR 3044), young adults (MOR 1125), and other adults (MOR 555) is dorsoventrally deep, in contrast to the shallow height of juveniles (BMRP 2002.4.1) (Carr, 2020). The floor of the sinus in CM 9380 (Figures 6(C), 7), young adults (MOR 1125), and other adults (MOR 555) is deepened by recesses, whereas the sinus is not deepened in juveniles (BMRP 2002.4.1) (Carr, 2020). Also, the floor in the type (Figures 6(C), 7), young adults (MOR 1125), and other adults (MOR 555) is crossed by a distinct strut that is absent from juveniles (BMRP 2002.4.1) (Carr, 2020).

3.21. Maxillary antrum

In medial view, the region above the medial foramen into the antrum in CM 9380 (Figure 7), young adults (UWBM 99,000), and other adults (MOR 980) is perforated by a large foramen that produces a dorsal opening into the antrum (Carr, 2020). In contrast, this region is imperforate in juveniles (BMRP 2002.4.1), subadults (MOR 3044), and young adults (MOR 1125) (Carr, 2020). The dorsal margin of the antrum in the type (Figure 7), subadults (MOR 3044), and some other adults (MOR 980) extends horizontally, whereas in juveniles (BMRP 2002.4.1), subadults (TMM 41,436–1), and young adults (MOR 1125) it extends rostroventrally (Carr, 2020). In caudal view in CM 9380, the caudal entrance into the antrum has a horizontal dorsal margin.

3.22. Jugal ramus

In lateral view the jugal ramus in CM 9380 (Figure 3B), young adults (MOR 1125), and other adults (AMNH FARB 5027) extends at a distinct angle from the alveolar region, whereas the ramus is straight in juveniles (CMNH 7541) or extends at a low angle in subadults (MOR 3044), young adults (LACM 150,167), and some adults (MOR 980) (Carr, 2020). In the type (Figure 3B), young adults (LACM 150,167), and adults (MOR 980) the two jugal processes are connected by a caudoventrally-extending web of bone, whereas in juveniles (BMRP 2002.4.1) they are separated by a deep notch (Carr, 2020).

In ventral and dorsal views the ramus in CM 9380 (Figure 6C), juveniles (BMRP 2002.4.1), subadults (MOR 3044), and some adults (MOR 555) is wide, whereas it is narrow in young adults (UWBM 99,000) and other adults (AMNH FARB 5027) (Carr, 2020).

3.23. Dorsal jugal process

In lateral view, the joint surface for the jugal on the process CM 9380 (Figure 3B), juveniles (CMNH 7541), young adults (UWBM 99,000), and some adults (AMNH FARB 5027) does not reach its dorsal margin, whereas in some young adults (LACM 150,167) and adults (MOR 980) it does (Carr, 2020).

3.24. Ventral jugal process

In lateral view, the ventral jugal process in CM 9380 (Figure 3B), subadults (MOR 3044), young adults (MOR 1125), and other adults (AMNH FARB 5027) is dorsoventrally deep, whereas it is shallow in juveniles (CMNH 7541) (Carr, 2020). The lateral surface of the process in the type (Figure 3B) and other adults (AMNH FARB 5027) has the form of a massive, dorsoventrally deep and convex strut that extends caudoventrally to the tip of the bone, whereas in juveniles (CMNH 7541) its lateral surface is flat (Carr, 2020). In subadults (MOR 3044), young adults (MOR 1125), and one adult (MOR 555), the lateral surface is subtly convex (Carr, 2020).

3.25. Joint surface for the jugal

In medial view in CM 9380 (Figure 6B), young adults (MOR 1125), and other adults (MOR 555) the joint surface for the jugal reaches the level of the second last alveolus, whereas in juveniles (BMRP 2002.4.1), subadults (MOR 3044), young adults (UWBM 99,000), and some adults (AMNH FARB 5027) it stops at or caudal to the last alveolus (Carr, 2020). In dorsal view in CM 9380 (Figure 6C), young adults (MOR 1125), and other adults (MOR 980) the joint surface is coarse, deep, and wide, whereas in juveniles it is a narrow slot (RSM 2347.1) or smooth and shallow (BMRP 2002.4.1) (Carr, 2020). It is shallow in subadults (MOR 3044), young adults (LACM 150,167), and some adults (MOR 555) (Carr, 2020).

3.26. Palatal process

In medial view, the palatal process of CM 9380 (Figure 5), subadults (MOR 3044), and other adults (AMNH FARB 5027) is sigmoid in shape, where it follows a shallow, but distinct, S-shape along its rostrodorsally

extending course from the ventral jugal process to the tip of the intermaxillary process. In contrast, the process is straight in juveniles (Carr, 2020). The caudal end of the process in the type (Figures 5, 6(B)), subadults (MOR 3044), young adults (UWBM 99,000), and other adults (AMNH FARB 5027) extends above the level of the level of the medial alveolar margin, whereas in juveniles (BMRP 2002.4.1) it extends below it (Carr, 2020). In medial and dorsal views, the caudal end of the process in CM 9380 (Figures 5, 6(B, C)), subadults (MOR 3044), young adults (MOR 1125), and other adults (MOR 980) is close to the dorsal jugal process, producing a narrow slot between them; in contrast, the structures are widely separate in juveniles (BMRP 2002.4.1) and young adults (UWBM 99,000) (Carr, 2020).

In dorsal view, the caudalmost extent of the trough medial to the tooth root bulges in the maxillary antrum in CM 9380 and one other adult (FMNH PR2081) is limited to the antrum; whereas in subadults (LACM 150,167) and other adults (MOR 555) it stops adjacent to the lateral interfenestral strut, and in juveniles (CMNH 7541), subadults (MOR 3044), and some young adults (MOR 1125) it extends to the caudal end of the palatal process (Carr, 2020). The groove that is between the medial interfenestral strut and the tooth root bulges in the type, young adults (LACM 150,167), and other adults (MOR 980), has a deeply inset caudal end, whereas in juveniles (BMRP 2002.4.1) and one young adult (UWBM 99,000) it fades over the palatal process (Carr, 2020).

In medial view in the type (Figures 5, 6(B)) and other adults (MOR 008) the tooth root bulges are completely obscured by overgrowth of bone, whereas in juveniles (CMNH 7541) and one adult (RSM 2523.8) they are distinct (Carr, 2020), They are partly obscured in young adults (MOR 1125) and some adults (MOR 980) (Carr, 2020), In CM 9380 (Figure 7), subadults (MOR 3044), young adults (MOR 1125), and other adults (AMNH FARB 5027), the margin of the bony choana extends from alveoli 5 to 7, indicating a rostral position, whereas in juveniles (BMRP 2002.4.1) it extends from alveoli 6 to 9, indicating a caudal position (Carr, 2020). In dorsal and ventral views, the contours of the process in the type, subadults (MOR 3044), young adults (MOR 1125), and other adults (AMNH FARB 5027) continuously widens rostrally without abrupt widening, whereas in juveniles (BMRP 2002.4.1) and one young adult (LACM 150,167) it widens abruptly where the palatine thins out rostrally (Carr, 2020).

3.27. Intermaxillary process

The intermaxillary process, as used here, refers to the rostral end of the palatal process that bears the joint surface for the complementary maxilla. In CM 9380 (Figure 7), subadults (MOR 3044), young adults (MOR 1125), and other adults (MOR 555), the joint surface for the maxilla extends caudally to the level of the promaxillary fenestra; in contrast, the joint surface in juveniles (BMRP 2002.4.1) stops rostral to the level of the fenestra (Carr, 2020). In ventral and dorsal views in the type (Figure 6C), subadults (MOR 3044), young adults (MOR 1125), and other adults (MOR 555) the intermaxillary process is wide, where it abruptly widens the rostral end of the palatal process (Carr, 2020). In contrast, the process is narrow in juveniles (Carr, 2020).

In medial view in CM 9380 (Figure 7), subadults (MOR 3044), young adults (MOR 1125), and other adults (AMNH FARB 5027) the process is situated a great distance above the ventral edge of the medial alveolar process, which is enhanced by the dorsomedial orientation of the process (Carr, 2020). In contrast, the process in juveniles (BMRP 2002.4.1) extends medially, and is positioned a short distance above the medial alveolar margin (Carr, 2020).

In the type (Figure 7), subadults (MOR 3044), young adults (LACM 150,167), and most adults (MOR 555), the intermaxillary process and the rest of the palatal process are continuous with each other; in contrast, a groove extends between the structures in juveniles (BMRP 2002.4.1), subadults (TMM 41,436-1), and a young adult (MOR 1125) (Carr, 2020). In the type, young adults (UWBM 99,000) and adults (AMNH FARB 5027), there are less than two teeth ahead of the intermaxillary process (Carr, 2020). In contrast, there are three ahead of the process in juveniles (BMRP 2002.4.1) (Carr, 2020).

3.28. Joint surface for the palatine

In medial view, the joint surface for the palatine in CM 9380 (Figure 6B), subadults (MOR 3044), young adults (MOR 1125), and other adults (MOR 555) is deep such that it exceeds the dorsoventral height of the medial alveolar process below it; in juveniles (BMRP 2002.4.1) the joint surface does not exceed the height of the process (Carr, 2020). In the type (Figure 6B), subadults (MOR 3044), young adults (UWBM 99,000), and other adults (RSM 2523.8), the joint surface is flat caudally and is grooved rostrally, whereas in juveniles (BMRP 2002.4.1) it is ridged caudally



and grooved rostrally (Carr, 2020). In some adults (MOR 980) the caudal end has a peg-in-socket form (Carr, 2020). In the type, the joint surface extends onto the ventral surface of the palatal process rostrally as a deep, coarse groove (Figure 6B).

In medial and ventral views in CM 9380 (Figure 6B), subadults (MOR 3044), young adults (MOR 1125), and other adults (MOR 980) the joint surface has a ridge and notch at its midlength, whereas in juveniles (BMRP 2002.4.1) this condition is absent (Carr, 2020). In the type and other adults (MOR 980) the ridge is long and the notch is deep, whereas in one young adult (MOR 1125) the ridge is short and the notch is shallow (Carr, 2020).

In dorsal view, the joint surface in the type, subadults (MOR 3044), young adults (LACM 150,167), and other adults (MOR 980) faces medially and is out of view, whereas in juveniles (BMRP 2002.4.1) its rostral half is visible as a deep groove (Carr, 2020).

3.29. Medial alveolar process

In medial view, the medial alveolar process in CM 9380 (Figures 5, 7), young adults (MOR 1125), and other adults (AMNH FARB 5027) is penetrated by large neurovascular foramina, whereas in juveniles (BMRP 2002.4.1) and some subadults (MOR 3044) they are small (Carr, 2020). The caudal end of the alveolar process, below the palatine, in the type (Figure 6B), subadults (MOR 3044), young adults (MOR 1125), and adults (MOR 980) is rugose in texture, whereas it is lightly coarse in juveniles (BMRP 2002.4.1) and some young adults (UWBM 99,000) and adults (UWGM 181) (Carr, 2020).

In medial view in CM 9380 (Figure 5), subadults (MOR 3044), young adults (MOR 1125), and other adults (MOR 980) the interdental pits do not occur caudal to alveolus 11 or less (between alveoli 9 and 10 in the type), whereas in juveniles (BMRP 2002.4.1) they reach alveolus 12 (Carr, 2020). In the type (Figure 7), subadults (TMM 41,436-1), young adults (MOR 1125), and other adults (AMNH FARB 5027) the rostral interdental pits are deeply concave, whereas they are shallow in juveniles (BMRP 2002.4.1) (Carr, 2020). In the type, the first three pits are the deepest.

3.30. Interdental plates

The apices of the interdental plates in CM 9380 (Figure 5), subadults (MOR 1125), and other adults (AMNH FARB 5027) are not close to the ventral margin of the bone, whereas in juveniles (RSM 2347.1), subadults (MOR 3044), and in one adult (MOR 008) they are close to the ventral margin (Carr, 2020). In ventral view, the rostral and caudal halves of the interdental plates of the type, subadults (MOR 3044), young adults (MOR 1125), and other adults (MOR 980) extend medially, whereas in juveniles (RSM 2347.1) they are parallel with the lateral alveolar process (Carr, 2020). The interdental septa in CM 9380 are oblique in orientation, as in young adults (MOR 1125) and other adults (AMNH FARB 5027), whereas in juveniles the septa are either normal to the lateral alveolar process (RSM 2347.1) or subtly oblique (BMRP 2002.4.1) (Carr, 2020).

In medial view, CM 9380 is similar to juveniles (BMRP 2002.4.1), subadults (MOR 3044), young adults (MOR 1125), and other adults (AMNH FARB 5027) in lacking distinct circular gaps between the bases of the interdental plates (Figure 5); in some young adults (LACM 150,167) and some adults (MOR 980) the gaps are present (Carr, 2020).

3.31. Lesions

In lateral view, there appears to be a healed notch in the alveolar margin at the caudal end of the fourth alveolus (Figure 1). A linear scour crosses the antorbital fossa (caudomedial to rostrolateral) between the jugal ramus and the lateral interfenestral strut (Figure 3A). A linear scar extends rostrolaterally from the caudal margin of the lateral interfenestral strut (Figure 3A). A lesion above the interfenestral strut within the antorbital fossa produces an irregular surface that resembles the subcutaneous surface (Figure 3A). The fossa and subcutaneous surface grade into each other ahead of the lesion and the fossa is sharply inset caudal to the lesion.

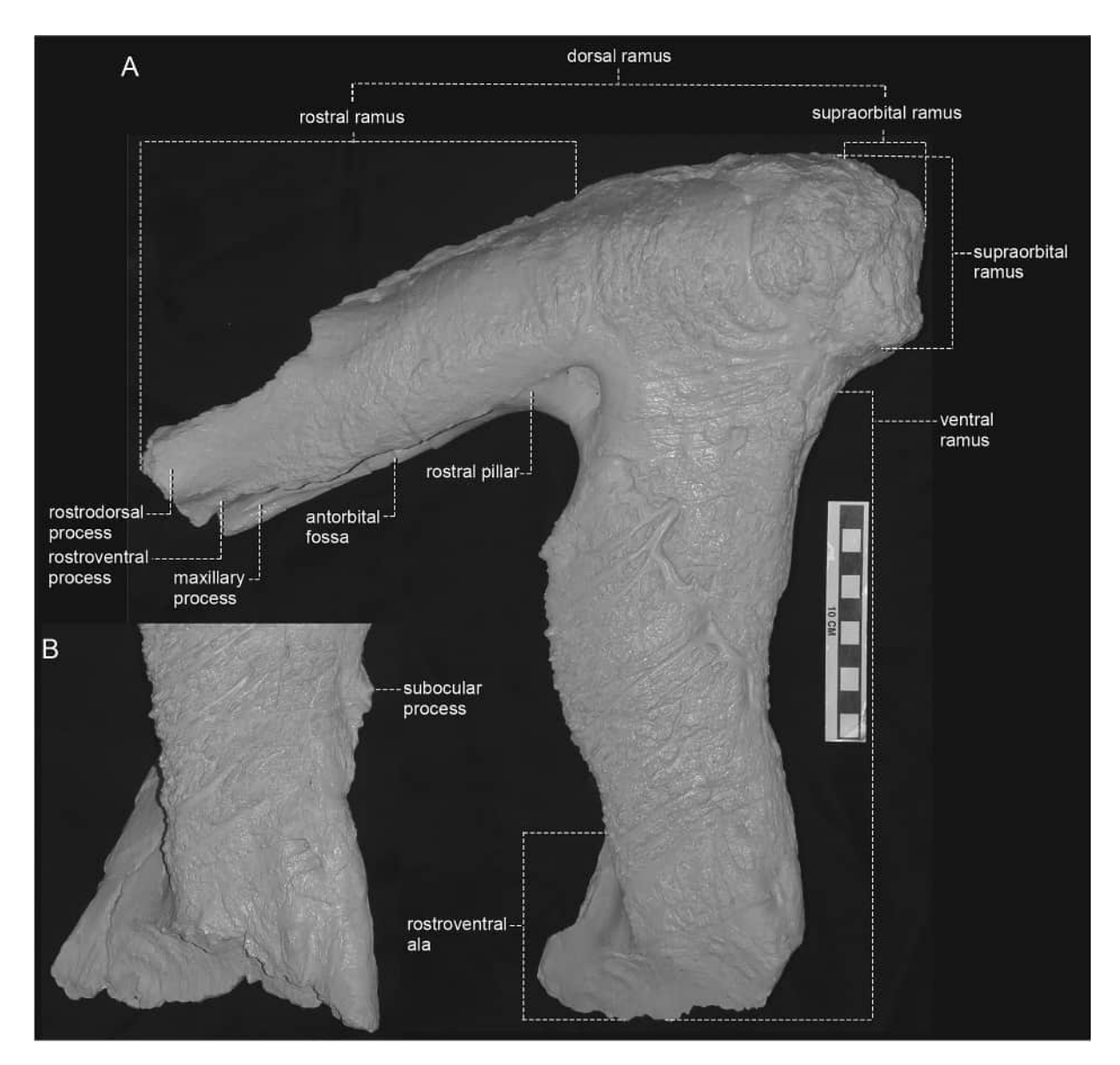


Figure 8. The left lacrimal of CM 9380 in (A) lateral view, scale bar equals 10 cm; (B) the right lacrimal in lateral view and reversed for ease of comparison. Images are not to scale.

3.32. Scavenging marks (?)

These marks are linear gouges that do not show evidence of healing; the tentative causal identification here does not necessarily exclude the possibility that these marks were damage that occurred during collection or preparation of the fossil. There are two parallel grooves rostral and rostroventral to the antorbital fossa (Figure 4A), one is short (26 mm) and the other is long (121 mm). A deep gouge is seen above the sixth alveolus (Figure 1).

4. Lacrimal

4.1. General description

Both lacrimals of CM 9380 are preserved; measurements of the bones are given in Table 2. In lateral view the lacrimal of CM 9380 (Figures 8, 9), subadults (RSM 2990.1), young adults (MOR 1125), and other adults (AMNH FARB 5027) is 7-shaped, where both the dorsal and ventral ramus extend rostroventrally, producing an acute angle between them (Carr, 2020). In contrast, in juveniles (FMNH PR2411) the bone is T-shaped where the rami form a right angle relative to each other (Carr, 2020).

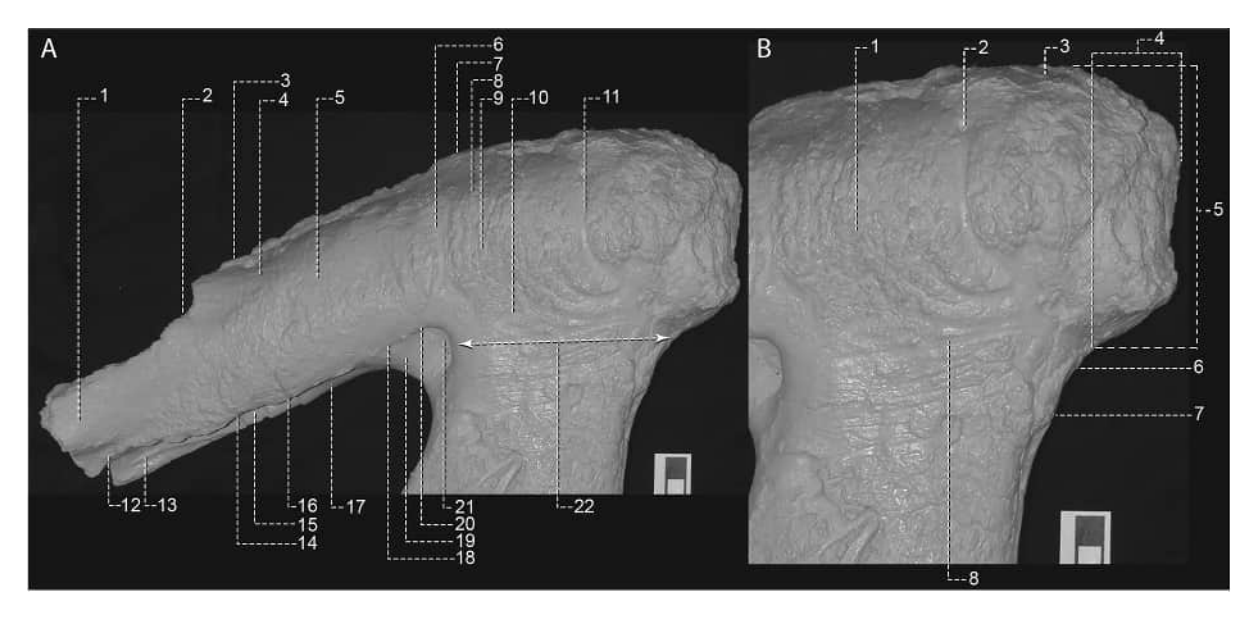


Figure 9. Detail of (A) the dorsal ramus of the left lacrimal of CM 9380 in lateral view; the numbers correspond to the features: 1, rostrodorsal process is dorsoventrally deep; 2, rostrodorsal margin is notched; 3, rostral ramus extends rostroventrally; 4, subcutaneous surface is coarse; 5, subcutaneous surface of the rostral ramus is more than twice as deep as the antorbital fossa; 6, dorsal ramus is several times deeper than the lacrimal pneumatic recess; 7, cornual process is obliterated by inflation; 8, dorsum extends dorsomedially; 9, discrete patch caudodorsal to recess; 10, region surrounding the lacrimal pneumatic recess is convex; 11, deep neurovascular sulci; 12, rostroventral process is shorter than the rostrodorsal process; 13, maxillary process is a sliver; 14, subcutaneous surface arcs dorsally in region of distal recess; 15, distal accessory recess faces ventrally, is minimally exposed laterally, and closely approaches the maxilla; 16, dorsolateral ala is reduced to a low ridge; 17, antorbital fossa is inflated and the septum between the accessory fossa and the lacrimal pneumatic recess is long; 18, subcutaneous surface and the antorbital fossa grade into each other ahead of the recess; 19, the ridge below the recess is inflated, extends rostrodorsally, and is imperforate; 20, recess extends a short distance ahead of the ventral ramus; 21, recess is less than half the length of the region behind it; 22, region caudal to the recess is long, deep, and inflated. (B) detail of the supraorbital ramus of the left lacrimal of CM 9380 in lateral view; the numbers correspond to the features: 1, caudolateral shelf is obliterated by inflation; 2, foramen that receives the sulcus that originates from the caudal surface of the bone; 3, dorsum extends into view above the supraorbital ramus; 4, supraorbital ramus is rostrocaudally short; 5, supraorbital ramus is dorsoventrally tall; 6, supraorbital ramus and ventral ramus grade into each other; 7, suborbital ligament scar is subtle, coarse, and laterally bulbous; 8, sulcus that extends from the caudal surface to the lacrimal pneumatic recess. Scale bar equals 10 cm.

4.2. Subcutaneous surface

In dorsal and lateral views, the subcutaneous surface of the bone in CM 9380 (Figures 8-10), young adults (MOR 1125), and other adults (AMNH FARB 5027) is coarse in texture, whereas in juveniles (FMNH PR2411), subadults (RSM 2990.1), and one young adult (TMP 1981.006.0001) it is lightly textured (Carr, 2020).

In CM 9380 (Figure 9B), young adults (MOR 1125), and other adults (AMNH FARB 5027) a discrete, coarse patch is present caudodorsal to the pneumatic recess, whereas in juveniles a low coarse ridge extends across this surface and the patch is absent from subadults (RSM 2990.1) and one young adult (TMP 1981.006.0001). In the type (Figures 8–10), young adults (MOR 1125) and other adults (FMNH PR2081) the dorsolateral surface of the dorsal ramus is rugose, bears spicule-like papillae, and is dissected by deep neurovascular sulci, whereas it is rough in juveniles (RMNH PR2411) and it is coarse in young adults (MOR 1125) and some adults (AMNH FARB 5027) (Carr, 2020).

4.3. Dorsal ramus

In lateral view, the dorsal ramus in CM 9380 (Figures 8, 9), subadults (RSM 2990.1), young adults (MOR 1125), and other adults (AMNH FARB 5027) is fully inflated, such that the height of the bone exceeds that of the lacrimal pneumatic recess, which is a relatively larger opening in juveniles (Carr, 2020). In the type

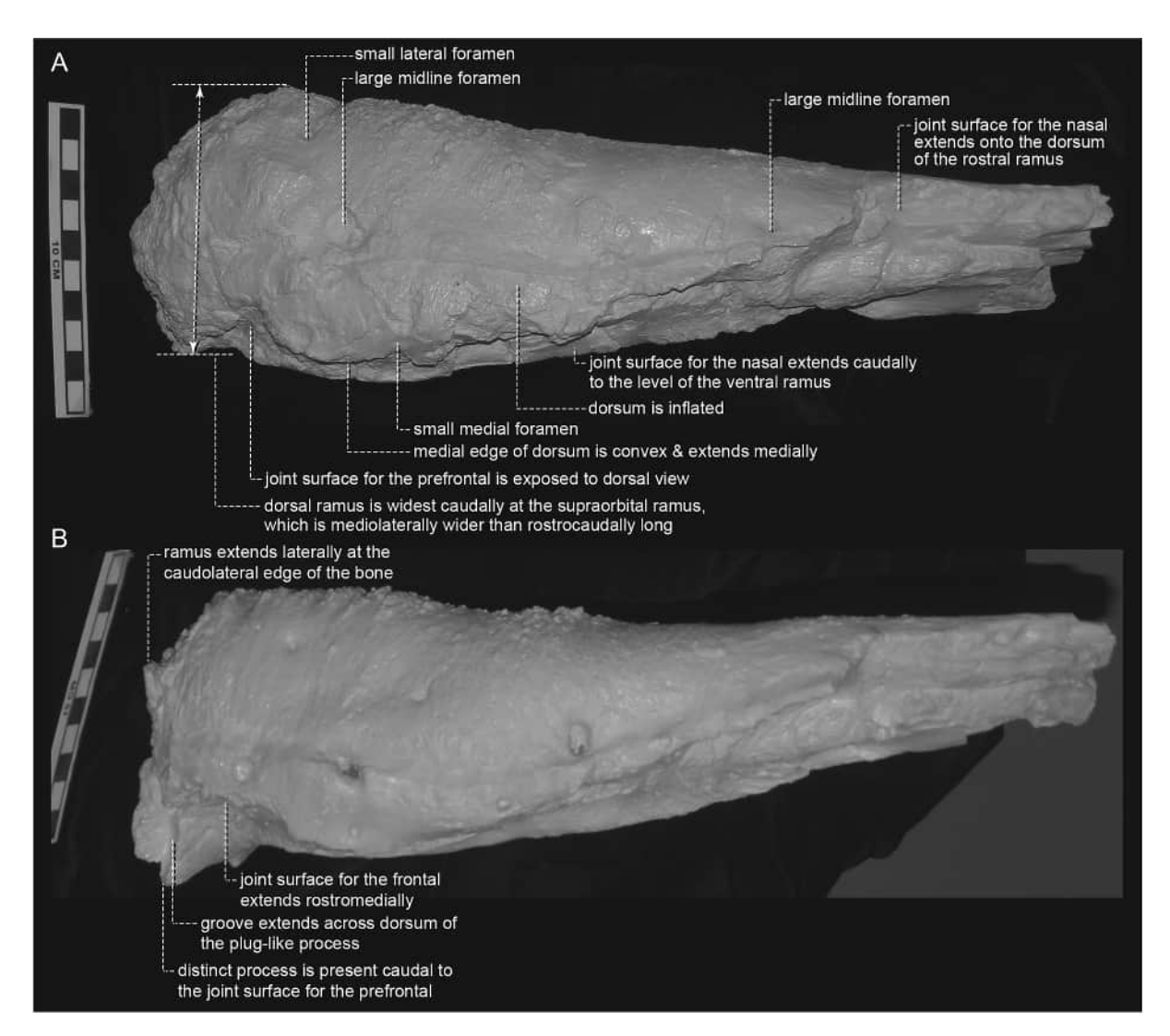


Figure 10. The left lacrimal of CM 9380 in (A) dorsal view; the right lacrimal in (B) dorsal view and reversed for ease of comparison. Scale bars equal 10 cm.

(Figures 9(A), 10, 11(A)), young adults (LACM 150,167) and other adults (LACM 23,844) the dorsum is inflated and extends dorsomedially, whereas in juveniles (FMNH PR2411) it extends ventromedially; in subadults (RSM 2990.1), young adults (MOR 1125), and some adults (AMNH FARB 5027) it is inflated and extends ventromedially (Carr, 2020).

In lateral view, the region dorsal and rostrodorsal to the pneumatic recess is convex in CM 9380 (Figure 9A), subadults (LACM 24,845), young adults (MOR 1125), and other adults (AMNH FARB 5027), whereas this region is concave in juveniles (FMNH PR2411) (Carr, 2020). The same pattern is seen caudal to the pneumatic recess, except that region is concave in one subadult (RSM 2990.1). In the type (Figure 9), young adults (MOR 1125), and other adults (AMNH FARB 5027) the region caudal to the recess is long, deep, and inflated, whereas in juveniles it is short and shallow; and intermediate condition is seen in subadults (RSM 2990.1) (Carr, 2020). Below the level of the supraorbital ramus, the recess is less than half the length of the region caudal to it in the type (Figure 9), subadults (RSM 2990.1), young adults (MOR 1125), and other adults (AMNH FARB 5027), whereas the recess is greater than half the length in juveniles (FMNH PR2411) (Carr, 2020).

In rostral view, the subcutaneous surface in the type (Figure 11A) and all other growth stages is marginally taller than the joint surface for the nasal, except it is distinctly taller in one juvenile (BMRP 2002.4.1) and one young adult (MOR 1125) (Carr, 2020). In dorsal view, the ramus in the type (Figure 10), young adults (MOR 1125), and other adults (MOR 980) the widest region is across the caudal end of the

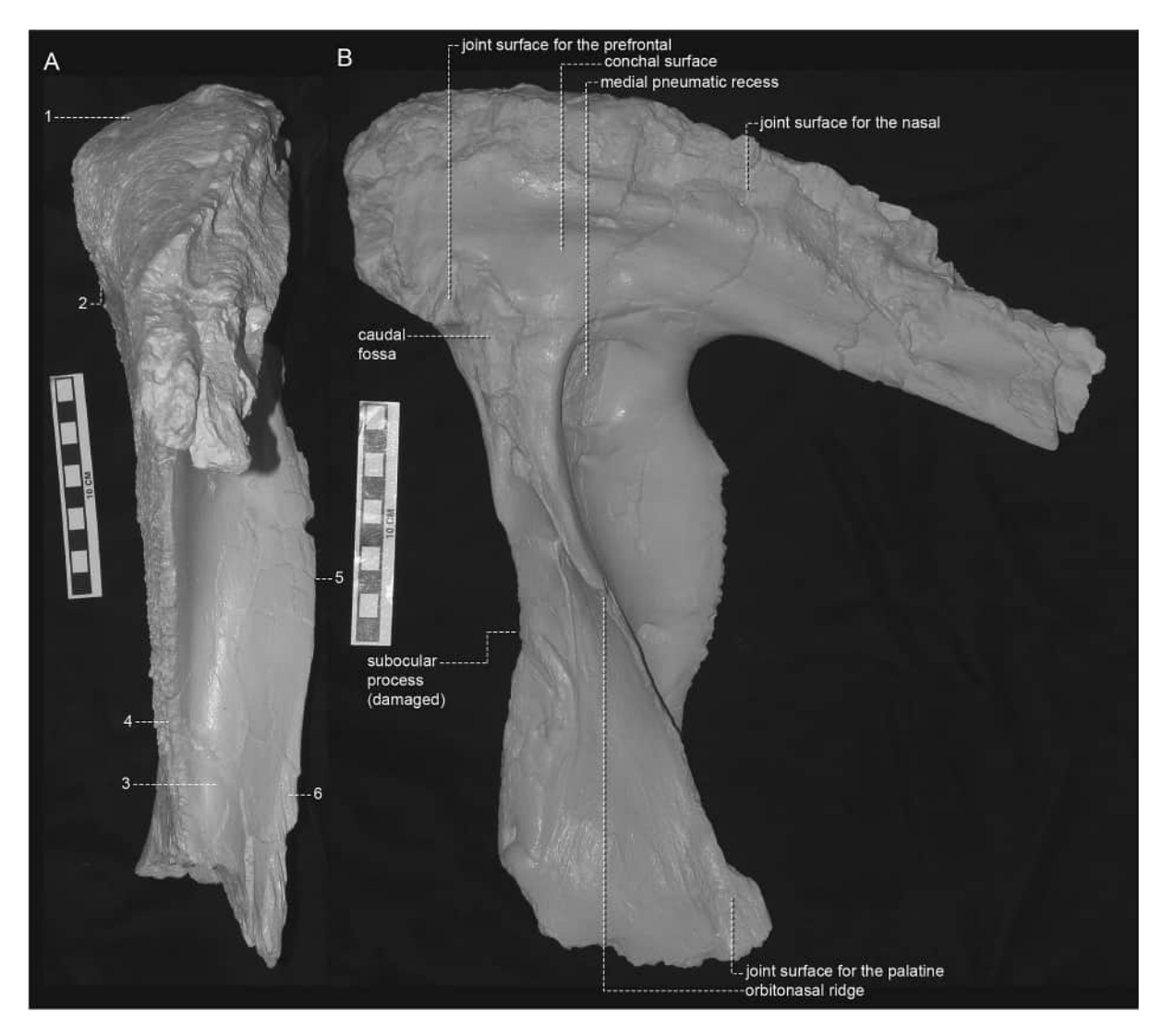


Figure 11. The right lacrimal of CM 9380 in (A) rostral view; numbers correspond to the features: 1, subcutaneous surface is marginally taller than the joint surface for the nasal; 2, region of the cornual process extends laterally beyond the ventral ramus; 3, the leading edge of the ventral ramus and the rostroventral ala are widely separated; 4, width of the ventral end of the ventral ramus is wide next to the junction with the rostroventral ala; 5, the orbitonasal ridge is wide proximodistally; 6, the joint surface for the palatine extends up the ventral two-thirds or more of the rostroventral ala. (B) left lacrimal in medial view with osteological landmarks labelled. Scale bars equal 10 cm.

ramus, whereas in small juveniles (FMNH PR2411) it is across the caudal end of the ventral ramus, and in large juveniles (BMRP 2002.4.1) and one young adult (LACM 150,167) at the rostral end of the ventral ramus (Carr, 2020). In some young adults (UWBM 99,000) and adults (RSM 2523.8) the widest point is across the midlength of the ventral ramus (Carr, 2020). In dorsal view the medial margin of the ramus in the type (Figure 10), subadults (RSM 2990.1), young adults (MOR 1125), and other adults (AMNH FARB 5027) is extended medially and convex, whereas in juveniles (FMNH PR2411) it is subtly convex and nearly straight (Carr, 2020).

In dorsal view in CM 9380 (Figure 10), the dorsum extends medially caudal to the rostrodorsal process, and it is pierced by three rostrocaudally-extending rows of foramina; the medial row of three small foramina pierce the medial edge of the bone. Lateral to the medial row, a row of three large foramina pierces the bone, possibly representing the row that pierces the dorsolateral surface of the nasal (Figure 10). The lateral-most row consists of small foramina that are scattered randomly over the dorsum (Figure 10).



4.4. Conchal surface (= medial fossa)

In medial view, the conchal surface in CM 9380 (Figures 11(B), 12), subadults (RSM 2990.1), young adults (MOR 1125), and other adults (MOR 980) is not bounded rostrally by a ridge, whereas in juveniles (FMN PR2411) a ridge is present (Carr, 2020). However, a prominent ridge bounds the conchal surface dorsally in the type (Figures 11(A), 12), a subadult (RSM 2990.1), and other adults (MOR 980), whereas a ridge bounds the surface only dorsally by a ridge in juveniles (FMNH PR2411) and one young adult (MOR 1125) (Carr, 2020). In the type (Figures 11(B), 12), subadults (RSM 2990.1), young adults (MOR 1125), and other adults (MOR 980), the caudal end of the ridge is inflated and dorsoventrally deep, whereas it is not inflated and shallow in juveniles (FMNH PR2411) (Carr, 2020).

The conchal surface in CM 9380 (Figures 11(B), 12), subadults (RSM 2990.1), young adults (MOR 1125), and other adults (MOR 980) is mediolaterally shallow, whereas it is deep and basin-like in juveniles (FMNH PR2411) and one adult (MOR 2822) (Carr, 2020). The conchal surface in the type (Figures 11(B), 12), young adults (MOR 1125), and other adults (MOR 555) is penetrated by a neurovascular foramen that is located close to the dorsal margin of the surface, whereas it is at the midheight of the surface in juveniles (BMRP 2002.4.1) (Carr, 2020). In the type, young adults (MOR 1125), and other adults (MOR 980) the surface above the medial pneumatic recess is convex, whereas in juveniles (FMNH PR2411) and subadults (RSM 2990.1) it is concave (Carr, 2020).

In CM 9380 (Figures 11(B), 12), subadults (RSM 2990.1), young adults (MOR 1125), and other adults (MOR 980), the caudodorsal surface of the conchal surface is convex, whereas in juveniles (FMNH PR2411) and one adult (MOR 2822) the surface is concave (Carr, 2020). In the type (Figures 11(B), 12), subadults (RSM 2990.1), and other adults (MOR 980) the caudal margin of the conchal surface extends caudally onto the base of the frontal process, whereas in juveniles (FMNH PR2411) and one young adult (MOR 1125) it is positioned rostrally, away from the process (Carr, 2020).

4.5. Cornual process

The region of the cornual process in CM 9380 (Figures 9(A), 10) is inflated, which has removed nearly all trace of the process, as is seen in subadults (LACM 23,845), young adults (MOR 1125), and other adults (AMNH FARB 5027), whereas the process is present in juveniles (BMRP 2002.4.1); it is retained as a low ridge in subadults (RSM 2990.1), young adults (UWBM 99,000) and one adult (MOR 008) (Carr, 2020). In the type a low ridge on the dorsomedial surface of the dorsal ramus might represent the process (Figure 10); on the left side its highest point is above the ventral ramus (Figures 8(A), 9(A)), whereas on the right it is rostral to the ramus.

In rostral view, the region of the cornual process extends laterally beyond the level of the ventral ramus in CM 9380 (Figure 11(A)), subadults (RSM 2990.1), young adults (MOR 1125), and other adults (MOR 980), whereas in juveniles (FMNH PR2411) it is level with the ramus (Carr, 2020).

4.6. Rostral ramus

In lateral view, the rostral ramus in CM 9380 (Figures 8(A), 9(A)) is inflated and dorsoventrally several times deeper than the pneumatic recess, as is seen in subadults (RSM 2990.1), young adults (MOR 1125), and other adults (AMNH FARB 5027) (Carr, 2020). In contrast, this region is shallow in juveniles (FMNH PR2411) (Carr, 2020). In tyrannosaurids, the rostral ramus is divided into a dorsal subcutaneous region and a ventral antorbital fossa region; in CM 9380 (Figures 8(A), 9(A)) the ramus is inflated to the extreme where both regions are inflated (Carr, 2020). In juveniles (FMNH PR2411) neither region is inflated; in subadult specimens (RSM 2990.1) the subcutaneous surface is inflated whereas the fossa is not inflated (Carr, 2020).

In lateral view, the rostrodorsal margin in CM 9380 (Figures 8(A), 9(A)), young adults (MOR 1125), and other adults (AMNH FARB 5027) extends abruptly rostroventrally above the distal recess, whereas in juveniles (BMRP 2002.41) it is convex; in subadults (RSM 2990.1) and young adults (LACM 150,167) it extends at a low rostroventral angle (Carr, 2020). The subcutaneous surface in the type (Figures 8(A), 9(A)), subadults (RSM 2990.1), young adults (MOR 1125), and other adults (AMNH FARB 5027) is twice

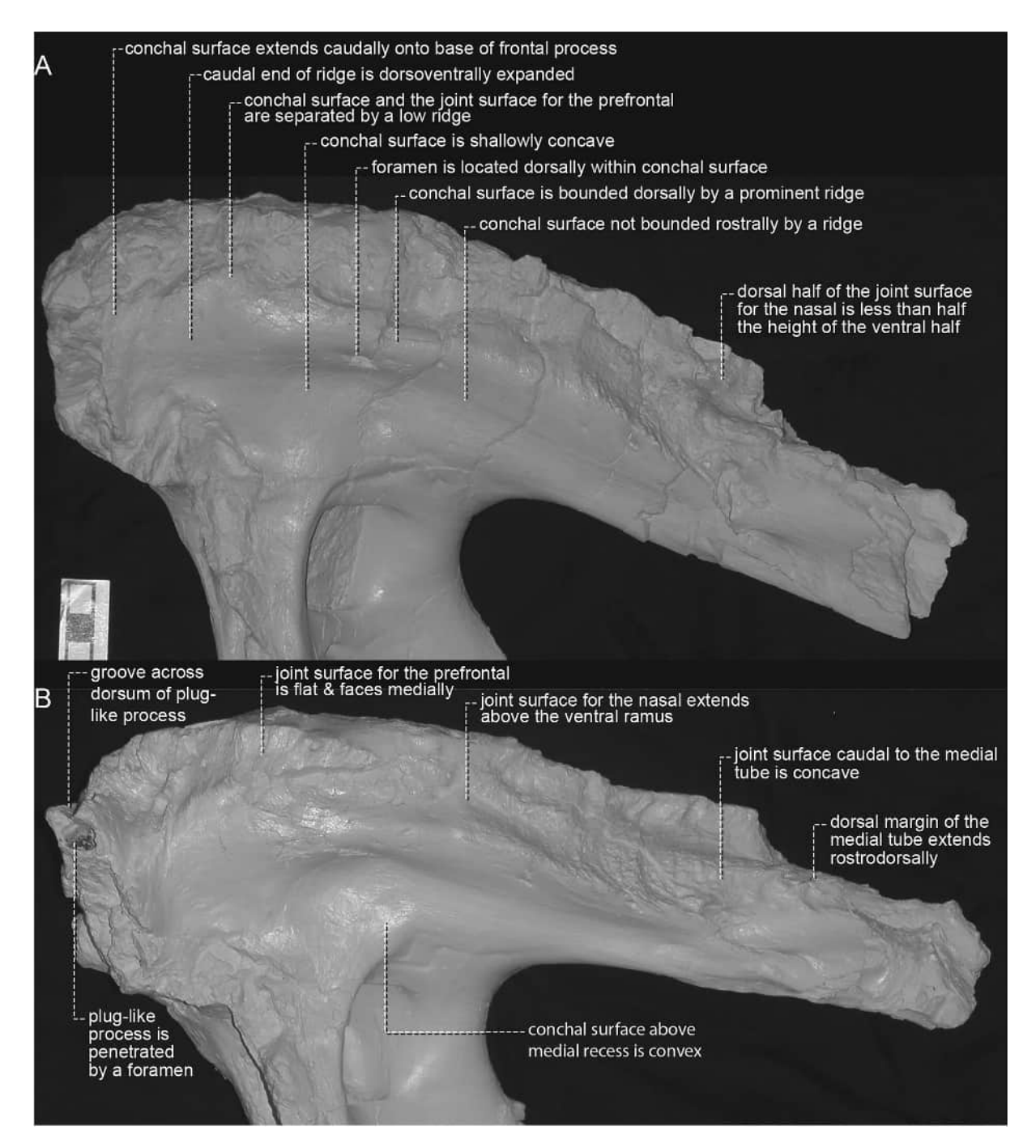


Figure 12. Detail of the dorsal ramus of the left lacrimal of CM 9380 in medial view, scale bar equals 10 cm.

as deep or more as the antorbital fossa below it, whereas in juveniles (BMRP 2020.4.1) it is less than half as deep as the fossa below it (Carr, 2020). The junction between the subcutaneous surface and the antorbital fossa in the type (Figures 8(A), 9(A)), subadults (RSM 2990.1), young adults (MOR 1125), and other adults (AMNH FARB 5027) is continuous between the surfaces ahead of the lacrimal pneumatic recess, whereas in juveniles (FMNH PR2411) the fossa undercuts the edge of the subcutaneous surface (Carr, 2020).

In medial view, the dorsal margin of the groove that extends rostrally from the medial tube in the type (Figure 12B), subadults (RSM 2990.1), young adults (MOR 1125), and other adults (MOR 980) extends

rostrodorsally, deepening the groove as it extends rostrally, whereas in juveniles (BMRP 2020.4.1) it is level with the dorsal margin of the tube and so the groove does not deepen (Carr, 2020).

4.7. Rostral processes

In lateral view, the rostrodorsal process in CM 9380 (Figures 8(A), 9(A)), subadults (RSM 2990.1), young adults (MOR 1125), and other adults (AMNH FARB 5027) is dorsoventrally deep, whereas it is shallow in juveniles (BMRP 2002.4.1) (Carr, 2020). The rostroventral process in the type (Figures 8(A), 9(A)), young adults (MOR 1125), and some other adults (MOR 555) is shorter than the rostrodorsal process, whereas the process is absent in juveniles; the process in some subadults (RSM 2990.1), young adults (TMP 1981.006.0001), and adults (MOR 980) is longer than the rostrodorsal process, whereas in some young adults (UWBM 99,000) and adults (AMNH FARB 5027) they are the same length (Carr, 2020). The maxillary process in the type (Figures 8 (A), 9(A)), subadults (RSM 2990.1), young adults (MOR 1125), and other adults (AMNH FARB 5027) is a sliver, whereas in juveniles (BMRP 2002.4.1) it is dorsoventrally tall (Carr, 2020). It is intermediate in depth in some young adults (LACM 150,167) (Carr, 2020).

4.8. Lacrimal pneumatic recess

In lateral view, the lacrimal pneumatic recess of CM 9380 (Figures 8(A), 9) is a small opening that extends a short distance ahead of the rostral margin of the ventral ramus and it is dorsoventrally shallow, which is seen in small juveniles (FMNH PR2411), young adults (UWBM 99,000), and other adults (AMNH FARB 5027) (Carr, 2020). In large juveniles (BMRP 2002.4.1), subadults (RSM 2990.1) and in one young adult (LACM 150,167) the opening is large, where it is tall and extends a great distance ahead of the ventral ramus (Carr, 2020).

4.9. Antorbital fossa

In lateral view, the antorbital fossa of CM 9380 (Figures 8(A), 9(A)), subadults (LACM 23,845), young adults (MOR 1125), and other adults (AMNH FARB 5027) is penetrated by one accessory pneumatic foramen. In contrast, the fossa is penetrated by two foramina in juveniles (BMRP 2002.4.1) and a subadult (RSM 2990.1) (Carr, 2020). The ridge below the recess in the type (Figures 8(A), 9(A)), subadults (RSM 29,901), young adults (MOR 1125), and other adults (MOR 980) is not penetrated by a foramen, whereas a foramen is seen in juveniles (FMNH PR2411) (Carr, 2020). The region below the recess in the type (Figures 8(A), 9(A)), young adults (MOR 1125), and other adults (AMNH FARB 5027) is inflated such that it extends rostrodorsally by merging with the septum rostral to the recess, whereas in juveniles (FMNH PR2411) the region is narrow and small and does not reach the septum; an intermediate condition is seen in subadults (RSM 2990.1) (Carr, 2020). In the type (Figures 8(A), 9(A)), a low ridge from the subcutaneous surface (= dorsolateral lamina of Carr, 1999) extends along the dorsal margin of the fossa.

The septum rostral to the recess is rostrocaudally long the type (Figures 8(A), 9(A)), young adults (MOR 1125), and other adults (AMNH FARB 5027), whereas it is short in juveniles (FMNH PR2411) and subadults (RSM 2990.1) (Carr, 2020). In the type (Figures 8(A), 9(A)), young adults (MOR 1125), and other adults (AMNH FARB 5027) the septum ahead of the recess is inflated, whereas in juveniles (FMNH PR2411) it is not inflated; an intermediate condition is seen in subadults (RSM 2990.1) and some young adults (LACM 150,167) (Carr, 2020). The septum in the type (Figures 8(A), 9(A)), young adults (MOR 1125), and other adults (AMNH FARB 5027) is penetrated by a foramen, whereas a foramen is absent from juveniles (BMRP 2002.4.1) and subadults (RSM 2990.1) (Carr, 2020).

In lateral view, the distal recess in the type (Figures 8(A), 9(A)), young adults (TMP 1981.006.0001), and other adults (AMNH FARB 5027) is oriented ventrally, and it is minimally exposed laterally, whereas in juveniles (BMRP 2002.4.1) it faces laterally; an intermediate condition is seen in subadults (RSM 2990.1) (Carr, 2020). The proximal pneumatic recess, between the lacrimal recess and the distal recess) in the type (Figures 8(A), 9(A)), subadults (RSM 2990.1), young adults (MOR 1125), and other adults (AMNH FARB 5027) has the form of a shallow fossa, whereas a deep fossa is seen in juveniles (BMRP 2002.4.1) (Carr, 2020). The septum between the proximal and distal recesses in the type (Figures 8(A), 9(A)), subadults (RSM 2990.1),



young adults (MOR 1125), and other adults (AMNH FARB 5027) is long, whereas in juveniles (BMRP 2002.4.1) and some young adults (LACM 150,167) it is short (Carr, 2020).

In lateral view, the accessory pneumatic recesses in CM 9380 (Figures 8(A), 9(A)), subadults (RSM 2990.1), young adults (MOR 1125), and other adults (AMNH FARB 5027) closely approach (if not reach) the maxilla, whereas in juveniles (BMRP 2020.4.1) they do not closely approach the maxilla (Carr, 2020). The distal accessory recess in the type (Figures 8(A), 9(A)), subadults (LACM 23,845), young adults (MOR 1125), and other adults (AMNH FARB 5027) is a large and discrete foramen, whereas in juveniles (BMRP 2002.4.1) it is a deep fossa (Carr, 2020). In subadults (RSM 2990.1) and one young adult (UWBM 99,000) it is a shallow fossa, and in some adults (MOR 980) it is a small neurovascular foramen (Carr, 2020).

The ventral edge of the subcutaneous surface ahead of the lacrimal pneumatic recess in the type (Figures 8(A), 9(A)), juveniles (FMNH PR2411), subadults (RSM 2990.01), young adults (MOR 1125), and some adults (AMNH FARB 5027) follows a dorsal arc, whereas in some young adults (UWBM 99,000) and adults (MOR 980) it extends rostroventrally, horizontally, or grades into the fossa (RSM 2523.8) without a clear orientation (Carr, 2020).

4.10. Joint surface for the nasal

In dorsal view in CM 9380 (Figure 10), subadults (RSM 2990.1), young adults (MOR 1125), and other adults (AMNH FARB 5027) the distal extent of the joint surface for the nasal is positioned on the dorsal surface of the rostral ramus, whereas in juveniles (BMRP 2002.4.1) and subadults (LACM 23,845) it is limited to the medial surface of the ramus (Carr, 2020). The joint surface in the type (Figures 11(B), 12), and other adults (MOR 980) extends medial to the level of the ventral ramus, whereas in juveniles (FMNH PR2411), subadults (RSM 2990.1) young adults (MOR 1125), and one adult (RSM 2523.8) it stops rostral to the ramus (Carr, 2020).

In medial view, the dorsal half of the joint surface in the type (Figures 11(B), 12), subadult (RSM 2990.1), young adults (MOR 1125), and other adults (MOR 980) is dorsoventrally shallower than the ventral half, whereas in juveniles (BMRP 2002.4.1) it is almost as deep as the ventral half (Carr, 2020). The joint surface caudal to the medial tube in the type (Figure 12B), subadults (RSM 2990.1), young adults (MOR 1125), and other adults (MOR 980) is concave, whereas in juveniles (FMNH PR2411) and one adult (MOR 555) it is convex (Carr, 2020).

4.11. Supraorbital ramus

In lateral, dorsal, and medial views, the supraorbital ramus of the type (Figures 8–12) is rostrocaudally short and dorsoventrally tall, the condition seen in subadults (RSM 2990.1), young adults (MOR 1125) and other adults (AMNH FARB 5027) (Carr, 2020). In contrast, the process is long in juveniles (FMNH PR2411) (Carr, 2020). The type (Figures 8(A), 9(A)) and LACM 23,844 can be differentiated from other adults in the extreme dorsalward inflation of the ramus that exceeds all others, where the dorsum extends into view above the rugose lateral surface of the supraorbital ramus (Carr, 2020). In the type (Figures 8(A), 9(A)) the joint surface for the epilacrimal is distinct and it excavates the caudodorsolateral surface of the ramus.

In lateral view, the caudolateral shelf in CM 9380 (Figures 8(A), 9(A)), subadults (RSM 2990.1), young adults (MOR 1125), and other adults (AMNH FARB 5027) is eliminated by inflation, whereas in juveniles (FMNH PR2411) it is present (Carr, 2020). In the type (Figures 8(A), 9(A)), young adults (MOR 1125), and other adults (AMNH FARB 5027) the angle between the supraorbital ramus and the ventral ramus is continuous and indistinct, whereas in juveniles (FMNH PR2411), subadults (RSM 2990.1), and some adults (FMNH PR2081) it is distinct (Carr, 2020).

In dorsal view, the ramus in the type (Figure 10B), young adults (MOR 1125), and other adults (MOR 980) extends laterally at the caudolateral edge of the bone, whereas in juveniles (FMNH PR2411) and subadults (RSM 2990.1) it curves caudomedially (Carr, 2020). The ramus in the type (Figure 10), subadults (RSM 2990.1), young adults (MOR 1125), and other adults (AMNH FARB 5027) is wider than long, whereas in small juveniles (FMNH PR2411) it is longer than wide and in large juveniles (BMRP 2002.4.1) it is as wide as long (Carr, 2020).

In dorsal view, the joint surface for the frontal in the type (Figure 10B), young adults (MOR 1125), and other adults (MOR 555) extends rostromedially, whereas in small juveniles (FMNH PR2411) it extends rostrocaudally and in large juveniles (BMRP 2002.4.1) it extends rostrolaterally (Carr, 2020). In the type (Figure 10B),

subadults (RSM 2990.1), young adults (MOR 1125), and other adults the medially extending process behind the joint surface for the prefrontal is distinct, whereas it is indistinct in juveniles (FMNH PR2411).

In caudal view in CM 9380, young adults (MOR 1125), and other adults (MOR 9890) the joint surface for the postorbital is above or lateral to that for the fontal (Carr, 2020). This joint surface is confluent with the laterally positioned joint surface for the epilacrimal osteoderm that caps the caudal surface of the ramus (Carr, 2020). In contrast, the joint surface is absent from juveniles (FMNH PR2411) since the lacrimal and postorbital are separated by a gap (Carr, 2020).

In caudal view in the type, young adults (LACM 150,167), and other adults (RSM 2523.8) the lateral extension of the caudal joint surface is positioned below the midheight of the ramus, whereas in juveniles (FMNH PR2411) there is no joint surface or extension present (Carr, 2020). In contrast, in young adults (MOR 1125) and some adults (MOR 555) the extension is at the midheight of the ramus. The ramus in the type and other adults (MOR 555) the ramus is wider than tall, whereas in juveniles (FMNH PR2411) and one young adult (MOR 1125) it is as wide as tall (Carr, 2020). In subadults (RSM 2990.1) it is deeper than wide (Carr, 2020).

4.12. Joint surface for the frontal

In medial view, the joint surface for the frontal is a conical plug-like structure in the type (Figure 12B), young adults (MOR 1125), and other adults (MOR 980); in contrast, this process is flat in juveniles (Carr, 2020). In the type (Figure 12B), young adults (MOR 1125), and other adults (MOR 555) a foramen penetrates the frontal process, whereas the process is imperforate in juveniles (FMNH PR2411) (Carr, 2020).

In dorsal and medial views, the dorsal surface of the peg that inserts into the frontal in CM 9380 (Figures 10(B), 12(B)), subadults (RSM 2990.1), young adults (MOR 1125), and other adults (MOR 555) is excavated by a deep mediolaterally-extending groove; the groove is absent from juveniles (FMNH PR2411) (Carr, 2020).

4.13. Ventral ramus

In lateral and medial views in CM 9380 (Figures 8(A), 11(B), 13), one juvenile (BMRP 2002.4.1), young adults (MOR 1125), and other adults (AMNH FARB 5027) spicules of bone extend rostrally beyond the rostrolateral edge of the ramus, forming an irregular fringe that impinges on the caudal margin of the antorbital fenestra (Carr, 2020). In contrast, marginal bone is absent from juveniles (BMNH PR2411), subadults (RSM 2990.1), and one young adult (LACM 150,167) (Carr, 2020).

In rostral view in CM 9380 (Figure 11A), young adults (MOR 1125), and other adults (MOR 980) the width of the ramus below the dorsal ramus is wide, whereas it is narrow in juveniles (FMNH PR2411) and subadults (RSM 2990.1) (Carr, 2020). In CM 9380 (Figure 11A), young adults (MOR 1125), and other adults (MOR 980) the leading edge of the ventral ramus and the rostroventral ala are widely separated from each other, whereas in juveniles (FMNH PR2411), subadults (RSM 2990.1), and one young adults (UWBM 99,000) they are not widely separated or merge together (Carr, 2020).

In rostral view in the type (Figure 11A), young adults (MOR 1125), and other adults (MOR 980) the width of the ventral end next to the junction with the rostroventral ala is wide, whereas in juveniles (FMNH PR2411) it is narrow (Carr, 2020). In the type (Figures 8(A), 9(A), 13(A)), young adults (MOR 1125), and other adults (AMNH FARB 5027) the rostrodorsal margin of the ramus is inflated, wide, and columnar, whereas in juveniles (FMNH PR2411) and subadults (RSM 2990.1) it is not inflated (Carr, 2020).

In lateral view in CM 9380 (Figure 13A), young adults (MOR 1125), and other adults (MOR 980) the leading edge of the ventral ramus and rostroventral ala (above the jugal contact) merge together, whereas they are separated by a groove or a crease in juveniles (FMNH PR2411), subadults (RSM 2990.1), and some adults (AMNH FARB 5027) (Carr, 2020). In the type (Figures 8(A), 13(A)), subadults (RSM 2990.1), young adults (MOR 1125), and other adults (AMNH FARB 5027) the proximal end of the ramus is wider than the distal end, whereas in juveniles (FMNH PR2411) the reverse is seen (Carr, 2020).

In lateral view in the type (Figure 13A), young adults (MOR 1125), and other adults (AMNH FARB 5027) the rostroventral extent of the ramus extends rostrally along the jugal, whereas the extension is absent from





Figure 13. Detail of (A) the ventral ramus of the left lacrimal of CM 9380 in lateral view; numbers correspond to the features: 1, proximal end of the ramus is wider than the distal end; 2, subocular process (damaged); 3, rostral extension along the joint surface for the jugal; 4, joint surface for the palatine extends onto the rostrolateral edge of the ala; 5, ventral ramus and rostroventral ala grade into each other; 6, rostroventral margin is concave; 7, marginal bone is present; 8, subcutaneous surface is rugose; 9, caudoventrally extending sulcus is present; 10, rostrodorsal margin of the ramus is concave; 11, antorbital fossa and subcutaneous surface grade into each other; 12, ridge and notch in caudal edge of ramus. (B) detail of the ventral ramus of the left lacrimal of CM 9380 in medial view; numbers correspond to the features: 1, joint surface for the prefrontal is peg-insocket in form; 2, orbitonasal ridge is wide proximally and thins distally; 3, medial recess is not crossed by a horizontal septum; 4, sulcus above recess is deeply inset; 5, medial recess is large; 6, recess is far caudal to the rostral edge of the bone; 7, caudoventral margin of the recess is absorbed; 8, orbitonasal ridge and ventral ramus grade into each other; 9, surface below the medial recess is concave; 10, orbitonasal ridge is not backswept; 11, orbitonasal ridge extends medially; 12, joint surface for the palatine covers one-quarter of the ala or less: 13, torturous sulci present: 14, orbitonasal ridge is far ahead of the caudal edge of the ventral ramus; 15, orbitonasal ridge extends rostroventrally above midheight; 16, joint surface for the prefrontal reaches the distal foramen; 17, subcutaneous surface extends medially. Scale bar equals 10 cm.

juveniles (BMRP 2002.4.1) and one adult (LACM 23,844) (Carr, 2020). In the type (Figures 8(A), 13(A)), young adults (MOR 1125), and other adults (MOR 980) the rostrodorsal margin of the ramus is concave, whereas it is convex in juveniles (FMNH PR2411), young adults UWBM 99,000), and some adults (MOR 555) or it is straight in subadults (RSM 2990.1), young adults (LACM 150,167), and some adults (AMNH FARB 5027) (Carr, 2020).

In lateral view, the subcutaneous surface of the ramus in CM 9380 (Figure 13A) and one other adult (LACM 23,844) is rugose, whereas it is wrinkled in juveniles (FMNH PR2411) and subadults (RSM 2990.1), and it is coarse in young adults (MOR 1125) and most adults (AMNH FARB 5027) (Carr, 2020). In medial view in the type (Figure 13B), subadults (RSM 2990.1), young adults (MOR 1125), and other adults (MOR 980) the coarse subcutaneous texture extends onto the caudal surface and reaches the caudal fossa, whereas in juveniles (FMNH PR2411) it does not extend onto the caudal surface of the ramus (Carr, 2020).

In lateral view in the type (Figures 8(A), 13(A)), subadults (LACM 23,845), young adults (MOR 1125), and other adults (AMNH FARB 5027) the rostroventral margin of the ramus is concave, whereas in juveniles (FMNH PR2411) it is convex, and in subadults (RSM 2990.1) and some adults (RSM 2523.8) it is straight (Carr, 2020). In the type (Figure 13A), young adults (MOR 1125), and other adults (AMNH FARB 5027) a caudoventrally extending sulcus extends across the ramus, whereas in juveniles (FMNH PR2411), subadults (RSM 2990.1), one young adult (LACM 150,167), and some adults (RSM 2523.8) it is absent (Carr, 2020). In the type (Figure 13A), the sulcus extends from the groove that extends into the lacrimal pneumatic recess.

In medial view in CM 9380 (Figure 13B), juveniles (FMNH PR2411), young adults (MOR 1125), and other adults (MOR 008) the surface ahead of the orbitonasal ridge and below the medial recess is concave in vertical and horizontal sections, whereas it is convex in vertical section in some adults (MOR 2822) (Carr, 2020). In the type (Figure 13B) and other adults (MOR 980) the medial surface of the caudal half of the ventral ramus is scoured by deep and torturous vascular sulci, whereas this surface is smooth in juveniles (FMNH PR2411), subadults (RSM 2990.1), and young adults (MOR 1125) (Carr, 2020). In the type (Figure 13B), young adults (MOR 1125), and other adults (MOR 555) the ventral margin of the rostral half of the ramus extends rostroventrally, whereas in juveniles (FMNH PR2411) and one adult (MOR 008) it extends rostrodorsally (Carr, 2020).

In lateral and medial views in CM 9380 (Figure 13), young adults (MOR 1125), and other adults (MOR 980) a prominent ridge along the caudal edge of the ramus is delimited ventrally by a notch is present, whereas the ridge and notch are absent from juveniles (BMRP 2020.4.1), subadults (RSM 2990.1), young adults (UWBM 99,000), and some adults (AMNH FARB 5027) (Carr, 2020). In lateral view in the type (Figures 9, 13(A)), juveniles (FMNH PR2411), young adults (MOR 1125), and adults (AMNH FARB 5027) the subcutaneous surface of the ventral ramus and the smooth antorbital fossa of the dorsal ramus merge together, whereas they are separated by a narrow groove in some juveniles (BMRP 2002.4.1) or by a wide groove in subadults (RSM 2990.1) and one young adult (LACM 150,167) (Carr, 2020).

In caudal view in CM 9380, young adults (MOR 1125), and other adults (MOR 980) the fossa between the prefrontal joint surface and the ventral ramus is deep and sharply delimited laterally by a ridge, whereas in juveniles (FMNH PR2411) and subadults (RSM 2990.1) the fossa is shallow (Carr, 2020).

4.14. Joint surface for the prefrontal

In medial and caudal views, the joint surface for the prefrontal in CM 9380 (Figure 13B) and other adults (MOR 555) extends ventrally to the level of the distal caudomedial foramen, whereas in young adults (UWBM 99,000) it extends below the level of the foramen, and in juveniles it does not extend below the level of the rostral ramus (Carr, 2020). The joint surface in the type (Figures 11(B), 12, 13(B)), young adults (MOR 1125), and other adults (MOR 555) is peg-in-socket in form, as in other adults; in contrast, the contact is abutting and coarse in juveniles (Carr, 2020). In medial view in the type (Figures 11(B), 12, 13(B)), subadults (RSM 2990.1), and other adults (MOR 980) the joint surface for the prefrontal and the conchal surface are separated by a low ridge, whereas in juveniles (FMNH PR2411) and one young adult (MOR 1125) the ridge is prominent (Carr, 2020).

In dorsal view, the joint surface in CM 9380 (Figure 10), young adults (LACM 150,167), and other adults (MOR 980) is exposed to view, whereas it is not exposed in juveniles (FMNH PR2411) (Carr, 2020). In caudal view in the type, young adults (MOR 1125), and other adults (MOR 555) the joint surface for the ventral process of the prefrontal is entirely in view, whereas in juveniles (FMNH PR2411) only the distal end is exposed to view (Carr, 2020).

4.15. Prefrontonasal contact

In CM 9380 (Figures 11(B), 12) and other adults (MOR 980) the prefrontonasal joint surface above the medial fossa is a flat, coarse, and medially-facing facet that caudally twists to face dorsally, whereas in juveniles (FMNH PR2411) it is a dorsoventrally shallow groove that faces medially (Carr, 2020). There is some variation:



in subadults (RSM 2990.1) it is flat and twists to face dorsally, and in young adults (MOR 1125) and some adults (MOR 555) it is a deep groove that caudally twists to face mediodorsally (Carr, 2020). In the type and other adults (MOR 555) the boundary between the joint surfaces are separated by a ridge, whereas in juveniles (BMRP 2002.4.1) they are continuous, and in young adults (MOR 1125) and some adults (MOR 980) they are separated by a groove (Carr, 2020).

4.16. Suborbital ligament scar

In lateral view in CM 9380 (Figures 8, 9, 13(A)), one juvenile (FMNH PR2411), subadults (RSM 2990.1), young adults (MOR 1125), and other adults (AMNH FARB 5027) the scar is subtle, whereas it is distinct in some juveniles (CMNH 7541) (Carr, 2020). The scar in the type (Figures 8, 9, 13(A)), young adults (MOR 1125), and other adults (AMNH FARB 5027) is coarse in texture, whereas the texture is lightly coarse in juveniles (FMNH PR2411) and subadults (RSM 2990.1) (Carr, 2020). In the type (Figures 8, 9, 13(A)) and one other adult (FMNH PR2081) the scar is laterally bulbous, whereas in juveniles (FMNH PR2411) it is flat and in subadults (RSM 2990.1), young adults (MOR 1125), and other adults (MOR 980) it is low in relief (Carr, 2020).

In caudal view in CM 9380, above the scar is a deep neurovascular foramen that extends onto the lateral surface of the bone and sends one sulcus dorsally and another branch rostrally that extends to the lacrimal pneumatic recess (Figures 8, 9). The dorsal branch splits into four sulci: the caudalmost to the joint surface for the epilacrimal and the other three to the dorsolateral surface of the bone (Figures 8, 9(B)). The rostralmost of the three enters a foramen on the dorsolateral surface of the dorsal ramus (Figures 8, 9(B)).

4.17. Subocular process

In lateral and medial views, the subocular process is present in the type (Figures 8(B), 13(A)), young adults (MOR 1125), and other adults (MOR 008) that extends from the caudal edge of the ventral ramus (Carr, 2020). This feature is absent from juveniles (FMNH PR2411), subadults (RSM 2990.1), and some adults (AMNH FARB 5027) (Carr, 2020).

4.18. Medial pneumatic recess

In medial view, a large medial pneumatic recess is present in CM 9380 (Figures 11(B), 12, 13(B)), subadults (RSM 2990.1), young adults (MOR 1125), and other adults (MOR 980); in contrast, this opening is absent from juveniles (FMNH PR2411) (Carr, 2020). In the type (Figures 11(B), 12, 13(B)), young adults (LACM 150,167), and other adults (MOR 980) the caudoventral margin of the recess is absorbed, whereas absorption is absent from subadults (RSM 2990.1), young adults (MOR 1125) and one adult (MOR 2822) (Carr, 2020). In the type (Figures 11(B), 12, 13(B)), young adults (MOR 1125), and other adults (MOR 980) the recess is positioned far caudal to the rostral margin of the ventral ramus, whereas in subadults (RSM 2990.1) and one young adult (LACM 150,167) it closely approaches the edge (Carr, 2020).

In rostromedial view in CM 9380, young adults (MOR 1125), and other adults (MOR 980) the recess is invasive such that it extends deeply caudodorsolaterally into the dorsal ramus, whereas in subadults (RSM 2990.1) and one adult (MOR 2822) it is a deep fossa of limited extent into the bone (Carr, 2020). In medial view in the type (Figures 11(B), 12, 13(B)), subadults (RSM 2990.1), young adults (LACM 150,167), and other adults (MOR 980) a horizontal septum at the midheight of the recess is absent, whereas a septum is seen in one young adult (MOR 1125) and an adult (MOR 2822) (Carr, 2020). In the type (Figures 11(B), 12, 13(B)), young adults (UWBM 99,000), and other adults (MOR 980) the vascular sulcus above the recess is deeply incised, whereas it is shallow in juveniles (FMNH PR2411), subadults (RSM 2990.1), young adults (MOR 1125), and some adults (MOR 2822) (Carr, 2020).

4.19. Orbitonasal ridge

In medial view in CM 9380 (Figures 11(B), 13(B)), subadults (RSM 2990.1), young adults (MOR 1125), and other adults (MOR 980) the ridge is wide proximally and narrow distally, whereas in juveniles (FMNH PR2411) both

ends are the same rostrocaudal length (Carr, 2020). In the type (Figures 11(B), 13(B)), subadults (RSM 2990.1), young adults (MOR 1125), and other adults (MOR 980) the ridge is not backswept, whereas in juveniles (FMNH PR241) the distal end of the ridge is backswept into a wing-like process (Carr, 2020).

In the type (Figures 11(B), 13(B)) and other adults the rostral margin of the ridge and the ventral ramus grade into each other, whereas a crease separates them in juveniles (FMNH PR1411) (Carr, 2020). In subadults (RSM 2990.1), young adults (MOR 1125), and one adult (MOR 008) the structures grade into each other dorsally and are separated by a crease ventrally (Carr, 2020). In the type (Figures 11(B), 13(B)), subadults (RSM 2990.1), young adults (MOR 1125), and other adults (MOR 980) the ridge is situated far ahead of the caudal edge of the ventral ramus, whereas it is situated close to the caudal edge in juveniles (FMNH PR2411). In the type (Figures 11(B), 13(B)), subadults (RSM 2990.1), young adults (MOR 1125), and other adults (MOR 980) the ridge extends rostroventrally proximally, at or above the midheight of the ventral ramus, whereas in juveniles (FMNH PR2411) it extends distally at the rostroventral ala (Carr, 2020).

In rostral view in CM 9380 (Figure 11A), young adults (MOR 1125), and adults (MOR 980) the ridge is proximodistally wide, whereas in juveniles (FMNH PR2411) the ridge is narrow and in subadults (RSM 2990.1) it is wide proximally and tapers ventrally (Carr, 2020).

In caudal view in CM 9380, young adults (MOR 1125), and other adults (MOR 980) the large foramen at the upper corner of the orbit is rounded, whereas in juveniles (FMNH PR2411), a young adult (UWBM 99,000), and an adult (MOR 555) it is dorsoventrally deep and narrow (i.e. oval) (Carr, 2020). In the type, young adults (MOR 1125), and other adults (MOR 980) the foramen is located in a deep pit, whereas in juveniles (FMNH PR2411), subadults (RSM 2990.1), and one young adult (UWBM 99,000) the pit is absent (Carr, 2020). In the type, young adults (MOR 1125), and other adults (MOR 980) the caudomedial edge of the ridge is mediolaterally wide, whereas in juveniles (FMNH PR2411) and a young adult (UWBM 99,000) it is narrow (Carr, 2020).

4.20. Rostroventral ala

In lateral view in CM 9380 (Figures 8, 13(A)), young adults (MOR 1125), and other adults (AMNH FARB 5027) the rostral margin of the ala is convex, whereas in small juveniles (FMNH PR2411) and one adult (MOR 555) it is concave and in large juveniles (BMRP 2002.4.1), subadults (RSM 2990.1), and one adult (MOR 980) it is straight (Carr, 2020).

4.21. Joint surface for the jugal

In lateral view, the contact for the jugal in CM 9380 (Figures 8, 13(A)), young adults (MOR 1125), and other adults (AMNH FARB 5027) is unequally divided between the rostroventral ala and the ventral ramus, where the length of the ramus exceeds that of the ala; in one adult (MOR 008) the contacts are equal in length (Carr, 2020). In juveniles (CMNH 7541) the contact with the ala exceeds that of the ramus (Carr, 2020). In the type (Figure 8A), large juveniles (BMRP 20,204.1), and one young adult (UWBM 99,000) the angle between the ramus and the jugal is less than 45 degrees, whereas in small juveniles (CMNH 7541), young adults (MOR 1125), and some adults (AMNH FARB 5027) the angle is 45 degrees or more. In the type, on the right side the

Table 3. Measurements (in millimetres) of the left squamosal of the type specimen of tyrannosaurus rex (CM 9380). All measurements were taken three times to the nearest hundredth, and the mean is documented here.

Structure measured	Measurement
Quadratojugal process, dorsal length	135.6
Quadratojugal process, ventral length	194.3
Quadratojugal process, rostral height	45.9
Quadratojugal process, midlength height	43.8
Quadratojugal process, basal height	30.9
Caudal process, dorsoventral height	114
Bone, total length (qj pr to cdl pr)	263.5
Postorbital process, basal height	65.1
Postorbital process, midlength height	66.8
Postorbital process, maximum height	78.2
Bone, dorsal length	272

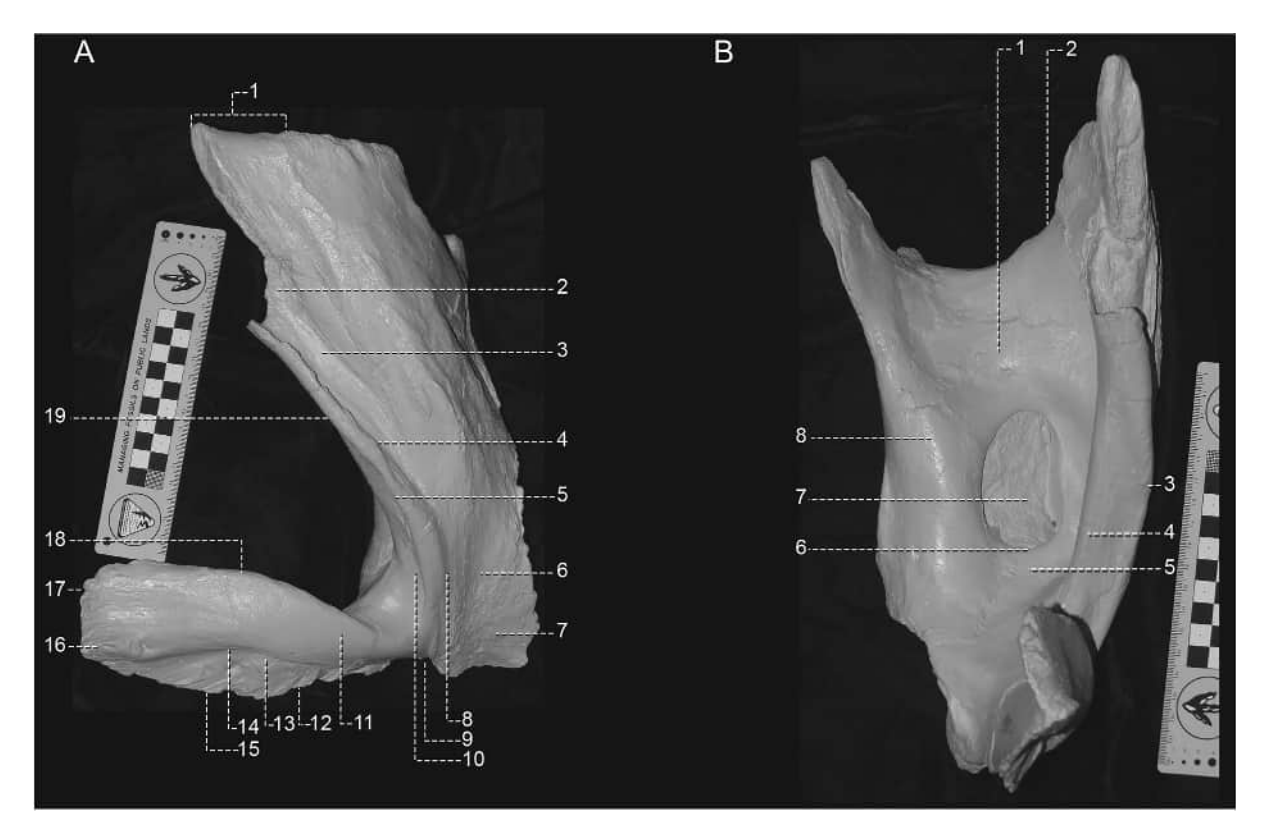


Figure 14. The left squamosal of CM 9380 in (A) lateral view; numbers correspond to the features: 1, rostrodorsal margin is short and deep; 2, joint surface is a long convexity; 3, joint surface overlaps ventral quarter to third of the process; 4, caudal end of joint surface does not approach the dorsal margin of the bone; 5, flange below joint surface is absent; 6, shallow groove separates inflated caudal process from rest of bone; 7, caudal process is rugose; 8, fossa is not bounded by a ventrally-extending ridge; 9, quadrate cotyle opens caudoventrally; 10, fossa extends onto the postorbital process; 11, proximal end of the process extends rostrodorsally; 12, rostral and caudal parts of the joint surface are continuous; 13, joint surface for the quadratojugal is deeply excavated, covers the ventral half of the process, does not cover the tip of the process, and is coarsened by ridges: 14, a slot excavates the dorsal edge of the joint surface: 15, joint surface for the quadratojugal forms a scalpel-shaped flange; 16, ventrolateral ridge; 17, distal end of quadratojugal process is deep, square, and ridged; 18, dorsal half of process extends dorsolaterally; 19, flange is continuous along process. (B) rostroventral view; numbers correspond to the features: 1, rostral bar is inflated and rostrocaudally long; 2, flange is absent from the rostral margin; 3, ridge extends more laterally than ventrally and is mediolaterally wide; 4, lateral strut is narrow and deep; 5, shelf caudal to foramen is present and inflated; 6, caudal end of the foramen reaches the level of the quadrate notch; 7, mediumsized pneumatic foramen is present; 8, medial strut is wide and convex. Scale bar equals 10 cm.

caudoventral margin of the jugal contact extends caudoventrally (Figure 8A,B), whereas in juveniles (CMNH 7541) and one adult (MOR 555) it extends 45 degrees, and on the left side in the type, young adults (MOR 1125) and most adults (AMNH FARB 5027) it extends greater than 45 degrees (Carr, 2020).

4.22. Joint surface for the palatine

In medial view in CM 9380 (Figures 11(B), 13(B)), young adults (MOR 1125), and adults (MOR 555) the joint surface for the palatine covers only a quarter or less of the distal end of the bone, whereas in juveniles (FMNH PR2411) it covers the rostral third of the bone (Carr, 2020). In the type (Figures 8, 11, 13), and other adults (MOR 980) the joint surface covers the medial, rostral, and lateral surfaces of the bone, whereas in juveniles (FMNH PR2411), subadults (RSM 2990.1), young adults (MOR 1125), and some adults (FMNH PR2081) it covers only the medial surface (Carr, 2020). In young adults (UWBM 99,000) and some adults (AMNH FARB 5027) the joint surface only covers the medial and rostral surfaces (Carr, 2020).

In medial view in CM 9380 (Figures 11(B), 13(B)), young adults (UWBM 99,000), and some adults (MOR 980) the joint surface is deeply inset, whereas in juveniles (FMNH PR2411) and one young adult (MOR 1125) it is



shallowly inset (Carr, 2020). In the type (Figure 11A), young adults (MOR 1125), and other adults (MOR 980) the joint surface extends up the ventral two-thirds or more of the ala, whereas in juveniles (FMNH PR2411) and one adult (MOR 555) it extends halfway up the ala (Carr, 2020).

5. Squamosal

5.1. General description

In CM 9380 the left squamosal is preserved; measurements of the bone are given in Table 3. In lateral view, in CM 9380 (Figure 14A), young adults (MOR 1125), and other adults (MOR 555) the fossa at the junction of the postorbital and quadratojugal rami excavates the postorbital process, whereas in juveniles (CMNH 7541) it is excavates the quadratojugal ramus only (Carr, 2020). In the type (Figure 14A), juveniles (CMNH 7541), young adults (UWBM 99,000), and some adults (FMNH PR2081) the fossa is not bounded above by a ridge, whereas in young adults (MOR 1125) and some adults (AMNH FARB 5027) the fossa is bounded by a ventrallyextending ridge that extends to the caudal end of the fossa (Carr, 2020).

5.2. Postorbital ramus

In lateral view in CM 9380 (Figure 14A), young adults (MOR 1125), and other adults (MOR 555) the flange from the lateroventral margin below the caudal end of the joint surface for the postorbital is absent, where the margin extends laterally above the laterotemporal fenestra (Carr, 2020). In contrast, the flange is seen in juveniles (BMRP 2002.4.1) and one adult (RSM 2523.8) (Carr, 2020). In the type (Figure 14A), young adults (MOR 1125), and other adults (MOR 555) the flange extends to the caudal end of the fenestra, whereas in juveniles (BMRP 2002.4.1) the flange arises distal to the caudal corner of the fenestra (Carr, 2020).

5.3. Joint surface for the postorbital

In lateral view in CM 9380 (Figure 14A), young adults (MOR 1125), and other adults (MOR 555) the caudal end of the joint surface does not approach the dorsal margin of the dorsal postorbital process, whereas it does approach the dorsal margin in juveniles (BMRP 2002.4.1) (Carr, 2020). In the type (Figure 14A), young adults (MOR 1125), and other adults (MOR 555) the joint surface overlaps the ventral guarter to third of the process, whereas in juveniles (BMRP 2002.4.1) the joint surface laps onto its ventral margin (Carr, 2020).

5.4. Dorsal postorbital process

In lateral view in CM 9380 (Figure 14A), young adults (MOR 1125), and other adults (MOR 555) the joint surface for the postorbital occupies the rostrodorsal region of the process as a long convexity, whereas in juveniles (BMRP 2002.4.1) and one subadult (LACM 150,167) the joint surface does not extend into this region (Carr, 2020). In the type (Figure 14A), young adults (MOR 1125), and other adults (MOR 555) the rostrodorsal margin of the process is short and deep, whereas in juveniles (BMRP 2002.4.1), young adults (UWBM 99,000), and some adults (FMNH PR2081) it is long and low (Carr, 2020).

5.5. Ventral postorbital process

In lateral and ventral views in CM 9380 (Figure 14), young adults (MOR 1125), and other adults (MOR 555) the flange that bounds the laterotemporal fossa is continuous, whereas in juveniles (BMRP 2002.4.1) a notch divides it into rostral and caudal parts (Carr, 2020). In ventral view in the type (Figure 14B), juveniles (BMRP 2002.4.1), young adults (MOR 1125), and other adults (MOR 980) the lateral ridge extends more laterally than ventrally, whereas in some adults (MOR 555) it extends more ventrally than laterally (Carr, 2020). In the type (Figure 14B), young adults (MOR 1125), and other adults (MOR 555) the width of the lateral ridge along the lateroventral flange is mediolaterally wide, whereas in juveniles (BMRP 2002.4.1) and one adult (MOR 980) it is narrow (Carr, 2020).

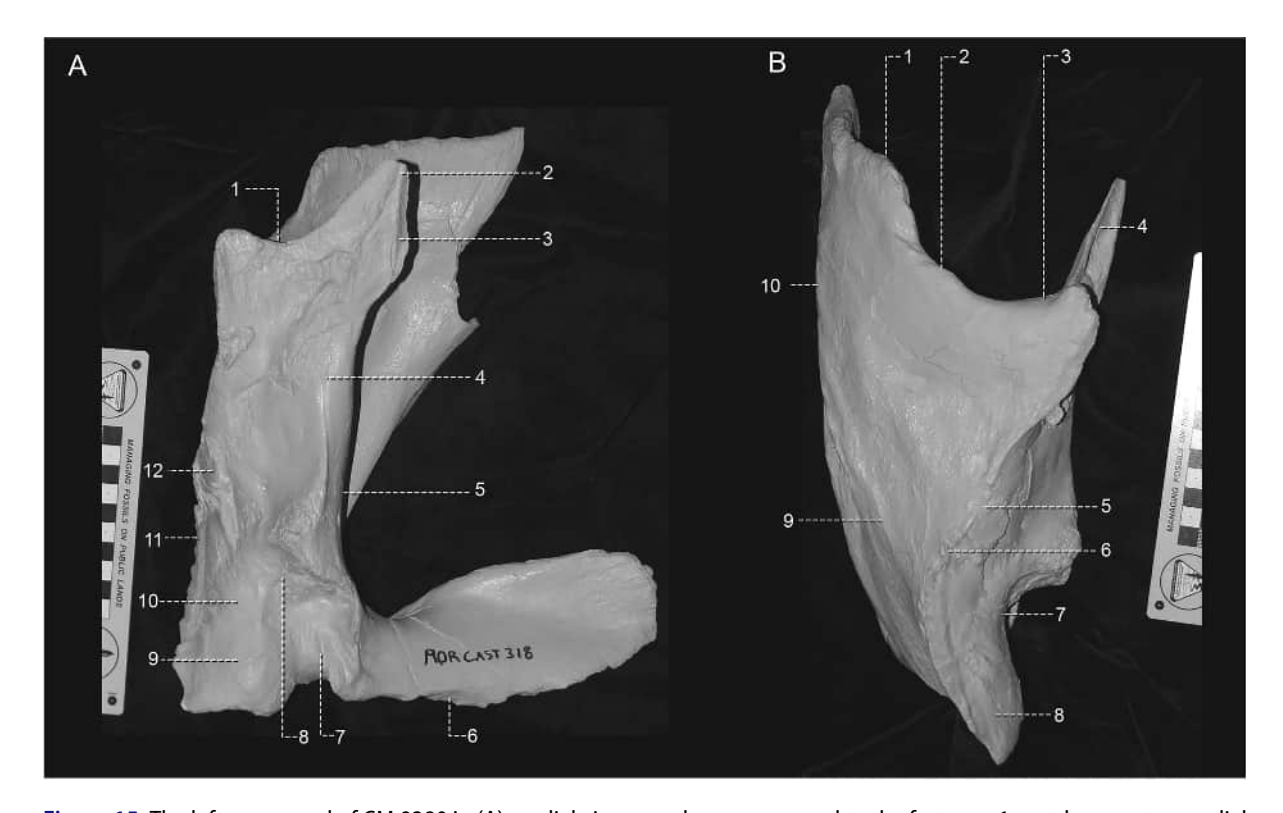


Figure 15. The left squamosal of CM 9380 in (A) medial view; numbers correspond to the features: 1, notch separates medial process from the dorsotemporal fenestra; 2, medial process extends sharply rostrodorsally; 3, ioint surface for the prootic is a deep flange; 4, medial process is inflated; 5, base of process is subtly concave; 6, joint surface for the quadratojugal is indistinct; 7, coarse ridges extend into the quadrate cotyle; 8, surface opposite the medial bar is filled by a pad of porous bone; 9, joint surface for the paroccipital process is deep; 10, joint surface above quadrate cotyle is convex; 11, dorsum extends medially over joint surface; 12, joint surfaces for otoccipital and paroccipital process are confluent. (B) dorsal view; numbers correspond to the features: 1, rostral margin of the dorsotemporal fenestra is angular; 2, flange is absent from the rostral margin; 3, medial end of dorsotemporal fenestra is notched; 4, joint surface faces more medially than dorsomedially; 5, medial margin of dorsum is subtly convex; 6, ridge fades before reaching the caudal process; 7, quadrate cotyle is positioned medially; 8, caudal process extends caudomedially; 9, ridge fades before reaching the caudal process; 10, ridge reaches the lateral edge of the bone. Scale bar equals 10 cm.

5.6. Dorsal surface

In medial view, in CM 9380 (Figure 15A), young adults (MOR 1125), and other adults (MOR 555) the dorsum extends medially and forms a shelf over the medial joint surface of the bone, whereas the shelf-like extension is absent from juveniles (CMNH 7541) (Carr, 2020). In dorsal view, the medial margin of the bone in the type (Figure 15B), young adults (MOR 1125), and other adults (MOR 555) is shallowly concave or subtly convex, whereas in juveniles (BMRP 2002.4.1) it is deeply concave (Carr, 2020).

In rostral view in CM 9380 (Figure 14B), young adults (MOR 1125), and other adults (MOR 555) a flange does not extend along the edge of the dorsotemporal fenestra, whereas a ridge is seen in juveniles (CMNH 7541) (Carr, 2020). In dorsal view in CM 9380 (Figure 15B), young adults (MOR 1125), and other adults (MOR 555) the rostral margin of the dorsotemporal fenestra is angular, whereas in juveniles (CMNH 7541) it is straight and extends rostrolaterally (Carr, 2020). In the type (Figure 15B), young adults (MOR 1125), and other adults (MOR 555) the medial end of the fenestra is deeply notched, whereas in juveniles (CMNH 7541), some young adults (LACM 150,167), and one adult (MOR 008) it is subtly notched (Carr, 2020).

In dorsal view in CM 9380 (Figure 15B), young adults (MOR 1125), and other adults (MOR 555) the ridge that bounds the dorsotemporal fossa fades before reaching the caudal process, whereas in juveniles (CMNH 7541), young adults (UWBM 99000), and one adult (MOR 008) it does reach the caudal process (Carr, 2020). In the type (Figure 15B), young adults (MOR 1125), and other adults (MOR 555) the ridge that extends caudally from the rostral end of the medial process fades before reaching the caudal process, whereas in juveniles (CMNH 7541) and some adults (MOR 008) it extends to the caudal process

(Carr, 2020). In the type (Figure 15B), young adults (UWBM 99,000), and other adults (MOR 555) the lateral margin of the fossa reaches the lateral margin of the dorsal postorbital process, whereas in juveniles (CMNH 7541) and young adults (MOR 1125) it does not reach the lateral margin of the process (Carr, 2020).

5.7. Pneumatic foramen

In ventral view, the ceiling of the dorsal ramus of the bone in CM 9380 (Figure 14B), young adults (MOR 1125), and other adults (FMNH PR2081) is penetrated by a medium-sized pneumatic foramen. In adults, this opening ranges from medium (CM 9380; Figure 14B) to large (RSM 2523.8) in size (Carr, 2020). In juveniles (BMRP 2002.4.1) a foramen is absent, but the ceiling of the bone is excavated by a shallow fossa (Carr, 2020). In the type (Figure 14B), young adults (UWBM 99,000), and other adults (MOR 008) the caudal end of the foramen extends to the level of the quadrate notch, whereas in one young adult (MOR 1125) and an adult (MOR 555) it is ahead of the level of the notch (Carr, 2020).

5.8. Circumfossa struts

In ventral view in CM 9380 (Figure 14B), young adults (MOR 1125), and other adults (MOR 555) the bar rostral to the pneumatic foramen is inflated and rostrocaudally long, whereas in juveniles (BMRP 2002.4.1) it is not inflated and short (Carr, 2020). In the type (Figure 14B), young adults (MOR 1125), and other adults (MOR 555) the strut lateral to the foramen is narrow and dorsoventrally deep, whereas in juveniles (BMRP 2002.4.1) it is low and wide (Carr, 2020). In the type (Figure 14B), young adults (MOR 1125), and other adults (MOR 555) the strut medial to the foramen is wide and convex, whereas in juveniles (BMRP 2002.4.1) and one young adult (LACM 150,167) it is deep and narrow (Carr, 2020). In the type (Figure 14B) and other adults (MOR 555) the shelf caudal to the foramen is present and inflated, whereas in juveniles (BMRP 2002.4.1) and young adults (MOR 1125) it is absent (Carr, 2020).

5.9. Joint surface for the prootic

In medial view in CM 9380 (Figure 15A) the joint surface excavates the medioventral surface of the medial process and it extends ventrally as a deep flange, whereas a low flange is seen in young adults (MOR 1125) and other adults (MOR 555) (Carr, 2020). In juveniles (BMRP 2002.4.1) and one adult (FMNH PR2081) it is limited to the distal end of the medial process and flattens its ventral surface (Carr, 2020).

5.10. Joint surface for the otoccipital

In medial view in CM 9380 (Figure 15A), young adults (MOR 1125), and other adults (MOR 555) the joint surface for the paroccipital process is dorsoventrally deep, whereas in juveniles (BMRP 2002.4.1) and one young adult (LACM 150,167) it is shallow (Carr, 2020). In the type (Figure 15A) and one other adult (FMNH PR2081) the joint surface above the quadrate cotyle is convex, whereas in juveniles (BMRP 2002.4.1), young adults (MOR 1125), and other adults (MOR 555) it is concave (Carr, 2020). In the type (Figure 15A), young adults (MOR 1125), and other adults (MOR 555) the joint surfaces for the otoccipital and that for the paroccipital process are confluent, whereas in juveniles (BMRP 2002.4.1) and one young adult (LACM 150,167) they are separated by a ridge (Carr, 2020).

5.11. Quadratojugal process

In lateral view, the distal end of the quadratojugal process in CM 9380 (Figure 14A), young adults (MOR 1125), and other adults (AMNH FARB 5027) is dorsoventrally deep and squared, which is the adult condition (Carr, 2020). In juveniles (BMRP 2002.4.1) the distal end is shallow and pointed (Carr, 2020). The joint surface for the quadratojugal deeply excavates the lateral surface of the process in the type (Figure 14A), young adults (LACM 150,167), and other adults (AMNH FARB 5027), whereas it is shallow in juveniles (BMRP 2002.4.1) and young adults (MOR 1125) (Carr, 2020).

In lateral view, the distal end of the process in the type (Figure 14A), young adults (MOR 1125), and other adults (AMNH FARB 5027) is coarsened by massive ridges, whereas in juveniles (BMRP 2002.4.1) and some adults (RSM 2523.8) it is coarsened by small ridges (Carr, 2020). The proximal end of the process in the type (Figure 14A), young adults (MOR 1125), and other adults (AMNH FARB 5027) extends rostrodorsally, whereas in juveniles (CMNH 7541) and one adult (MOR 980) it extends rostrally (Carr, 2020). In the type (Figure 14A) and some other adults (MOR 008) the rostral and caudal parts of the joint surface for the quadratojugal are continuous with each other, whereas in juveniles (BMRP 2002.4.1), young adults (MOR 1125), and other adults (AMNH FARB 5027) a distinct concavity in the ventral margin of the process separates the joint surface into rostral and caudal parts (Carr, 2020).

In medial view in CM 9380 (Figure 15A), young adults (MOR 1125), and other adults (MOR 008) the proximal part of the joint surface is indistinct, whereas in juveniles (BMRP 2002.4.1) and one young adult (UWBM 99,000) it is distinct (Carr, 2020). In rostral view in CM 9380 (Figure 14B) and juveniles (BMRP 2002.4.1) the dorsal half of the ramus extends dorsolaterally, whereas in young adults (MOR 1125) and other adults (AMNH FARB 5027) it extends dorsomedially (Carr, 2020). In the type (Figure 14A), young adults (MOR 1125) and other adults (AMNH FARB 5027) the long axis of the dorsal end of the process has a distinct twist such that the nonjoint surface extends sharply ventrolaterally to culminate in a laterally-jutting ridge; in juveniles (BMRP 2002.4.1) it is vertical with a subtle ventrolateral curvature (Carr, 2020).

5.12. Joint surface for the quadratojugal

In lateral view in the type (Figure 14A), young adults (MOR 1125) and other adults (AMNH FARB 5027) the joint surface covers the ventral half of the quadratojugal process and does not cover the tip of the process; in contrast, in juveniles (BMRP 2002.4.1) it covers almost the entire depth, except dorsally, and it covers the tip of the process (Carr, 2020). In the type (Figure 14A), young adults (MOR 1125) and other adults (AMNH FARB 5027) the joint surface is a deep, scalpel-shaped flange, whereas in juveniles (BMRP 2002.4.1) it is shallow (Carr, 2020). In the type (Figure 14A), young adults (MOR 1125), and other adults (AMNH FARB 5027) the joint surface is coarsened throughout by distinct rostroventrally-extending ridges, whereas in juveniles (BMRP 2002.4.1) the surface is mottled with ridges at the tip of the process (Carr, 2020).

In lateral view in the type (Figure 14A), young adults (UWBM 99,000), and other adults (AMNH FARB 5027), the dorsal margin of the rostral part of the joint surface is deeply concave; in contrast, it is bounded by a shallow ridge in juveniles (BMRP 2002.4.1) and in young adults (MOR 1125) and one adult (FMNH PR2081) the dorsal margin grades into the lateral surface of the bone (Carr, 2020). In the type (Figure 14A), young adults (UWBM 99,000), and other adults (AMNH FARB 5027) a slot excavates the dorsal margin of the joint surface, whereas a slot is absent from juveniles (BMRP 2002.4.1), young adults (MOR 1125), and one adult (FMNH PR2081) (Carr, 2020).

5.13. Caudal process

In lateral view, the caudal process in CM 9380 (Figure 14A), young adults (MOR 1125), and other adults (AMNH FARB 5027) is pneumatically inflated and it is demarcated from the rest of the bone by a shallow groove; in contrast, in juveniles (BMRP 2002.4.1) the process is apneumatic such that a deep groove separates the body of the bone from the process (Carr, 2020). In caudal view, the process in the type, young adults (MOR 1125), and other adults (FMNH PR2081) is mediolaterally wide, whereas it is narrow in juveniles (CMNH 7541) and young adults (LACM 150,167) (Carr, 2020). The process in the type (Figure 14A) and other adults (AMNH FARB 5027) is coarsely rugose in texture, whereas it is lightly rugose in juveniles (CMNH 7541), young adults (MOR 1125), and one adult (MOR 980) (Carr, 2020). In dorsal view in CM 9380 (Figure 15B), young adults (MOR 1125), and other adults (AMNH FARB 5027) the process extends caudomedially, whereas in juveniles (CMNH 7541) it extends caudally (Carr, 2020).

5.14. Medial process

In medial view in CM 9380 (Figure 15A), young adults (MOR 1125), and other adults (MOR 555), the medial process is inflated, whereas it is not inflated in juveniles (BMRP 2002.4.1) (Carr, 2020). The process extends steeply rostrodorsally in the type (Figure 15A), young adults (MOR 1125), and other adults (MOR 555), whereas it extends at a low angle in juveniles (BMRP 2002.4.1) (Carr, 2020). The ventral margin of the base of the process in the type, young adults (MOR 1125), and other adults (MOR 555), is shallowly concave, whereas in juveniles (BMRP 2002.4.1) it is distinctly dorsally concave (Carr, 2020). In the type (Figure 15A), young adults (MOR 1125), and other adults (MOR 555), the margin of the dorsotemporal fenestra and the base of the process are separated by a notch, whereas the notch is absent in juveniles (BMRP 2002.4.1) and some young adults (LACM 150,167) (Carr, 2020). In the type (Figure 15A), young adults (MOR 1125), and other adults (MOR 555), the ridge that extends distally along the medial joint surface is short and fades caudal to the dorsotemporal fenestra, whereas in juveniles (BMRP 2002.4.1) it is long and extends far caudally to the margin of the fenestra (Carr, 2020).

In dorsal view in the type (Figure 15B), young adults (MOR 1125), and other adults (MOR 555), the rostral half of the medial joint surface faces more medially than dorsomedially, whereas in juveniles (BMRP 2002.4.1) it faces more dorsomedially than medially (Carr, 2020).

5.15. Joint surface for the quadrate

In lateral view in CM 9380 (Figure 14A), young adults (MOR 1125), and other adults (MOR 555) the lateral notch of the quadrate cotyle opens caudoventrally, whereas in juveniles (BMRP 2002.4.1) and some adults (MOR 008) it opens ventrally (Carr, 2020).

Table 4. Measurements (in millimetres) of the right ectopterygoid of the type specimen of tyrannosaurus rex (CM 9380). All measurements were taken three times to the nearest hundredth. and the mean is documented here.

Structure measured	Measurement
Jugal process, dorsoventral height at midlength	67.8
Jugal process, height of base	68.9
Jugal process, length of base	89.4
Jugal process, ratio of height to length	77%
Joint surface for the jugal, height proximal end	60.3

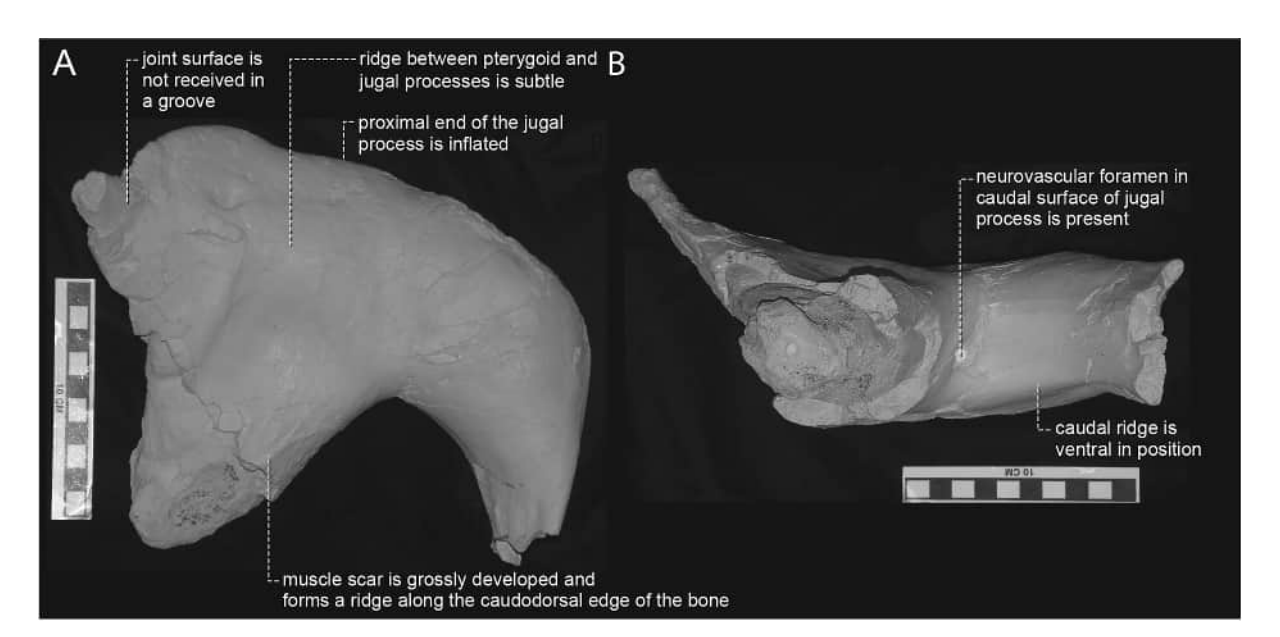


Figure 16. The left ectopterygoid of CM 9380 in (A) dorsal view and (B) caudal view. Scale bar equals 10 cm.

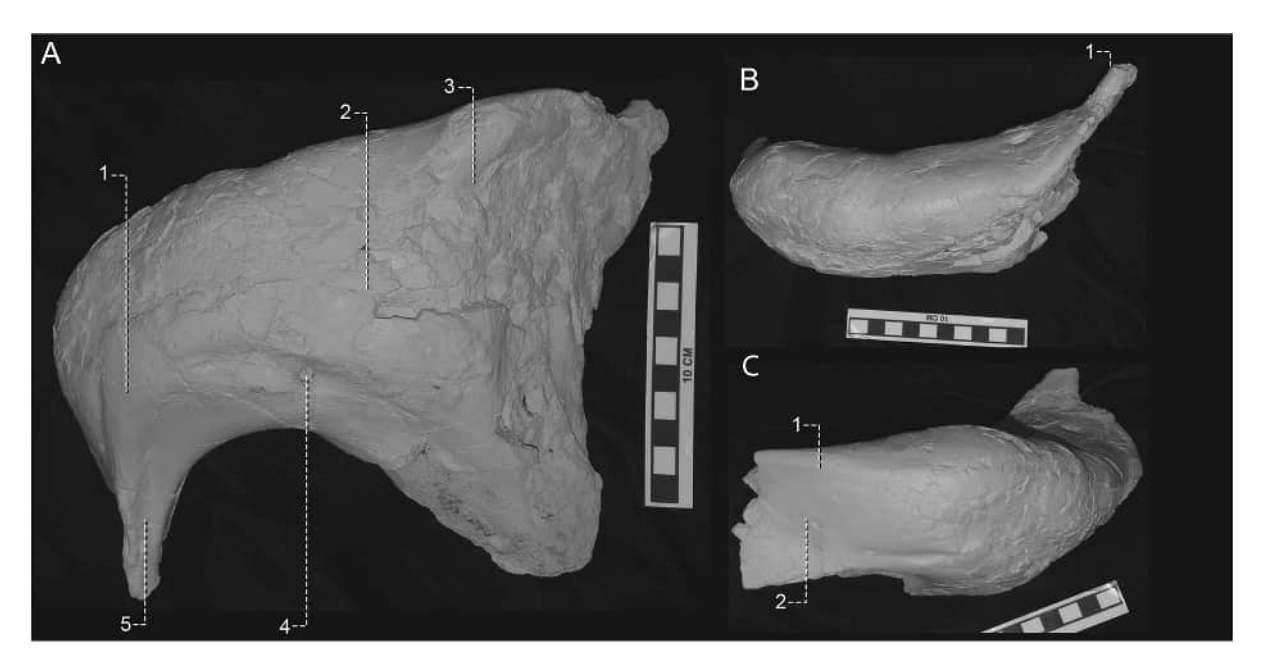


Figure 17. The left ectopterygoid of CM 9380 in (A) ventral view; numbers correspond to the features: 1, ridge medial to flange is indistinct; 2, proximal end of the jugal process is inflated; 3, a fossa is present rostral to the pneumatic recess; 4, neurovascular foramen in caudal surface of jugal process is present; 5, distal end of the jugal process is not inflated. (B) rostral view; number corresponds to the feature: 1, pterygoid process extends mediodorsally at a steep angle. (C) lateral view; numbers correspond to the features: 1, region above joint surface extends laterally relative to the joint surface; 2, proximodorsal part of joint surface is concave. Scale bar equals 10 cm.

In medial view in CM 9380 (Figure 15A), young adults (MOR 1125), and other adults (MOR 555) the joint surface opposite the medial bar is filled with a convex pad of porous bone, whereas in juveniles (BMRP 2002.4.1) the surface is concave and a pad is absent (Carr, 2020). In the type (Figure 15A), young adults (UWBM 99,000), and other adults (MOR 555) coarse ridges extend into the quadrate cotyle, whereas in juveniles (BMRP 2002.4.1) ridges are absent, and in young adults (MOR 1125) and some adults (FMNH PR2081) the ridges are subtle (Carr, 2020).

In dorsal view in CM 9380 (Figure 15B), young adults (MOR 1125), and other adults (MOR 555) the quadrate notch is displaced far medially from the lateral margin of the medial joint surface, whereas in juveniles (BMRP 2002.4.1) it closely approaches the lateral edge (Carr, 2020). In medial and ventral views in CM 9380 (Figure 15A), young adults (LACM 150,167), and other adults (MOR 555) the medial strut is so swollen that it extends caudally, making the rostral surface of the quadrate cotyle convex, whereas the strut is not swollen and the surface is concave in juveniles (BMRP 2002.4.1), young adults (MOR 1125), and one adult FMNH PR2081) (Carr, 2020).

6. Ectopterygoid

6.1. General description

In CM 9380 the left ectopterygoid is preserved, although it is missing the tip of the jugal process, the caudal process, and most of the pterygoid process. Measurements of the ectopterygoid are given in Table 4. In dorsal view in CM 9380 (Figure 16A), young adults (LACM 150,167), and other adults (MOR 555) the ridge that extends between the pterygoid and jugal processes is absent or vanishingly low, whereas in juveniles (BMRP 2002.4.1) and some young adults (MOR 1125) the ridge is present but low (Carr, 2020).

6.2. Jugal ramus

In caudal view (Figure 16B), the jugal ramus of CM 9380, one young adult (UWBM 99,000), and some adults (MOR 555) is penetrated by a neurovascular foramen, whereas the process is imperforate in juveniles (BMRP



2002.4.1), young adults (MOR 1125), and some adults (FMNH PR2081) (Carr, 2020). In the type (Figure 17A), the foramen pierces the ventral surface lateral to the pneumatic recess and ahead of the caudal margin of the jugal process.

The proximal end of the ramus in the type, one young adult (UWBM 99,000), and other adults (AMNH FARB 5027) is inflated (Figures 16, 17); in contrast, it is not inflated in juveniles (BMRP 2002.4.1) and in some young adults (MOR 1125) (Carr, 2020). The distal end of the ramus is not inflated in the type (Figures 16(A), 17 (A)), juveniles (BMRP 2002.4.1), and some young adults (MOR 1125), whereas in other young adults (LACM 150,167) and adults (FMNH PR2081) it is inflated (Carr, 2020).

In caudal view in CM 9380 (Figure 16B), young adults (LACM 150,167), and other adults (MOR 555) the process is inflated, whereas in juveniles (BMRP 2002.4.1), young adults (MOR 1125), and one adult (FMNH PR2081) the process is not inflated (Carr, 2020). In the type (Figure 16B), young adults (MOR 1125), and other adults (MOR 555) the ridge along the caudal surface of the process is towards its ventral edge, whereas in juveniles (BMRP 2002.4.1) it extends dorsolaterally towards the dorsal edge of the process (Carr, 2020). In rostral and lateral views in CM 9380 (Figure 17C), young adults (MOR 1125), and other adults (MOR 555) the region above the joint surface for the jugal is inflated and extends laterally over the joint surface, whereas it is not inflated in juveniles (BMRP 2002.4.1) (Carr, 2020).

6.3. Jugal flange

In ventral view CM 9380 (Figure 17A), young adults (MOR 1125), and one other adult (RSM 2523.8) the ridge medial to the jugal flange is distinct, whereas in juveniles (BMRP 2002.4.1), young adults (LACM 150,167), and some adults (AMNH FARB 5027) it is indistinct (Carr, 2020).

6.4. Joint surface for the jugal

In ventral view, when the bone is lain flat, in CM 9380, young adults (MOR 1125), and other adults (MOR 555) the joint surface faces ventrolaterally and so is in view, whereas in juveniles (BMRP 2002.4.1) it faces dorsolaterally and so is not in view (Carr, 2020). In lateral view in the type (Figure 17C), young adults (MOR 1125), and other adults (MOR 555) the proximodorsal part of the joint surface is concave, whereas it is flat in juveniles (BMRP 20,02.4.1) (Carr, 2020).

6.5. Pneumatic recess

In ventral view in CM 9380 (Figure 17A), young adults (MOR 1125), and other adults (AMNH FARB 5027) there is a fossa next to the rostral end of the recess, whereas a fossa is absent from juveniles (BMRP 2002.4.1) and one adult (MOR 555) (Carr, 2020).

6.6. Pterygoid process

In rostral view in CM 9380 (Figure 17B), young adults (MOR 1125), and other adults (MOR 555) the process extends mediodorsally at a steep angle, whereas in juveniles (BMRP 2002.4.1) and one young adult (LACM 150,167) it extends at a low angle (Carr, 2020).

6.7. Dorsal joint surface for the pterygoid

In dorsal view in CM 9380 (Figure 16A), young adults (MOR 1125), and other adults (MOR 555) the pterygoid is not received in a groove, whereas in juveniles (BMRP 2002.4.1) a groove is present (Carr, 2020).

6.8. Caudal process

In rostrolateral and dorsal views in CM 9380 (Figure 16A), young adults (MOR 1125), and other adults (MOR 555) the muscle attachment surface is grossly developed and makes a ridge along the caudodorsal edge of the process, whereas in juveniles (BMRP 2002.4.1) it makes a swelling along the caudodorsal surface (Carr, 2020).

Table 5. Measurements (in millimetres) of the left and right dentaries of the type specimen of tyrannosaurus rex (CM 9380). All measurements were taken three times to the nearest hundredth, and the mean is documented here. Asterisk (*) indicates measurement taken to the nearest millimetre, tilde (~) indicates measurement taken once, plus sign (+) indicates an incomplete structure.

Structure measured	Measurement left	Measurement right
Tooth row, rostrocaudal length*	518.4	531
Bone, maximum rostrocaudal length	832.5	815+
Bone, dorsal length	597	605
Bone, maximum dorsoventral height	315*	295*
Bone, dorsoventral height at alveolus 1	95.8	82.9
Bone, dorsoventral height at alveolus 2	167.8	139.6
Bone, dorsoventral height at alveolus 3	195.8	168.4
Bone, dorsoventral height at alveolus 4	198.2	194.5
Bone, dorsoventral height at alveolus 5	188.2	189.6
Bone, dorsoventral height at alveolus 6	174.9	179.7
Bone, dorsoventral height at alveolus 7	165.1	167.5
Bone, dorsoventral height at alveolus 8	158.6	163.9
Bone, dorsoventral height at alveolus 9	165.8	166.3
Bone, dorsoventral height at alveolus 10	170.9	174.1
Bone, dorsoventral height at alveolus 11	192.2	189.3
Bone, dorsoventral height at alveolus 12	211.3	206.5
Bone, dorsoventral height at alveolus 13	240*~	220.5
Alveolus 1, mesiodistal length	26.9	38
Alveolus 2, mesiodistal length	45*~	35.4
Alveolus 3, mesiodistal length	43*~	52.6
Alveolus 4, mesiodistal length	55*~	51.7
Alveolus 5, mesiodistal length	45*~	55
Alveolus 6, mesiodistal length	43*~	47*~
Alveolus 7, mesiodistal length	39*~	43*~
Alveolus 8, mesiodistal length	36*~	41*~
Alveolus 9, mesiodistal length	28*~	36*~
Alveolus 10, mesiodistal length	35*~	35*~
Alveolus 11, mesiodistal length	26*~	34*~
Alveolus 12, mesiodistal length	27*~	21*~
Alveolus 13, mesiodistal length	22*~	15*~
Alveolus 1, labiolingual width	30.1	27.3
Alveolus 2, labiolingual width	43.7	42.3
Alveolus 3, labiolingual width	40*~	46.4
Alveolus 4, labiolingual width	40*~	45.3
Alveolus 5, labiolingual width	33*~	43*~
Alveolus 6, labiolingual width	37*~	36
Alveolus 7, labiolingual width	35*~	34*~
Alveolus 8, labiolingual width	32*~	31*~
Alveolus 9, labiolingual width	21.2	27.6
Alveolus 10, labiolingual width	23.7	25*~
Alveolus 11, labiolingual width	18*	21.3
Alveolus 12, labiolingual width	18*~	15.9
Alveolus 12, labiolingual width	14.5*~	14*~
Bone, labiolingual width at alveolus 1	57.3	43.2
Bone, labiolingual width at alveolus 2	77.6	78.3
Bone, labiolingual width at alveolus 3	95.4	91
Bone, labiolingual width at alveolus 4	-	-
Bone, labiolingual width at alveolus 5	-	-
Bone, labiolingual width at alveolus 6		-
Bone, labiolingual width at alveolus 7	74.9	73.9~
Bone, labiolingual width at alveolus 8	70.1	72.3
Bone, labiolingual width at alveolus 9	69.2	68.9
Bone, labiolingual width at alveolus 10	68.7	68.9
Bone, labiolingual width at alveolus 11	65.4	64.5
Bone, labiolingual width at alveolus 12	62.9	63.3
Bone, labiolingual width at alveolus 13	60	61.8

6.9. Lesions

The foramen that penetrates the jugal process appears to be associated with a lesion in the ventral surface of the process (Figure 17A). A shallow, coarse furrow with a remodelled and highly vascularised surface, extends laterally from the foramen (Figures 16(B), 17(A)).

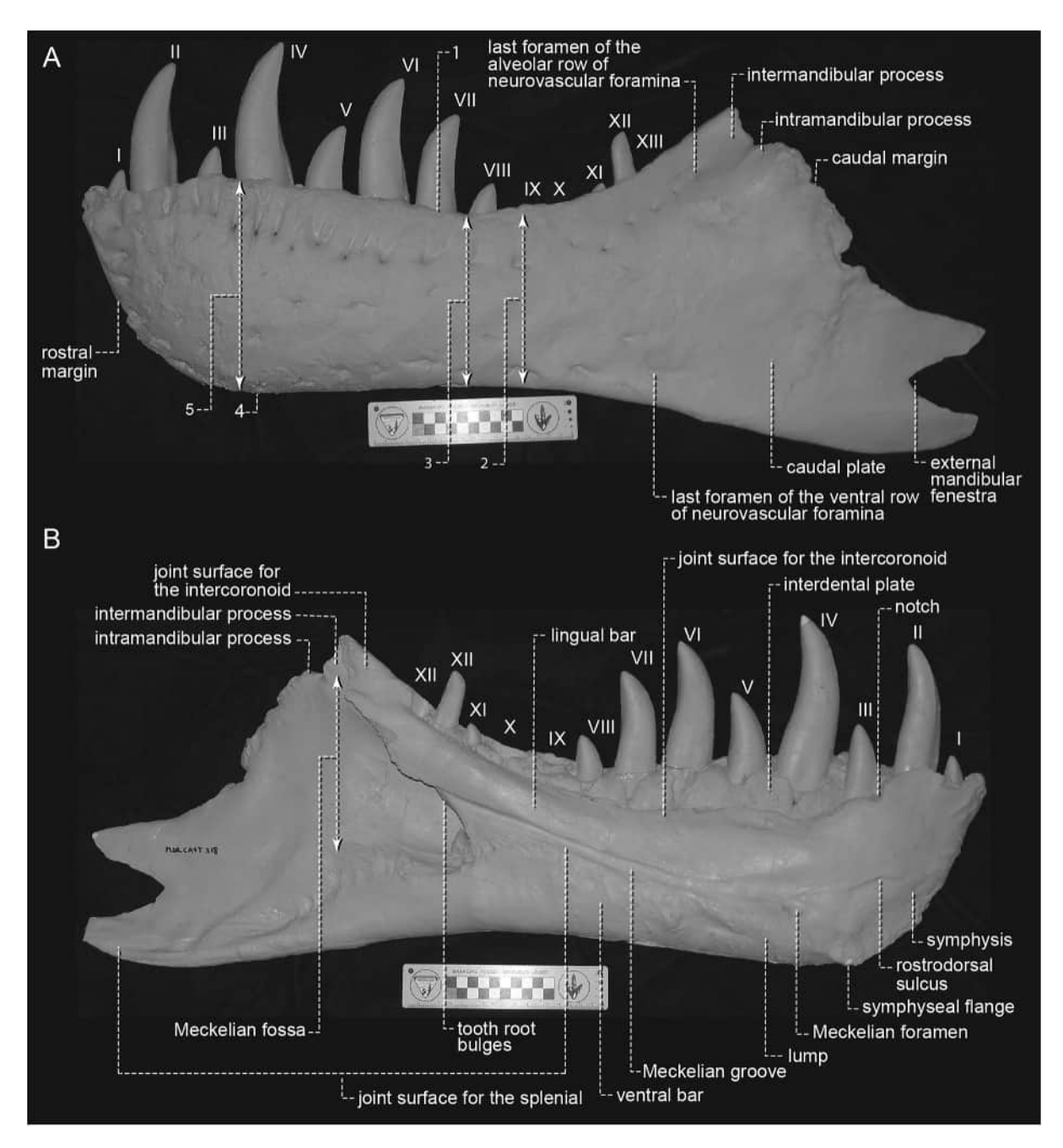


Figure 18. The left dentary of CM 9380 in (A) lateral view; numbers correspond to the following features: 1, convex margin extends to alveolus #7; 2, deepest point of curvature is at alveolus #9; 3, bone is dorsoventrally deep and shallowest point of bone is at alveoli #7 and 8; 4, ventral margin extends uninterrupted to the chin; 5, chin is positioned below alveolus #4. (B) medial view. Roman numerals indicate open alveoli. Scale bar equals 10 cm.

7. Dentary

7.1. General description

In CM 9380 both dentaries are preserved; measurements of the bones are given in Table 5. In lateral view in CM 9380 (Figure 18A), subadults (LACM 23,845), young adults (MOR 1125), and other adults (AMNH FARB 5027) the dentary is dorsoventrally deep, whereas it is shallow in small juveniles (LACM 28,471) and intermediate in height in large juveniles (CMNH 7541) (Carr, 2020). The ratio of the rostral end of the dentary through the chin to the maximum height of the bone is nearly constant across all growth stages in *T. rex*: in CM 9380, the ratio is 64% to 72%, which overlaps with that seen in juveniles (BMRP 2002.4.1), young adults

(MOR 1125), and most other adults (MOR 980). In one adult (NHMUK R7994) the ratio is high, at 82%, whereas in another (MOR 555) the ratio is low, at 57%.

In lateral view in CM 9380 (Figure 18A), young adults (UWBM 99,000), and other adults (AMNH FARB 5027) the rostral margin of the bone (from the chin to the alveolar margin) extends at a steep angle (more dorsal than rostral); the steep angle of the rostral margin is enhanced by the dorsal and ventral margins of the bone that diverge from each other as they extend rostrally (Carr, 2020). In contrast, in juveniles (LACM 28,471), young adults (MOR 1125), and some adults (MOR 008) the margin extends at a low angle (more rostral than dorsal) (Carr, 2020).

The deepest point of curvature along the alveolar margin in CM 9380 (Figure 18A), young adults (MOR 1125), and other adults (AMNH FARB 5027) is at alveolus 9, whereas in juveniles (BMRP 2002.4.1) it is at alveoli 10 and 11, and in young adults (UWBM 99,000) and some adults (MOR 555) it is at alveolus 8 (Carr, 2020). In the type (Figure 18A), young adults (MOR 1125), and other adults (MOR 555) the shallowest point of the bone caudal to the chin is at alveoli 7 and 8, whereas in small juveniles (CMNH 7541) and some adults (AMNH FARB 5027) it is at alveolus 9, and in large juveniles (BMRP 2002.4.1) it is at alveoli 10 and 11 (Carr, 2020). In the type, young adults (MOR 1125), and other adults (MOR 980) the ratio of the shallowest point of the dentigerous region to the length of the tooth row is 28% or greater (31% in CM 9380), whereas in juveniles (BMRP 2002.4.1) it is 21% (Carr, 2020).

In lateral view in CM 9380 (Figure 18A), small juveniles (CMNH 7541), young adults (MOR 1125), and other adults (MOR 555) the convex margin of the tooth row extends caudally to alveolus 7, whereas in large juveniles (BMRP 2002.4.1), young adults (UWBM 99,000), and some adults (AMNH FARB 5027) it extends to alveolus 8, and in one adult (MOR 008) it extends to alveolus 9 (Carr, 2020). In the type (Figure 18A), young adults (MOR 1125), and other adults (AMNH FAR 5027) the ventral margin of the bone extends uninterrupted to the chin, whereas in juveniles (BMRP 2002.4.1) and young adults (LACM 150,167) the margin is concave as it approaches the chin (Carr, 2020).

In dorsal view in CM 9380, young adults (MOR 1125), and other adults the dentigerous region of the bone curves rostromedially towards the symphysis, whereas the region is straight in juveniles (BMRP 2002.4.1) (Carr, 2020). In the type, young adults (UWBM 99,000), and some adults (MOR 555) the lateral surface of the bone is widest at the rostral and caudal ends of the tooth row, whereas in juveniles (AMNH FARB 5050) it is

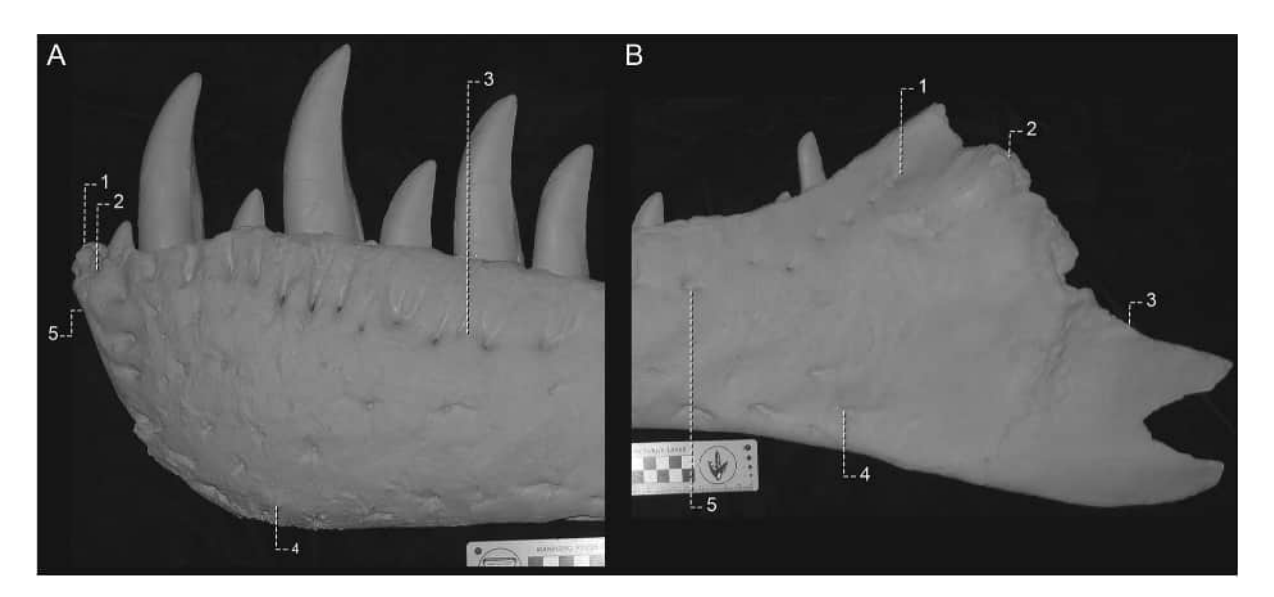


Figure 19. Detail of the rostral region of the left dentary of CM 9380 in (A) lateral view; numbers correspond to the following features: 1, first alveolus is expressed as a shallow dimple; 2, enlarged rostral foramen faces more rostrally than laterally; 3, sulcus of dorsal row of foramina is subtle but present; 4, region of chin is coarsely rugose; 5, rostral margin is subtly concave. (B) detail of the caudal region of the left dentary of CM 9380 in lateral view; numbers correspond to the following features: 1, sulcus of last foramen of the dorsal row emits a dorsoventrally deep sulcus and the foramen is positioned caudal to the last dental alveolus; 2, proximal end of the joint surface for the surangular is mediolaterally wide; 3, caudal margin of the caudal plate is deeply concave; 4, last foramen of the ventral row is positioned rostral to the last alveolus; 5, ventral-most foramen of the dorsal row is at less than 40% of the total height of the bone below its dorsal edge. Scale bar equals 10 cm.

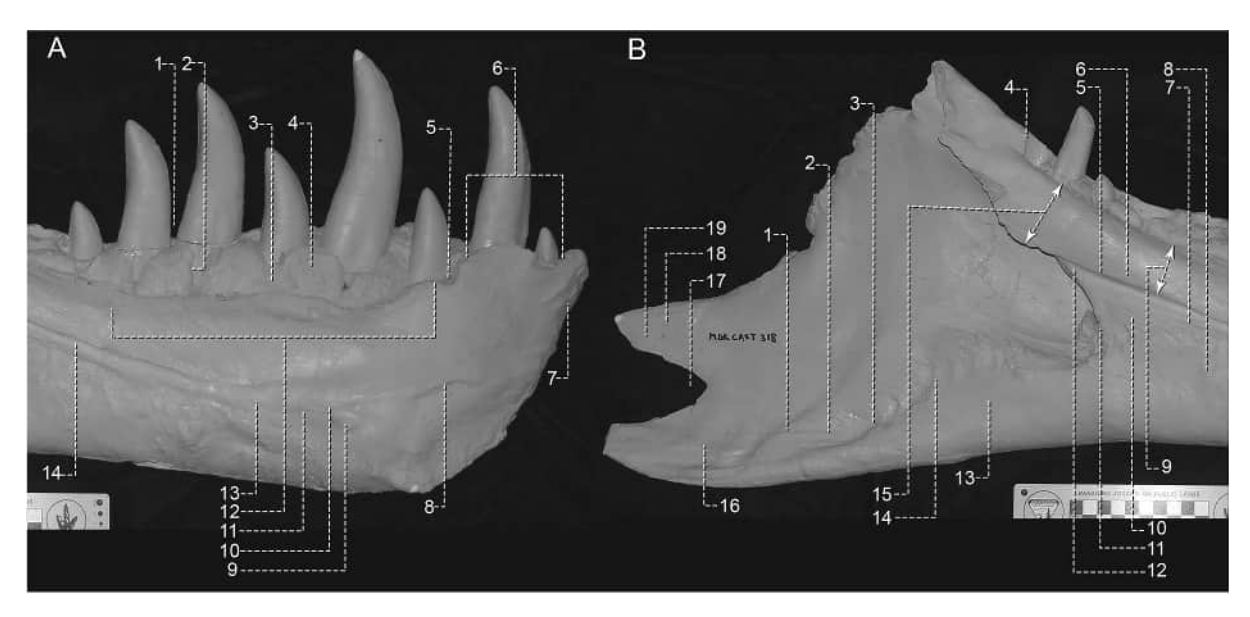


Figure 20. Detail of (A) the rostral region of the left dentary of CM 9380 in medial view; numbers correspond to the following features: 1, alveolus length decreases at alveoli 6 and 7; 2, notches present in rostral margins of interdental plates in the midregion of the tooth row; 3, more than two adjacent plates contact each other; 4, interdental plates are large and they do not approach the dorsal margin of the bone; 5, deep notch at rostral end of the joint surface for the intercoronoid; 6, combined lengths of the first two alveoli are longer than the third; 7, symphysis is fringed by low ridges; 8, Meckelian groove rostrodorsal to the Meckelian foramen is deeply inset; 9. Meckelian foramen is below alveolus 4: 10. rugose patch is situated caudodorsal to the Meckelian foramen; 11, ventral margin of the Meckelian groove reaches the Meckelian foramen; 12, coarse patch on lingual bar; 13, rostral end of the Meckelian groove is at the midheight of the bone; 14, Meckelian groove is deeply inset. (B) detail of the caudal region of the left dentary of CM 9380 in medial view; numbers correspond to the following features: 1, elevated joint surface is present dorsal to the ventral bar; 2, ridges of the joint surface for the splenial are distinct; 3, peg-in-socket joint surface for the splenial; 4, caudal edge of last alveolus extends steeply caudodorsally; 5, dorsal edge of the Meckelian groove is not enclosed by a ridge; 6, joint surface for the splenial on the lingual bar is deeply inset; 7, ventral margin of Meckelian groove is enclosed by a distinct ridge; 8, proximal end of ventral bar is dorsoventrally deep; 9, 'waist' of the lingual bar; 10, joint surface for the splenial is reinforced by rostroventral ridges; 11, rostral end of the Meckelian fossa is at the level of the 11th tooth; 12, caudal end of the Meckelian groove is above the midheight of the bone; 13, ventral bar below the joint surface for the splenial is dorsoventrally deep; 14, inflection point present in ventral bar; 15, caudal end of the lingual bar is significantly deeper than the 'waist'; 16, ridges extend rostrally from the ventral mandibular fenestra process; 17, external mandibular fenestra is a deep notch; 18, a ridge that extends rostrally from the dorsal process is absent; 19, dorsal process above external mandibular fenestra is present. Scale bar equals 10 cm.

widest at the caudal end of the tooth row, and in young adults (MOR 1125) and some adults (AMNH FARB 5027) it is widest caudally and intermediately wide rostrally (Carr, 2020).

In ventral view in CM 9380, young adults (MOR 1125), and other adults (AMNH FARB 5027) the dentigerous region approximately doubles in width in the rostralmost region, whereas in juveniles (LACM 28,471) it is uniform in the dentigerous region but becomes narrow rostrally (Carr, 2020). In the type, young adults (UWBM 99,000), and other adults (MOR 555) the lateral surface is convex rostrally and concave caudally, whereas in small juveniles (AMNH FARB 5050) it is subtly sinuous and in large juveniles (BMRP 2002.4.1) and one young adult (MOR 1125) it is straight (Carr, 2020).

In rostral view in CM 9380, young adults (MOR 1125), and other adults (AMNH FARB 5027) the bone is wide, where the lateral margin is convex, whereas in juveniles the bone is narrow and the lateral surface is flat (Carr, 2020).

7.2. Chin

In lateral view, the chin in CM 9380 (Figure 18A), juveniles (LACM 28,471), young adults (MOR 1125), and some adults (MOR 555) is positioned below the fourth alveolus, whereas it is positioned rostrally below the

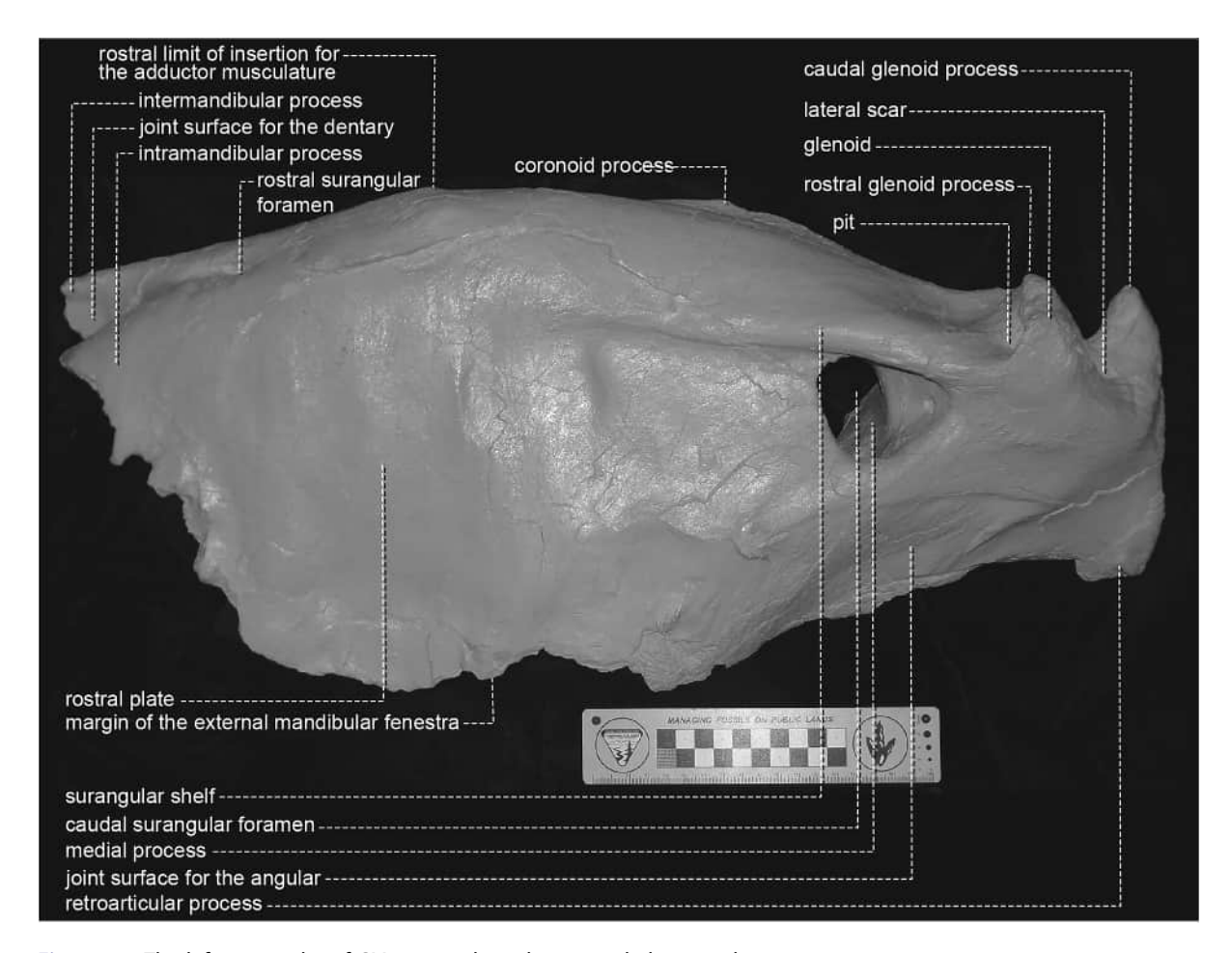


Figure 21. The left surangular of CM 9380 in lateral view, scale bar equals 10 cm.

third alveolus in other adults (AMNH FARB 5027) (Carr, 2020). In medial view, the chin in the type (Figure 18B), young adults (MOR 1125), and other adults (AMNH FARB 5027) is enhanced by the presence of a distinct flange that is located rostroventral to the Meckelian foramen, whereas the flange is low in juveniles (LACM 28,471) and in some adults (LACM 23,844) (Carr, 2020). In the type (Figure 19A), young adults (UWBM 99,000), and some adults (AMNH FARB 5027) the rostral margin below the enlarged rostral foramen is concave, whereas in juveniles (CMNH 7541), young adults (MOR 1125), and some adults (MOR 008) it is convex and continuous with the rest of the rostral margin of the chin (Carr, 2020).

7.3. Subcutaneous surface

In lateral view in CM 9380 (Figure 19A), young adults (LACM 150,167), and other adults (AMNH FARB 5027) the surface in the region of the chin is highly rugose, whereas it is lightly textured in juveniles (LACM 28,471), young adults (MOR 1125), and one adult (CM 1400) (Carr, 2020).

7.4. Lateral foramina

In lateral view in CM 9380 (Figure 19A) the dorsal row of neurovascular foramina are alternatively united by a groove that is present from the level of alveoli four to six on the left side, and at the level of the first six alveoli on the right side (Carr, 2020). A partial groove is also seen in young adults (MOR 1125) and other adults (AMNH FARB 5027). The groove is absent from small juveniles (LACM 28,471), whereas it is present along the entire foramen row in large juveniles (BMRP 2002.4.1) (Carr, 2020).

In lateral view in CM 9380 (Figure 19A), young adults (MOR 1125), and other adults (AMNH FARB 5027) the enlarged rostral foramen faces more rostrally than laterally, whereas in juveniles (CMNH 7541) it faces more laterally than rostrally (Carr, 2020). The last foramen of the dorsal row in the type (Figure 19B), young adults (LACM 150,167), and other adults (AMNH FARB 5027) emits a dorsoventrally deep sulcus, whereas in juveniles (AMNH FARB 5050), young adults (MOR 1125), and one adult (MOR 555) it is shallow (Carr, 2020). In the type (Figure 19B), large juveniles (BMRP 2002.4.1), young adults (LACM 150,167), and other adults (AMNH FARB 5027) the last foramen is positioned caudal to the last alveolus, whereas in small juveniles (AMNH FARB 5050) and one young adults (MOR 1125) it is positioned beside the alveolus (Carr, 2020).

In lateral view in CM 9380 (Figure 18A), young adults (MOR 1125), and other adults (AMNH FARB 5027) the ventralmost foramen of the dorsal row is less than 40% of the depth of the bone (i.e. close to dorsal margin), whereas in juveniles (BMRP 2002.4.1) it is greater than 40% of the height of the dentigerous region (i.e. far ventral to dorsal margin) (Carr, 2020).

In lateral view in the type (Figure 19B), large juveniles (BMRP 2002.4.1), young adults (MOR 1125), and other adults (AMNH FARB 5027) the last foramen of the ventral row is positioned ahead of the last alveolus, whereas in small juveniles (AMNH FARB 5050) and some adults (MOR 555) it is below the alveolus (Carr, 2020).

7.5. Interdental plates

In medial view in CM 9380 (Figures 18(B), 20(A)), large juveniles (BMRP 2002.4.1), young adults (MOR 1125), and other adults (FMNH PR2081) the interdental plates are large, whereas in small juveniles (AMNH FARB 5050) they are small triangular spikes situated at the base of the interdental septa (Carr, 2020). In the type (Figures 18(B), 20(A)), young adults (TMP 1981.006.0001), and other adults (MOR 555) the interdental dates are not situated close to the alveolar margin of the bone, whereas in juveniles (LACM 28,471), young adults (MOR 1125), and in one adult (MOR 008), the plates are situated close to the alveolar margin (Carr, 2020). Regardless of their height, the plates are large in the type (Figures 18(B), 20(A)) and in all growth stages, aside from small juveniles (AMNH FARB 5050) (Carr, 2020).

In CM 9380 (Figure 20A), young adults (MOR 1125), and other adults (MOR 555) more than two plates touch each other, whereas in small juveniles (AMNH FARB 5050) they are separate from each other, in large juveniles (BMRP 2002.4.1) and one adult (NMMNH P-3698) two plates touch each other (Carr, 2020). In the type (Figure 20A), large juveniles (BMRP 2002.4.1), young adults (MOR 1125), and other adults (RSM 2523.8) the rostral margin of the plates in the midregion of the tooth row are notched, whereas in juveniles (AMNH FARB 5050) and some adults (MOR 555) notches are absent (Carr, 2020).

7.6. Lingual bar

In medial view in CM 9380 (Figure 20B), young adults (UWBM 99,000), and other adults (MOR 555) the joint surface for the intercoronoid on the dorsal edge of the free end of the bar is displaced dorsally by a ridge, whereas in juveniles (BMRP 2002.4.1), some young adults (MOR 1125), and some adults (FMNH PR2081) it is not displaced dorsally (Carr, 2020). In the type (Figure 20A), young adults (MOR 1125), and other adults (MOR 555) a distinct coarse patch is present below alveoli three to six (three to seven in CM 9380), whereas in juveniles (BMRP 2002.4.1) a patch is absent (Carr, 2020). In the type (Figure 20B), young adults (MOR 1125), and other adults (MOR 555) the bar rostrodorsal to the joint surface for the splenial is dorsoventrally shallow, producing a 'waist' in the bar, whereas in juveniles (AMNH FARB 5050) the bar has a constant depth and so lacks a 'waist' (Carr, 2020).

In CM 9380 (Figures 18(B), 20(A)), young adults (UWBM 99,000), and other adults (MOR 980) the notch at the rostral end of the joint surface for the intercoronoid is dorsoventrally deep, whereas in juveniles (BMRP 2002.4.1), young adults (MOR 1125), and some adults (MOR 555) it is shallow (Carr, 2020). In the type (Figures 18(B), 20(B)), young adults (UWBM 99,000), and other adults (MOR 555) the caudal end of the bar below the last alveoli is one-third deeper relative to the shallowest point of the bar, whereas in juveniles (BMRP 2002.4.1) and young adults (MOR 1125) it is only moderately deeper (Carr, 2020). In the type (Figures 18(B), 20(B)), young adults (MOR 1125), and other adults (AMNH FARB 5027) the caudal end of the bar is shallow between the intercoronoid and Meckelian groove, whereas it is deep in juveniles (AMNH FARB 5050) (Carr, 2020).

In dorsal view in CM 9380, young adults (MOR 1125), and other adults (MOR 555) the bar is widened medially, whereas in juveniles (AMNH FARB 5050) it is narrow along its entire length (Carr, 2020). In the type, young adults (MOR 1125), and other adults (MOR 555) the joint surface for the intercoronoid is distinct and caudal to the midregion it is a wide and medioventrally sloping joint surface and rostrally it is wide and coarse; in contrast, in juveniles (AMNH FARB 5050) it is narrow and indistinct along the top of the lingual bar (Carr, 2020).

7.7. Meckelian groove

In medial view the Meckelian groove in CM 9380 (Figures 18(B), 20), juveniles (AMNH FARB 5050), young adults (MOR 1125), and adults (AMNH FARB 5027) is deeply inset, whereas the groove is shallowly inset in small juveniles (LACM 28,471) (Carr, 2020). In the type (Figures 18(B), 20(A)) and other adults (AMNH FARB 5027) the groove is positioned at the midheight of the bone rostrally, and it is above the midheight caudally (Figures 18(B), 20(B)); in contrast, the groove in small juveniles (AMNH FARB 5050) is below midheight rostrally and at the midheight caudally, and in large adults (BMRP 2002.4.1), young adults (MOR 1125), and some other adults (FMNH PR2081) it is below midheight rostrally and above midheight caudally (Carr, 2020).

In CM 9380 (Figure 20B), young adults (MOR 1125), and other adults (AMNH FARB 5027) the dorsal margin of the proximal end of the groove is not bounded by a ridge, whereas in juveniles (BMRP 2002.4.1), young adults (UWBM 99,000), and one adult (FMNH PR2081) it is bounded by a sharp, ventrally-extending and blade-like ridge (Carr, 2020). In the type (Figure 20B), young adults (MOR 1125), and other adults (MOR 555) the proximal end of the ventral margin is delimited by a distinct ridge, whereas in juveniles (AMNH FARB 5050) a ridge is absent (Carr, 2020).

In CM 9380 (Figures 18(B), 20(A)), young adults (MOR 1125), and other adults (AMNH FARB 5027) the ventral margin of the groove extends ahead of the joint surface for the splenial and closely approaches the Meckelian foramen, whereas in juveniles (AMNH FARB 5050) it fades ahead of the joint surface (Carr, 2020). In the type (Figures 18(B), 20(A)), young adults (MOR 1125), and other adults (MOR 555) the rostral end of the groove that extends rostrodorsal to the Meckelian foramen is deeply inset, whereas in juveniles (BMRP 2002.4.1), young adults (UWBM 99,000), and some adults (MOR 980) is shallowly inset (Carr, 2020).

7.8. Meckelian foramen

In medial view in CM 9380 (Figures 18(B), 20(A)), young adults (MOR 1125) and other adults (AMNH FARB 5027) the foramen is below alveolus four, whereas in juveniles (BMRP 2002.4.1), and one adult (MOR 555) it is below alveolus five (Carr, 2020). In the type (Figure 20A), young adults (UWBM 99,000), and other adults (MOR 555) the rugosity associated with the foramen is located caudodorsal to the opening, whereas in juveniles (BMRP 2002.4.1) and some adults (NHMUK R7994) it is rostrodorsal to the foramen (Carr, 2020).

7.9. Ventral bar

In medial view, the rostral end of the ventral bar in CM 9380 (Figures 18(B), 20(A)), young adults (MOR 1125), and other adults (AMNH FARB 5027) is expanded into a medially-extending lump; in contrast, the lump is absent in juveniles (BMRP 2002.4.1) or it is a low swelling in young adults (UWBM 99,000) (Carr, 2020). In the type (Figures 18(B), 20(B)), young adults (MOR 1125), and other adults (AMNH FARB 5027) the proximal end of the bar is deep in that it is approximately a third deeper than the distal end of the bar, whereas in juveniles it is shallow and is not significantly deeper than the distal end of the bar (Carr, 2020). In the type (Figures 18 (B), 20(B)), young adults (MOR 1125), and other adults (AMNH FARB 5027) the bar is significantly deeper than the caudal end of the lingual bar, whereas in juveniles (LACM 28,471) it is less than or marginally deeper than the lingual bar rostrally (Carr, 2020). In the type (Figures 18(B), 20(B)), young adults (MOR 1125), and other adults (AMNH FARB 5027) the bar below the Meckelian fossa is dorsoventrally deep, whereas in juveniles (AMNH FARB 5050) and subadults (LACM 23,845) it is shallow (Carr, 2020).

In CM 9380 (Figures 18(B), 20(B)), young adults (MOR 1125), and other adults (MOR 555) the bar below the fossa is tall such that it has a distinct inflection point, whereas in juveniles (AMNH FARB 5050), subadults (LACM 23,845), and subadults (TMP 1981.006.0001) it is shallow and has only a subtle inflection point (Carr, 2020). In the type (Figures 18(B), 20(B)), young adults (MOR 1125), and other adults (MOR 555) the lingual and ventral bars split from each other below alveoli 10 to 11, whereas in juveniles (BMRP 2002.4.1) and one adult (FMNH PR2081) they separate below alveolus 13 or 14 (Carr, 2020).

7.10. Symphysis

In medial view, the rostral margin of the symphysis in CM 9380 (Figure 20A), young adults (MOR 1125), and other adults (AMNH FARB 5027) is fringed by a series of ridges; in contrast, a low irregular ridge is seen in juveniles (BMRP 2002.4.1) and in one young adult (LACM 150,167) (Carr, 2020).

7.11. Caudal plate

In lateral and medial views in CM 9380 (Figure 18), young adults (MOR 1125), and other adults (AMNH FARB 5027) the margin of the external mandibular fenestra is a deep notch that produces a distinct dorsal process above the opening, a condition seen in all adults (Carr, 2020). In contrast, the margin of the fenestra is a shallow fenestra and the dorsal process is absent from juveniles (CMNH 7541) (Carr, 2020).

In lateral view in CM 9380 (Figure 19B), young adults (MOR 1125), and other adults (MOR 555) the ridge that extends rostrally from the dorsal process of the external mandibular fenestra is absent, whereas in juveniles (CMNH 751) and one adult (FMNH PR2081) it is present (Carr, 2020). Also, in medial view in the type (Figure 20B), young adults (UWBM 99,000), and other adults (MOR 555) prominent ridges extend rostrally from the region of the external mandibular fenestra and ventral mandibular fenestra process, whereas in juveniles (BMRP 2002.4.1) and young adults (MOR 1125) they are absent or indistinct (Carr, 2020).

In CM 9380 and other adults (MOR 980) the secondary intermandibular process is present, whereas it is absent from juveniles (BMRP 2002.4.1), young adults (LACM 150,167), and one adult (FMNH PR2081), and in young adults (MOR 1125) it is represented by a low ridge (Carr, 2020). In the type (Figure 18), young adults (LACM 150,167), and other adults (MOR 555) the caudal margin of the plate is deeply concave, whereas in juveniles (BMRP 2002.4.1), young adults (MOR 1125), and one adult (SDSM 12,047) it is straight to subtly concave (Carr, 2020).

In ventral view in CM 9380 and other adults (FMNH PR2081) the ventral surface of the plate extends to its lateral edge, whereas in juveniles (AMNH FARB 5050) it is limited to the medial edge (Carr, 2020). In caudolateral view in the type, young adults (UWBM 99,000), and other adults (MOR 980) the caudodorsolateral edge is a caudally convex, mediolaterally wide, and coarse joint surface for the surangular, whereas in juveniles (BMRP 2002.4.1), young adults (MOR 1125), and other adults (MOR 555) it is a narrow and blade-like edge (Carr, 2020).

In medial view in CM 9380 (Figures 18(B), 20(B)), young adults (UWBM 99,000), and other adults (MOR 555) there is an elevated joint surface along the caudoventrally extending part of the ventral bar, whereas in juveniles (BMRP 2002.4.1) and young adults (MOR 1125) it is absent (Carr, 2020). In the type (Figures 18(B), 20 (B)), young adults (MOR 1125), and other adults (MOR 980) the ridges that extend dorsal and caudodorsal to the ventral bar in the region of the joint surface for the splenial are prominent, whereas in juveniles (AMNH FARB 5050) they are absent or indistinct (Carr, 2020).

7.12. Meckelian fossa

In medial view in CM 9380 (Figures 18(B), 20(B)), young adults (MOR 1125), and other adults (MOR 555) the rostral margin of the fossa extends ventromedially to blend with the dorsomedial edge of the ventral bar, whereas in juveniles (AMNH FARB 5050) and some adults (MOR 008) it extends ventrolaterally (Carr, 2020). In the type, young adults (MOR 1125), and other adults (MOR 555) there are two pits lateral to the ridge that extends to the ventral bar, whereas one large pit is seen in juveniles (BMRP 2002.4.1) (Carr, 2020).

In medial view in CM 9380 (Figures 18(B), 20(B)) and other adults (MOR 555) the rostral margin of the fossa stops below the second to fourth last dentary tooth (below third [L] or fourth [R] in the type), whereas in juveniles (BMRP 2002.4.1) and young adults (LACM 150,167) it is below tooth four or higher (Carr, 2020). In



the type (Figures 18(B), 20(B)), young adults (MOR 1125), and other adults (MOR 555) the tooth root bulges in the rostrodorsal corner of the fossa bulge ventrally below the level of the Meckelian groove, whereas in juveniles (AMNH FARB 5050) they do not extend below the level of the groove (Carr, 2020).

In caudal view in CM 9380, young adults (MOR 1125), and other adults (MOR 555) the fossa is rectangular in outline owing to a wide ventral shelf, whereas in juveniles (BMRP 2002.4.1) it is triangular (Carr, 2020).

7.13. Joint surface for the splenial

In medial view, the joint surface for the splenial in CM 9380 (Figures 18(B), 20(B)), young adults (MOR 1125), and other adults (MOR 980) is a coarse peg-in-socket contact below the Meckelian fossa, whereas in juveniles (BMRP 2002.4.1), some young adults (UWBM 99,000) and adults (MOR 555) the contact is secured by longitudinal ridges and grooves (Carr, 2020).

In CM 9380 (Figure 20B), young adults (UWBM 99,000), and other adults (MOR 555) the joint surface on the lingual bar is distinct and deeply inset, whereas in juveniles (AMNH FARB 5050) it is indistinct, and in some young adults (MOR 1125) and some adults (FMNH PR2081) it is a flat elevation (Carr, 2020). In caudomedial view in the type, young adults (MOR 1125), and other adults (MOR 555) the rostromedial edge of the joint surface for the splenial has the form of a socket, whereas in juveniles (AMNH FARB 5050) it is a groove (Carr, 2020). In medial view in CM 9380 (Figure 20B), young adults (UWBM 99,000), and other adults (MOR 555) the joint surface ahead of the Meckelian fossa is reinforced by rostroventrally trending grooves and ridges, whereas in juveniles (AMNH FARB 5050), young adults (MOR 1125), and one adult (CM 1400) the joint surface is nearly smooth or it is a coarse facet (Carr, 2020).

7.14. Alveoli

In dorsal view in CM 9380, young adults (LACM 150,167), and other adults (AMNH FARB 5027) the first open alveolus is substantially smaller than the second and third alveoli, whereas in juveniles (LACM 28,471) and in young adults (MOR 1125) the first two open alveoli are substantially smaller than the third alveolus (Carr, 2020). Also, the combined lengths of the first two alveoli in the type, young adults (MOR 1125), and other adults (AMNH FARB 5027) are longer than the third alveolus, which is seen in most other adults (Carr, 2020). In contrast, the first two alveoli are the same length as the third in juveniles (LACM 28,471) and in one young adult (LACM 150,167) (Carr, 2020).

In the type, young adults (UWBM 99,000), and other adults (AMNH FARB 5027) the first tooth is small and the second and third teeth are twice as large and similar in length to each other, whereas in juveniles (LACM 28,471) and young adults (MOR 1125) the first three teeth increase incrementally in size from mesially to distally (Carr, 2020).

In dorsal view the type, young adults (MOR 1125), and other adults (AMNH FARB 5027) the dentigerous region of the bone curves rostromedially towards the symphysis as in other adults, whereas in juveniles (BMRP 2002.4.1) the row of alveoli is straight (Carr, 2020). In the type (Figure 19A), young adults (MOR 1125), and other adults (AMNH FARB 5027) the first alveolus is

Table 6. Measurements (in millimetres) of the left surangular of the type specimen of tyrannosaurus rex (CM 9380). All measurements were taken three times to the nearest hundredth, and the mean is documented here. Asterisk (*) indicates measurement taken to the nearest millimetre, tilde (~) indicates measurement taken once.

Structure measured	Measurement (mm)
Caudal surangular foramen, dorsoventral height	50.6
Caudal surangular foramen, rostrocaudal length	68.3
Bone, maximum length	642*
Dorsoventral height through lateral glenoid fossa	116.9
Dorsoventral height through caudal glenoid process	153.4
Surangular shelf, dorsoventral height above caudal surangular foramen	25.6
Length caudal to caudal surangular foramen	140.4
Joint surface for the angular, rostrocaudal length	417.3*
Mediolateral width above caudal surangular foramen	78.3
Foramen within caudal surangular foramen, length	6.3
Foramen within caudal surangular foramen, height	8.4~

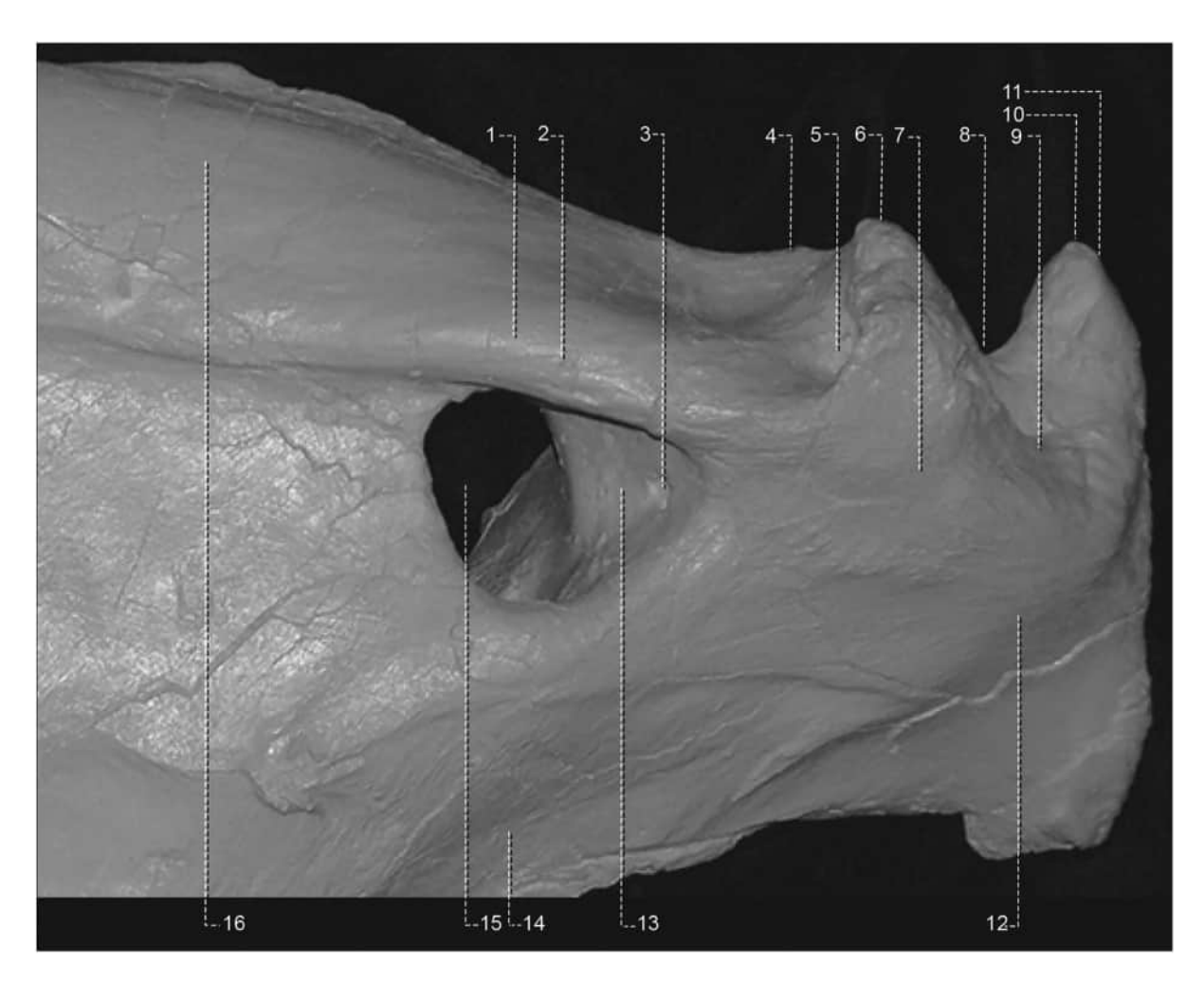


Figure 22. Detail of the glenoid region of the left surangular of CM 9380 in lateral view; numbers correspond to the following features: 1, surangular shelf long axis extends rostrodorsally; 2, surangular shelf extends dorsolaterally; 3, accessory foramen present; 4, rostral glenoid process is continuous with the coronoid process; 5, deep pit in rostral glenoid process is present; 6, rostral glenoid process extends rostrodorsally; 7, surangular shelf fades below glenoid region; 8, glenoid fossa is short and deep; 9, lateral scar is rugose and shallowly inset; 10, caudal glenoid process is as tall as the rostral glenoid process; 11, caudal glenoid process is not split by a sulcus; 12, depression-like scar below glenoid region is absent; 13, embayment behind caudal glenoid process is shallow; 14, joint surface for the angular is crossed by an inflection point; 15, caudal surangular foramen is small and situated ahead of the glenoid; 16, coronoid region is dorsoventrally deep.

expressed as a shallow dimple, whereas in juveniles (LACM 28,471) it is present, open, and supports a tooth (Carr, 2020). In CM 9380 the dimples are separated from the first open alveolus by an interdental septum, but there is no interdental plate. Both dimples are expressed as pit that are oriented from distolingually to mesiolabially. On the left side a sulcus connects the dimple to the first foramen of the alveolar row, whereas on the right side they are separated by a ridge. On both sides the dimples are positioned medial to the foramen and rostral to the first open alveolus, and they are rostrocaudally shorter (L: 4 mm, R: 8 mm) than lateromedially wide (L: 12 mm, R: 15 mm).

In dorsal view in CM 9380, juveniles (BMRP 2002.4.1), young adults (MOR 1125), and some adults (MOR 555) alveolus length begins to decrease at alveoli six to seven, whereas in young adults (UWBM 99,000) and some adults (MOR 980) length decreases at alveoli four to five (Carr, 2020). In medial view in the type (Figure 20B), young adults (UWBM 99,000), and other adults (MOR 980) the caudal margin of the last alveolus extends vertically or at a steep caudodorsal angle (steep in CM 9380), whereas it extends at a low angle caudodorsally in juveniles (BMRP 2002.4.1) and young adults (MOR 1125) (Carr, 2020).

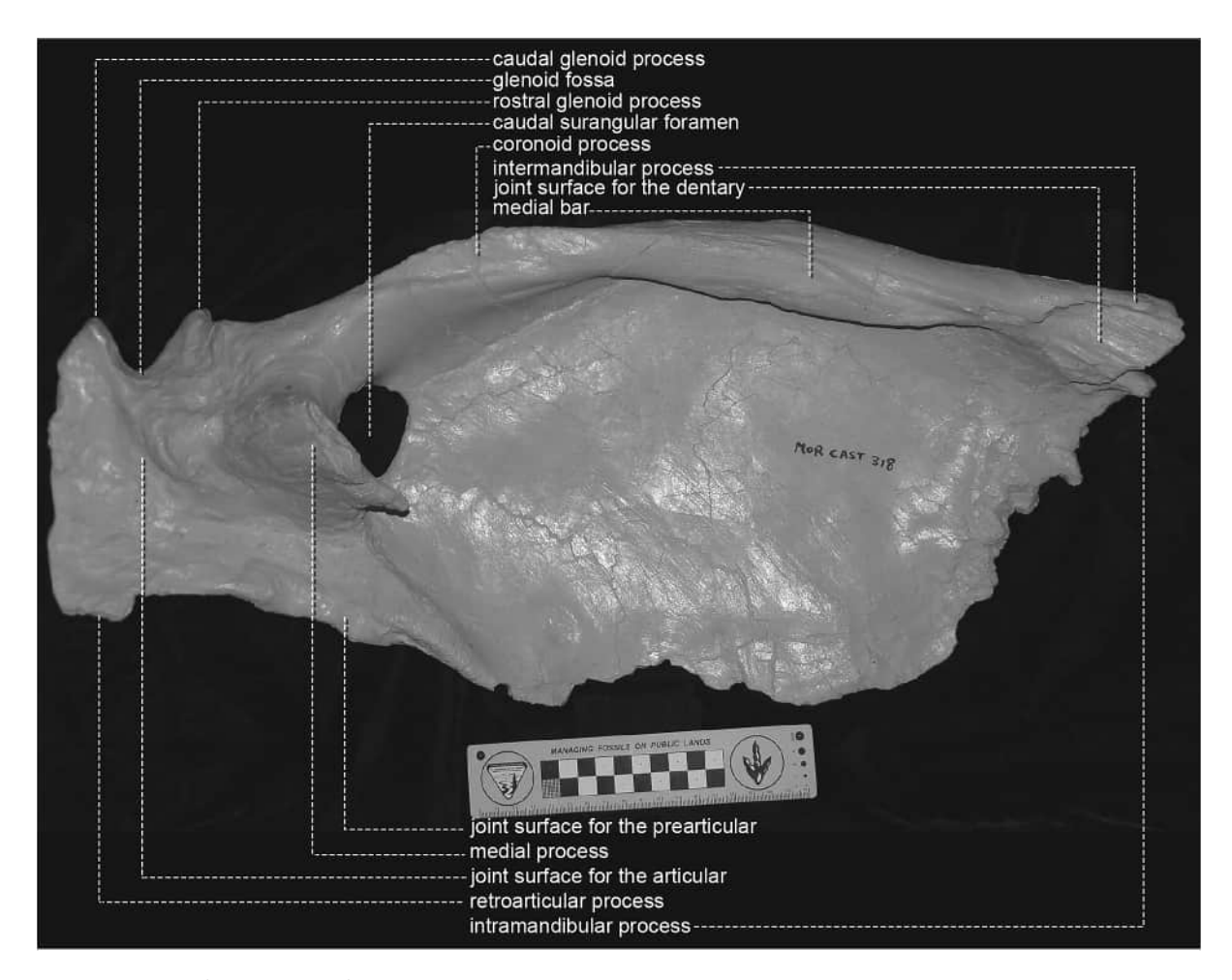


Figure 23. The left surangular of CM 9380 in medial view, scale bar equals 10 cm.

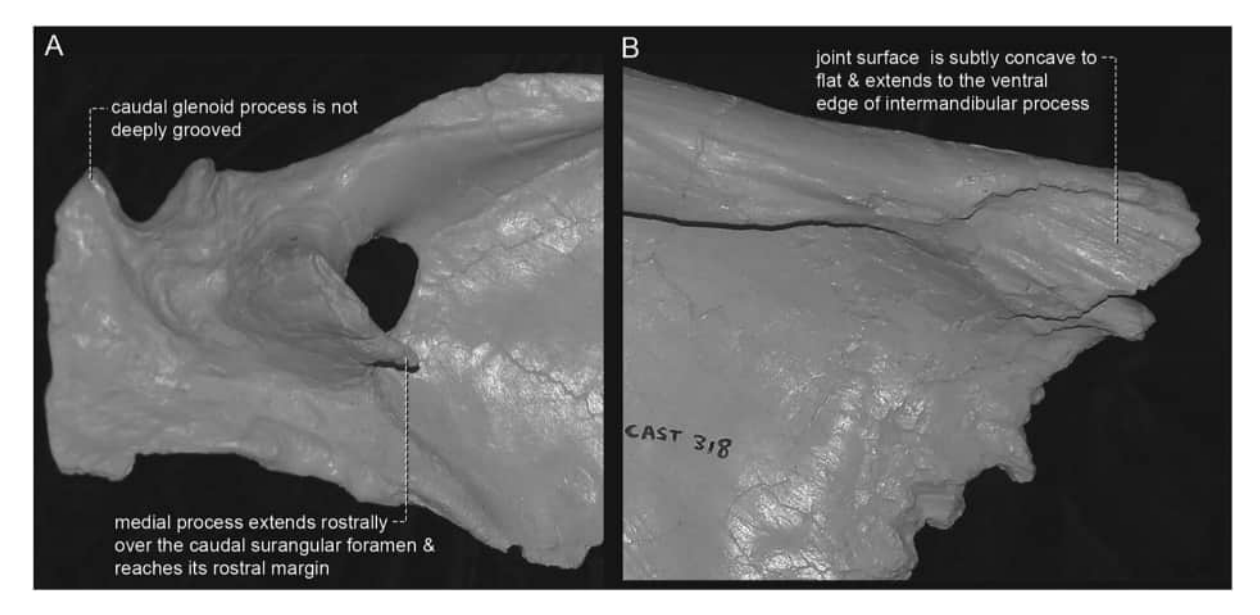


Figure 24. Detail of (A) the glenoid region of the left surangular of CM 9380 in medial view, and (B) the rostral region of the left surangular of CM 9380 in medial view, scale bar equals 10 cm.



In dorsal view in CM 9380, young adults (MOR 1125), and some adults (RSM 2523.8) more than seven interdental septa extend rostrolaterally, whereas in juveniles (BMRP 2002.4.1) and some adults (MOR 555) the first seven extend rostrolaterally, and in some young adults (UWBM 99,000) and some adults (AMNH FARB 5027) less than the first seven septa extend rostrolaterally (Carr, 2020).

7.15. Lesions

In the right dentary there are two remodelled gouges on the lower margin of the bone below the third and fourth alveoli.

8. Surangular

8.1. General description

In CM 9380 the left surangular is preserved; measurements of the bone are given in Table 6. In lateral view in CM 9380 (Figure 21), subadults (LACM 23,845), young adults (MOR 1125), and other adults (AMNH FARB 5027) the bone is dorsoventrally deep, whereas it is shallow in juveniles (CMNH 7541) (Carr, 2020).

8.2. Surangular shelf

In lateral view in CM 9380 (Figures 21, 22) and one other adult (MOR 008), the surangular shelf extends dorsolaterally, whereas the shelf extends laterally in juveniles (LACM 28,471), subadults (LACM 23,845), and young adults (UWBM 99,000) (Carr, 2020). In other adults, the shelf extends lateroventrally (AMNH FARB 5027) (Carr, 2020). In the type (Figures 21, 22), subadults (LACM 23,845), young adults (MOR 1125) and other adults (AMNH FARB 5027) the rostrocaudal orientation of the shelf extends rostrodorsally (Carr, 2020). In one adult, LACM 23,844, it extends rostroventrally on the left side and rostrodorsally on the right (Carr, 2020). In contrast, in juveniles (CMNH 7541) and in some young adults (LACM 150,167) the shelf extends horizontally (Carr, 2020).

In lateral view in CM 9380 (Figure 21), subadults (LACM 23,845), young adults (MOR 1125), and other adults (AMNH FARB 5027) the shelf extends to the level of the external mandibular fenestra before fading, whereas in juveniles (BMRP 2002.4.1) and one young adult (UWBM 99,000) it stops short of the fenestra (Carr, 2020). In the type (Figure 22) and juveniles (LACM 28,471) the shelf fades caudally below the glenoid region, whereas in young adults (MOR 1125) and other adults (AMNH FARB 5027) it is wide and differentiated below the region (Carr, 2020).

8.3. Glenoid region

In lateral view in CM 9380 (Figures 21, 22), large juveniles (BMRP 2002.4.1), and other adults (MOR 980) the scar below the glenoid region is rugose in texture and shallowly excavated into the bone, whereas in small juveniles (LACM 28,471) it is smooth and shallow, and in young adults (MOR 1125) and some adults (AMNH FARB 5027) it is rugose and deep (Carr, 2020).

In lateral view in CM 9380 (Figures 21, 22), young adults (MOR 1125), and other adults (AMNH FARB 5027) the glenoid is rostrocaudally short and dorsoventrally deep, whereas in juveniles (LACM 28,471) it is long and shallow (Carr, 2020). In the type (Figures 21, 22), young adults (MOR 1125), and other adults (AMNH FARB 5029) a distinct muscle scar below the lateral scar is absent, whereas a distinct depression-like scar is seen in juveniles (BMRP 2002.4.1) and some adults (AMNH FARB 5027) (Carr, 2020). The scar is vanishingly shallow in one young adult (UWBM 99,000) (Carr, 2020).

8.4. Rostral glenoid process

In dorsal view in CM 9380, young adults (MOR 1125), and other adults (AMNH FARB 5027) the process is wide and extends to the coronoid process, whereas in juveniles (LACM 28,471) it is narrow and does not extend to the process (Carr, 2020). In the type (Figures 21, 22), young adults (MOR 1125), and

other adults (AMNH FARB 5027) the rostral glenoid process is penetrated by a large and deep pit, whereas in juveniles (LACM 28,471) it is pierced by a small foramen (Carr, 2020). In one adult (FMNH PR2081) it is excavated by a large and deep concavity (Carr, 2020). In lateral view in CM 9380 (Figures 21, 22), juveniles (LACM 28,471), young adults (MOR 1125), and other adults (AMNH FARB 5027) the process extends rostrodorsally, whereas in one juvenile (BMRP 2002.4.1) it extends dorsally (Carr, 2020).

8.5. Caudal glenoid process

In lateral view in CM 9380 (Figures 21, 22), juveniles (LACM 28,471), young adults (MOR 1125), and other adults (AMNH FARB 5027) the caudal process is as tall as the rostral process, whereas in one juvenile (BMRP 2002.4.1) it is shorter than the rostral process (Carr, 2020). In the type (Figures 21, 22), juveniles (LACM 28,471), young adults (MOR 1125), and other adults (AMNH FARB 5029) the apex of the process is not split into two parts by a sulcus, whereas it is split in one juvenile (BMRP 2002.4.1) (Carr, 2020). In medial view in CM 9380 (Figures 23, 24(A)), subadults (LACM 23,845), young adults (MOR 1125), and other adults (MOR 980) the medial surface of the process is not deeply grooved, whereas it is deeply grooved by a pair of sulci in one juvenile (BMRP 2002.4.1) (Carr, 2020).

8.6. Caudal surangular foramen

In lateral and medial views in CM 9380 (Figures 21, 23), subadults (LACM 23,845), young adults (LACM 150,167), and other adults (MOR 980) the caudal surangular foramen is small in size, which is seen in other adults; in contrast, the opening is large in juveniles (CMNH 7541) and some young adults (MOR 1125) (Carr, 2020). In the type (Figures 21, 22), subadults (LACM 23,845), young adults (MOR 1125) and other adults (MOR 008) the embayment immediately caudal to the foramen is reduced; in contrast, the embayment is present and distinct in juveniles (CMNH 7541), young adults (UWBM 99,000), and in some adults (MOR 980) (Carr, 2020). In lateral view in the type (Figures 21, 22), young adults (MOR 1125), and other adults (AMNH FARB 5027) the foramen is situated far rostral to the glenoid, whereas it is situated partly below the glenoid in juveniles (LACM 28,471) (Carr, 2020).

8.7. Coronoid region

In lateral view in CM 9380 (Figures 21, 22), young adults (MOR 1125), and other adults (AMNH FARB 5027) the coronoid region is deep such that the surangular shelf does not approach the dorsal margin of the bone, whereas the region is shallow and the shelf does approach the dorsal margin in juveniles (CMNH 7541) (Carr, 2020). In the type (Figures 21, 22), subadults (LACM 23,845), young adults (MOR 1125), and other adults (AMNH FARB 5027) the coronoid process is deep and extends caudally to merge with the rostral glenoid process, whereas in juveniles (LACM 28,471) it stops before reaching the glenoid region (Carr, 2020). In medial view in CM 9380 (Figures 23, 24(B)), subadults (LACM 23,845), young adults (MOR 1125), and other adults (AMNH FARB 5027) the coronoid process is distinct rostrally as it extends across the medial bar, whereas it fades rostrally in juveniles (BMRP 2002.4.1) (Carr, 2020).

8.8. Joint surface for the angular

In CM 9380 (Figures 21, 22) and one young adult (MOR 1125) there is an inflection point in the joint surface, where the upper region extends ventromedially and the lower region extends ventrolaterally to vertically, whereas in juveniles (BMRP 2002.4.1), young adults (LACM 150,167), and other adults (LACM 23,844) it extends vertically (Carr, 2020).

8.9. Intermandibular process

In CM 9380 (Figure 24B), young adults (MOR 1125), and other adults (MOR 980) the joint surface on the medial surface of the intermandibular process reaches its ventral edge, whereas in juveniles (BMRP 2002.4.1) a flange extends along the ventral edge of the process, preventing the joint surface from reaching the edge (Carr, 2020).

The joint surface in the type (Figure 24B), young adults (MOR 1125), and other adults (MOR 980) is subtly concave to flat, whereas in juveniles (BMRP 2002.4.1) and one adult (FMNH PR2081) it is deeply concave (Carr, 2020).

8.10. Medial process

In medial view in CM 9380 (Figures 23, 24(A)), juveniles (BMRP 2002.4.1), young adults (UWBM 99,000), and one other adult (LACM 23,844) the medial process extends rostrally over the caudal margin of the caudal surangular foramen, whereas in young adults (MOR 1125) and other adults (MOR 980) it is widely separate from the foramen and extends caudomedially away from it (Carr, 2020). In the type (Figures 23, 24(A)), young adults (MOR 1125), and other adults (AMNH FARB 5027) the process extends rostrally below the foramen, almost reaching or reaching its rostral margin, whereas in juveniles (BMRP 2002.4.1) it extends marginally ahead of the caudal margin (Carr, 2020).

8.11. Retroarticular process

In caudal view in CM 9380, young adults (LACM 150,167), and other adults (AMNH FARB 5027) the medial flange is positioned above the midheight of the process, whereas in juveniles (BMRP 2002.4.1) it is at the midheight, and in some young adults (MOR 1125) it is below the midheight (Carr, 2020).

Table 7. Measurements (in millimetres) of the dentary teeth of the type specimen of tyrannosaurus rex (CM 9380). All measurements were taken three times to the nearest hundredth, and the mean is documented here

Structure measured	Left dentary	Right dentary
Tooth #1, basal crown length	-	17.1
Tooth #1, basal crown width	-	24
Tooth #1, ratio width/length	-	140%
Tooth #2, basal crown length	38.1	-
Tooth #2, basal crown width	35.1	-
Tooth #2, ratio width/length	92%	-
Tooth #3, basal crown length	-	44.6
Tooth #3, basal crown width	-	39.2
Tooth #3, ratio width/length	-	88%
Tooth #4, basal crown length	45.9	-
Tooth #4, basal crown width	38.6	-
Tooth #4, ratio width/length	84%	-
Tooth #5, basal crown length	-	44
Tooth #5, basal crown width	-	33.9
Tooth #5, ratio width/length	-	77%
Tooth #6, basal crown length	42.8	-
Tooth #6, basal crown width	-	-
Tooth #6, ratio width/length	-	-
Tooth #7, basal crown length	36.6	-
Tooth #7, basal crown width	30.1	-
Tooth #7, ratio width/length	82%	-
Tooth #8, basal crown length	-	36.8
Tooth #8, basal crown width	-	-
Tooth #8, ratio width/length	-	-
Tooth #9, basal crown length	-	-
Tooth #9, basal crown width	-	-
Tooth #9, ratio width/length	-	-
Tooth #10, basal crown length	-	30.8
Tooth #10, basal crown width	-	23.3
Tooth #10, ratio width/length	-	76%
Tooth #11, basal crown length	-	-
Tooth #11, basal crown width	-	-
Tooth #11, ratio width/length	-	-
Tooth #12, basal crown length	20.8	-
Tooth #12, basal crown width	15.6	-
Tooth #12, ratio width/length	75%	-
Tooth #13, basal crown length	-	-
Tooth #13, basal crown width	-	-
Tooth #13, ratio width/length	-	-

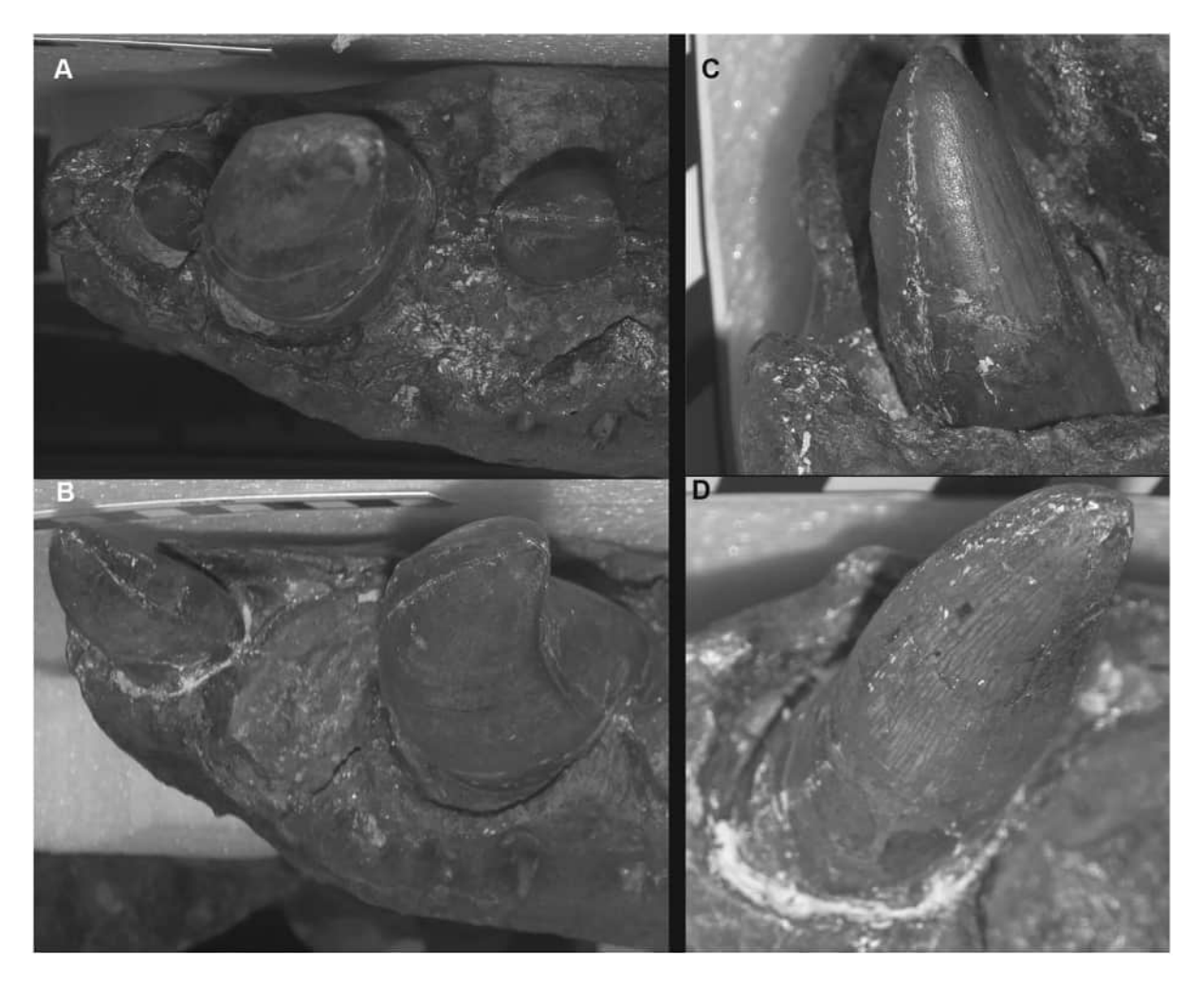


Figure 25. Mesial three alveoli of CM 9380 in (A) left dorsal view and (B) right dorsolateral view. Mesial-most tooth of CM 9380 in (C) left rostrolateral view and (D) right rostrodorsolateral view. Scale bars are in centimetres; right views are reversed for ease of comparison.

9. Dentition

9.1. Maxilla

9.1.1. General description

In CM 9380, there are 12 open alveoli. The dentition is incomplete: the first, third, and fourth teeth are reconstructed in plaster, the eighth, eleventh, and twelfth crowns are missing; the second, seventh, and ninth crowns are represented by their bases; the fifth tooth is not fully erupted; the sixth and tenth crowns are the only erupted teeth, and the sixth tooth is too shattered and plaster-repaired to take measurements.

The maxillary teeth are incrassate (i.e. w/l: 0.65+) (Carr, 2020). The last alveolus in the type and young adults (MOR 1125) is positioned below the last alveolar foramen, whereas in juveniles (RSM 2347.1) it is positioned caudal to the foramen (Carr, 2020). In several adults (AMNH FARB 5027) it is positioned ahead of the foramen (Carr, 2020). In the type, young adults (MOR 1125), and other adults (MOR 008) the mesiodistally longest tooth is at alveolus five to three, whereas in juveniles (BMRP 2002.4.1) it is at the sixth alveolus; the longest tooth in the type was presumably at alveolus 4 (Carr, 2020; Table 1).

9.2. Dentary

9.2.1. General description

In CM 9380, young adults (LACM 150,167), and other adults (MOR 980) there are 13 open alveoli in both dentaries; whereas in juveniles (BMRP 2002.4.1) there are up to 17 alveoli and in some adults (MOR 555) as



few as 12 (Carr, 2020). The mesiodistally longest teeth of the series in the type, young adults (UWBM 99,000), and other adults (AMNH FARB 5027) are at alveolus 5 or less, whereas in juveniles (BMRP 2002.4.1) it is at alveolus 8 (Carr, 2020). The longest tooth in the type is at alveolus 4 (Carr, 2020). Measurements of the dentition of both bones are given in Table 7.

9.2.2. Ratio of first to second tooth

In CM 9380 (Figure 25), young adults (MOR 1125), and other adults (MOR 980) the first dentary tooth is large relative to the second dentary tooth, whereas in juveniles (LACM 28,471), some young adults (LACM 150,167), and some adults (FMNH PR2081) it is half the length of the second tooth (Carr, 2020). The ratio of the first tooth to the second in the type is difficult to quantify since the first tooth is not fully erupted from the left side and the second tooth is missing from the right side.

9.2.3. First tooth morphology

The tooth in CM 9380 (Figure 25), young adults (LACM 150,167), and other adults is subincisiform in shape, whereas it is subconical in juveniles (LACM 28,471) (Carr, 2020). In dorsal view on the left side of the type (Figure 25A, C) the tooth is subincisiform, where the terms mesial and distal do not apply to the carina, and instead here are referred to as labial and lingual in reference to their position relative to the tooth row. The external (labial) surface extends mesiolabially. The labial carina is situated towards the distolabial surface, but well lingual to the external surface of the tooth. The lingual carina is positioned at the lingual margin of the tooth, at the midlength of the crown. The distal surface between the carinae is subtly convex, whereas the external surface is strongly convex.

The first tooth of the right side in dorsal view (Figure 25B) has an oblique (mesiolabial to distolingual) long axis relative to that of the dentary. It is subincisiform (Figure 25D), where the carinae are positioned at the distal end of the crown and the crown distal to them is shorter than the crown ahead of them. The labial carina is along the distolabial surface of the crown, opposite the alveolar septum. The lingual carina is distal to the crown midlength, and it extends basally towards the distolingual corner of the tooth, but does not reach the distal surface. The distal convexity between the carinae is shorter than the convexity ahead of them.

9.2.4. Second tooth morphology

The second dentary tooth in CM 9380 (Figure 25A), young adults (UWBM 99,000), and other adults (AMNH FARB 5027) is incrassate with a distolingual to mesiolabial long axis that displaces the carinae onto the sides of the crown, whereas in small juveniles (LACM 28,471) it is subincisiform and twisted axially, and in large juveniles it is incrassate, blade-like and transitional in form with a mesiodistally oriented long axis (Carr, 2020).

The second tooth of the left side of the type in dorsal view is subconical (Figure 25A). The labial carina extends along the distolabial surface, but ahead of the distal margin of the tooth and distal to the crown midlength. The lingual carina extends mesially ahead of crown midlength to the mesiolingual surface. A distolingual 'heel' (i.e. basal strut) is present (Figure 25A); the mesiolabial corner is the most strongly convex region. The long axis of the crown is oriented oblique to the long axis of the dentary; i.e. from distolingual to mesiolabial.

9.3. Osteological inferences in CM 9380

9.3.1. Premaxilla

The dorsoventrally tall joint surface for the premaxilla on the maxilla indicates that the alveolar region (= body) of the premaxilla was dorsoventrally tall. The coarse subcutaneous surface of the maxilla would have continued onto the premaxilla.

9.3.2. Nasals

The peg-in-socket joint surface for the nasal in the maxilla indicates that the nasals in the type had a reciprocal joint surface. The coarse subcutaneous surface of the maxilla would have continued onto the nasals. The mediolaterally expanded lacrimals indicate that the nasals abruptly tapered in width between those bones.

9.3.3. Jugal

The coarse subcutaneous surface of the maxilla would have continued from the lacrimal and maxilla onto the jugal.

9.3.4. Postorbital

The coarse lateral surface of the squamosal would have continued onto the postorbital. Based on the form of the joint surface for the postorbital on the squamosal, the squamosal process of the postorbital was dorsoventrally deep and extended at a steep caudoventral angle.

9.3.5. Prefrontal

The peg-in-socket form the joint surface for the prefrontal on the lacrimal indicates that the corresponding joint surface on the prefrontal had a complementary joint surface.

9.3.6. Epilacrimal and epipostorbital

The presence of an extensive joint surface on the caudal surface of the lacrimal indicates that the accessory osteoderms were present. The epilacrimal would have been wedged between the lacrimal and postorbital, and the epipostorbital extended from the lateral surface of the postorbital to the caudolateral surface of the lacrimal.

9.3.7. Quadratojugal

The long quadratojugal process of the squamosal indicates that the quadratojugal in CM 9380 had a rostrally-expanded dorsal process, as is seen in other tyrannosaurids.

9.3.8. Splenial

The coarse joint surfaces for the splenial on the dentary had a corresponding form on the splenial.

9.3.9. Angular

The coarse joint surface for the angular on the surangular had a corresponding form on the angular.

10. Discussion

10.1. Diagnosis of tyrannosaurus rex

Based on Carr (2020) and Carr and Napoli et al. (2022) the craniodental diagnostic characters of *T. rex* that can be seen in CM 9380 include: giant size, absence of a swelling on the lateral surface of the supraorbital ramus of the lacrimal (present in *T. bataar*), absence of a subcutaneous ridge along the antorbital fossa (present in *T. bataar*), short ventral ramus of the prefrontal as shown by the joint surface on the lacrimal (long in *T. bataar*), rostral ramus of the lacrimal splits into three processes (two in *T. bataar*), fewer than 15 dentary teeth (15 in *T. bataar*). The maxillary tooth count of 12 in CM 9380 overlaps with that of *T. bataar*, but it is greater than the minimum count (11) of *T. rex*. The dentary tooth count of 13 in CM 9380 is less than that of *T. bataar*, but it is greater than the minimum count (12) of *T. rex*.

10.2. Clarifications

10.2.1. Proportions of the first three dentary teeth

The size of the first three dentary teeth have been a focus of attention given the hypothesis that their sizes are taxonomically informative (Larson, 2008; Paul et al., 2022), although this hypothesis has been challenged (Carr and Napoli et al., 2022). Specifically, the type specimen has been claimed to have a small first tooth, in contrast to much larger second and third teeth, which is thought, in part, to diagnose *T. rex* (Larson, 2008; Paul et al., 2022). Measurements of the left teeth 2 (55 mm) and 3 (54 mm) of the left side were given by Larson (2008) and measurements of the same teeth were given – but transposed – by Paul et al. (2022). The importance of the ratio of the third to the second tooth was to establish the similarity in size between the teeth; i.e. to quantify whether or not the second tooth is significantly smaller than the third. If the second tooth was found to be smaller than the third tooth, then that was taken as evidence of the presence of two small mesial teeth.

Unfortunately, in neither work is it indicated whether or not the measurements correspond to measurements of tooth crowns or to measurements of alveoli (Larson, 2008; Paul et al., 2022).

In the examination of CM 9380 made by Carr and Napoli et al. (2022), it was found that the third tooth of the left side is an erupting crown, and the second tooth of the right side is missing; therefore, it is not possible to obtain a ratio between the teeth of either side. However, they did obtain a ratio of 1.55 between the alveoli of the right side, and the inference might be drawn that the second tooth was small. Ergo, this side shows evidence for *T. 'imperator'* in having two mesial incisors. This result conflicts with the observations of Larson (2008) and Paul et al. (2022).

Added here to this comparison are the measurements of the alveoli of the left side (alveolus 2: 45 mm, alveolus 3: 43 mm, ratio: 0.96), which conflicts with the data from the right side. Ergo, the left side has a single incisiform tooth and so, according to Paul et al. (2022), it might be referable to either *T. rex* or *T. 'regina'*. It must be emphasised that it is not possible to obtain a ratio of the basal crown lengths of the sequential teeth for either side, because one or the other is missing or not fully erupted (Table 7).

10.3. Number of lateral maxillary foramina rows

Cullen et al. (2023) claimed that *T. rex* had a single row of neurovascular foramina extending along the ventral margin of the lateral surface of the maxilla. However, six rows that penetrate the maxilla of CM 9380 were counted here (Figure 4B), and multiple rows are typical of Tyrannosauridae in general. Also, the distribution of neurovascular foramina in tyrannosaurids extends across the dorsum of the snout, which is more extensive than that seen in living crocodylians (e.g. *Alligator mississippiensis*) where dorsal rows in the nasals are not seen. Therefore, the pattern in tyrannosaurids cannot be described as 'low density, linear pattern' (Cullen et al., 2023: 1349). In both clades, the largest foramina follow the ventral margin of the upper jaw, whereas those piercing the rest of the snout are smaller in diameter (Cullen et al., 2023: Figure 2C,E).

10.4. Retention of juvenile features

Several character states in the type are similar to those seen in juveniles, but it is not always evident if they reflect a true reversal to the juvenile state, represent individual variation, or are an artefact of a unique state seen in another adult. Each of the 'juvenile' states seen in CM 9380 are summarised and assessed here.

10.4.1. Maxilla, maxillary fenestra close to the ventral margin of the antorbital fossa

In adults this character is almost certainly an epiphenomenon of the enlargement of the teeth and horizontal ramus. The dorsalward dental expansion results in a reduction of the antorbital fossa above it; this hypothesis can be tested through a geometric morphometric comparison of juvenile and adult maxillae. Therefore, the state seen in adults is not homologous to what is seen in juveniles. Regardless, the transition from a nonexpanded dentigerous region to an expanded region that subsumes part of the antorbital fossa is regarded here as ontogenetically informative.

10.4.2. Maxilla, fossa present in base of interfenestral strut

A fossa is present in all growth stages of *T. rex*, so its presence in CM 9380 is not exceptional (Carr, 2020). However, this region is perforated in one adult, which is expected to be seen in other mature adults. Therefore, the state seen in adults is homologous to what is seen in juveniles, and the growth change from fossa to perforation is tentatively regarded here as ontogenetically informative.

10.4.3. Maxilla, circumfossa ridge is present

A distinct ridge is seen in juveniles, whereas it is absent from most young adults and adults. However, it is subtle in some adults, including CM 9380. It is hypothesised that the reduction and elimination of the ridge is an epiphenomenon of two processes, namely the expansion of the teeth and horizontal ramus, and remodelling of the subcutaneous surface of the maxilla. Therefore, the state seen in adults is homologous to what is seen in juveniles, and the transition from a ridge that is distinct to absent is regarded here as ontogenetically informative.

10.4.4. Maxilla, one foramen in the tract of the subnarial foramen

A single neurovascular foramen in the tract of the subnarial foramen is seen throughout the growth series of *T. rex* (Carr, 2020). Two foramina are seen in a single juvenile. However, there appears to be a difference in homology between the foramen in the growth stages: the foramen in small juveniles has a ventral position, whereas in large adults, young adults, and adults – including CM 9380 - it has a dorsal position (Carr, 2020). Therefore, the state seen in adults is homologous to what is seen in juveniles; the dorsal position might be an epiphenomenon of a deepened maxilla. The transition from a ventral to a dorsal foramen is regarded here as ontogenetically informative, whereas the presence of two foramina represents individual variation.

10.4.5. Maxilla, joint surface for the lacrimal in the ascending ramus is shallow

This joint surface is shallow in small juveniles, young adults, and in CM 9380, whereas it is deep in large juveniles, young adults, and other adults. It is presumed here that the condition seen in the type represents a developmental lag. Therefore, the characters seen in adults is homologous to what is seen in juveniles, and the transition in state from shallow to deep is tentatively regarded as ontogenetically informative.

10.4.6. Maxilla, alveolar skirts are absent

Alveolar skirts in *T. rex* are seen in one young adult and two adults; as such, the absence of these structures, as is seen in CM 9380, is the dominant pattern in *T. rex*. Therefore, the state seen in adults is homologous to what is seen in juveniles, and the transition from skirts that are absent to present is tentatively regarded here as ontogenetically informative.

10.4.7. Maxilla, antorbital fossa reduces in height below the antorbital fenestra

A reduction in height of the antorbital fossa below the antorbital fenestra and towards the jugal ramus is seen throughout the growth series of *T. rex*, including CM 9380 (Carr, 2020). A fossa that keeps a constant height towards the jugal ramus is seen in some juveniles, young adults, and one adult. It is presumed here that the condition seen in the type is the same as that in other growth stages; therefore, the state seen in adults is homologous to what is seen in juveniles. The two states are regarded here as representing individual variation and so they are not ontogenetically informative.

10.4.8. Maxilla, round gaps are absent between the interdental plates

In juveniles, subadults, young adults, and adults, including CM 9380, round gaps do not separate the bases of the interdental plates from each other (Carr, 2020). However, gaps are seen in some young adults and adults. It is presumed here that the condition seen in the type is homologous to what is seen in juveniles. The transition from the absence of gaps to their presence is tentatively regarded here as ontogenetically informative.

10.4.9. Maxilla, joint surface for the jugal does not reach the dorsal edge of the jugal ramus

In juveniles, young adults, and adults, including CM 9380, the jugal is prevented from reaching the dorsal margin of the jugal ramus by a ridge (Carr, 2020). In contrast, the joint surface for the jugal reaches the dorsal margin, eliminating the ridge, in several young adults and adults. It is presumed here that the condition seen in the type represents a lag in elimination of the ridge. Therefore, the state seen in some adults is homologous to what is seen in juveniles and the transition from not reaching the dorsal edge to reaching the edge is tentatively regarded here as ontogenetically informative.

10.4.10. Maxilla, jugal ramus is wide in ventral view

The jugal ramus is mediolaterally wide in juveniles, subadults, and two adults, including CM 9380, whereas it is narrow in most young adults and adults (Carr, 2020). It is presumed here that the condition seen in the type represents a lag in reaching the mature condition. Therefore, the wide state seen in adults is homologous to what is seen in juveniles. The transition from wide to narrow is tentatively regarded here as ontogenetically informative.

10.4.11. Lacrimal, lacrimal pneumatic recess is small

In small juveniles, the small size of the recess is the result of the steep angle of the dorsal margin of the recess, whereas in adults the size is reduced as the result of fusion between the strut that encloses the recess rostrally and the dorsal edge of the antorbital fossa (Carr, 2020). Therefore, the state seen in adults is not



homologous to what is seen in juveniles. Regardless, the transition - from small to large and back to small - is regarded here as ontogenetically informative.

10.4.12. Lacrimal, subcutaneous surface is marginally taller than the joint surface for the nasal

Throughout the growth series, including CM 9380, the subcutaneous surface of the dorsum of the bone is not much taller than the joint surface for the nasal, whereas the tall condition is only seen in one juvenile and one young adult (Carr, 2020). It is presumed here that the type reflects the dominant morphology for T. rex, and the tall condition reflects individual variation. Therefore, the state seen in adults is homologous to what is seen in juveniles. The occurrence of a significantly taller subcutaneous surface is regarded here as individual variation, and so it is not ontogenetically informative.

10.4.13. Lacrimal, subcutaneous ala arcs dorsally

In juveniles, young adults, and some adults including CM 9380, the antorbital fossa is dorsally convex ahead of the lacrimal pneumatic recess (Carr, 2020). However, in juveniles the rostrodorsally extending margin starts from the rostral end of the recess, whereas in young adults and adults – including the type – it occurs further rostrally, above the distal accessory pneumatic recess (Car, 2020). Therefore, the state seen in adults is not homologous to what is seen in juveniles. Regardless, the transition from a proximal convexity to a distal convexity is regarded here as ontogenetically informative.

10.4.14. Lacrimal, surface ahead of orbitonasal ridge is concave

In juveniles, these regions are separated by a crease, and in some subadults and adults, including CM 9380, the surface is concave in vertical and horizontal sections, and in some adults it is convex (Carr, 2020). Therefore, the state seen in the type and adults is homologous to what is seen in juveniles and the transition – from crease to concave to convex – is regarded here as ontogenetically informative.

10.4.15. Lacrimal, antorbital fossa and ventral ramus grade into each other

In juveniles, young adults, and adults, including CM 9380, these surface grade into each other, whereas they are separated by a narrow groove in one juvenile, and they are widely separated in one subadult and one young adult (Carr, 2020). The intermediate state seen in the subadult and the young adult indicates that juvenile and adult conditions arise from different processes, and so are not considered here to be homologous. Regardless, the progression from grade to groove, to wide separation, and then to grade is tentatively considered to be ontogenetically informative.

10.4.16. Lacrimal, suborbital ligament scar is subtle

The scar is subtle in all growth stages, aside from two juveniles where it is distinct (Carr, 2020). Therefore, the state seen in the type and other specimens is homologous to what is seen in juveniles. This transition – from subtle to distinct to subtle - is tentatively regarded here as ontogenetically informative.

10.4.17. Squamosal, dorsal half of quadratojugal process extends dorsolaterally

In juveniles and CM 9380 the process extends dorsolaterally, in contrast to the dorsomedial orientation that is seen in young adults and other adults (Carr, 2020). The condition seen in the type is regarded here as a lag in growth. Therefore, the state seen in the type is homologous to what is seen in juveniles, and the transition from dorsolateral to dorsomedial is regarded here as ontogenetically informative.

10.4.18. Squamosal, dorsal ridge extends to the caudal edge of fossa

The ridge extends caudally in juveniles, some young adults and a few adults, including CM 9380 (Carr, 2020). The condition seen in the type is regarded here as a lag in growth. Therefore, the state seen in the type is homologous to what is seen in juveniles, and the transition from caudal to rostral is regarded here as ontogenetically informative.

10.4.19. Squamosal, ridge of ventral postorbital process extends laterally

The lateral orientation is seen in juveniles, young adults, and a few adults, including CM 9380. The lateral condition seen in the type and other adults is regarded here as a lag in growth. Therefore, the state seen in



the type is homologous to what is seen in juveniles and the transition from lateral to ventral is regarded here as ontogenetically informative.

10.4.20. Ectopterygoid, distal end of the jugal process is not inflated

The growth-related process of inflation in the pneumatic bones of tyrannosaurids are assumed here to follow the same proximal-to-distal pattern. As such, the distal end of the process of juveniles is not inflated, whereas inflation is seen in adults (Carr, 2020). The uninflated condition in CM 9380 presumably represents an individual lag in inflation relative to other adults. Therefore, the state seen in adults is homologous to what is seen in juveniles and the transition from not inflated to inflated is regarded here as ontogenetically informative.

10.4.21. Dentary, chin is below 4th alveolus

In juveniles the 'chin' - the point of angulation between the horizontal ventral margin of the bone and its rostral margin is positioned below the fourth alveolus (Carr, 2020). In contrast, the inflection point in young adults and adults tends to be rostrally shifted, as far ahead as between alveoli 2 and 3 (Carr, 2020). The condition in CM 9380 is presumed here to represent individual variation; i.e. a lag in growth. Therefore, the state seen in adults is homologous to what is seen in juveniles and the transition from caudal to rostral is regarded here as ontogenetically informative.

10.4.22. Dentary, ratio through chin to deepest point of bone

This ratio is 72% or less in all growth stages, aside from one adult (NHMUK R7994), where the ratio is 82%. The condition seen in the type is regarded here as typical for the taxon (Carr, 2020. Therefore, the state seen in the type is homologous to what is seen in juveniles, although this ratio character reflects individual variation and so it is not ontogenetically informative.

10.4.23. Dentary, convex dorsal margin extends to alveolus 7

The convex dorsal margin of the dentary in juveniles, young adults, and some adults, including CM 9380, is limited to the first seven alveoli, whereas in young adults and some adults it extends caudally to alveolus nine (Carr, 2020). The condition seen in the type and other adults is regarded here as a lag in growth. Therefore, the state seen in the type is homologous to what is seen in juveniles; this character is tentatively regarded here as ontogenetically informative.

10.4.24. Dentary, alveoli decrease in length at alveoli 6 or 7

In juveniles, young adults, and some adults, including CM 9380, the alveoli begin to decrease in mesiodistal length at the sixth or seventh alveolus, whereas in young adults and most adults this shifts mesially to alveolus five to four (Carr, 2020). The condition seen in the type is regarded here as a lag in growth. Therefore, the state seen in the type is homologous to what is seen in juveniles; this character is regarded here as ontogenetically informative.

10.4.25. Surangular, rostral glenoid process extends rostrodorsally

In all growth stages this process extends rostrodorsally, including CM 9380, aside from a dorsal orientation that is seen in one juvenile and one adult (Carr, 2020). The condition seen in the type is regarded here as the dominant pattern for the species. Therefore, the state seen in the type is homologous to what is seen in juveniles; this character is regarded here as not ontogenetically informative.

10.4.26. Surangular, caudal glenoid process is tall

In all growth stages, including the CM 9380, this process is tall, aside from a short process that is seen in one juvenile (Carr, 2020). The condition in the type is regarded here as the dominant pattern for the species. Therefore, the state seen in the type is homologous to what is seen in juveniles; this character is regarded here as not ontogenetically informative.



10.4.27. Surangular, caudal glenoid process is not split

In all growth stages, including CM 9380, this process is not split, aside from a split process that is seen in one juvenile (Carr, 2020). The condition in the type is regarded here as the dominant pattern for the species. Therefore, the state seen in the type is homologous to what is seen in juveniles; this character is regarded here as not ontogenetically informative.

10.4.28. Surangular, shelf is indistinct below glenoid region

In juveniles and CM 9380, the shelf fades below the glenoid region, whereas in young adults and all other adults it is a distinct ridge (Carr, 2020). The condition in the type is regarded here as a lag in development. Therefore, the state seen in the type is homologous to what is seen in juveniles; this character is regarded here as ontogenetically informative.

10.4.29. Surangular, medial process extends rostrally

In juveniles, one young adult, and two adults, including CM 9380, the process extends rostrally, whereas in all other adults it extends caudomedially (Carr, 2020). The condition in the type is regarded here as a lag in development. Therefore, the state seen in the type is homologous to what is seen in juveniles; this character is regarded here as ontogenetically informative.

10.5. Homoplasy among large, deep-skulled theropods

10.5.1. Subocular process of the lacrimal

In addition to T. rex, a similar process or flange that extends from the caudal edge of the ventral ramus of the lacrimal (Figure 8) is also seen in abelisaurids (e.g. Abelisaurus, Majugasaurus) and allosauroids (e.g. Acrocanthosaurus, Caracharodontosaurus). The process of the lacrimal is situated opposite that of the postorbital in Abelisaurus, Carcharodontosaurus, Majungasaurus, and T. rex, indicating that together they mark the ventral limit of the eyeball-containing part of the orbital fenestra. The presence of a subocular process – either on the lacrimal, postorbital, or both – represents a ventralward deepening of the skull frame, where the eyeball maintains its dorsal position below the frontal, owing to the association of CNs II, III, IV, and VI with the extrinsic muscles of the eyeball.

11. Conclusions

In conclusion, the skull of CM 9380, the type specimen of T. rex, was characterised here in the context of a comparison of variation in the growth series of the species. The type was found to be comparable with other adults, aside from several characters that represent lags in growth, which are seen in some other adults. Several characters that were presumed to be ontogenetically informative in Carr (2020) were reassessed here and some were found to be uninformative. Unlike all other T. rex specimens, the lateral interfenestral strut of CM 9380 is pneumatically breached that has resulted in a large opening at the caudodorsal corner of the structure and has produced a 'twist' in the rostral margin of the antorbital fenestra. Several lesions were identified in the maxilla, ectopterygoid, and dentaries. Inferences were made regarding the appearance of the missing bones that once surrounded the bones collected of the type specimen. A comparison of the lengths of the second and third alveoli of the left and right dentaries found conflicting patterns, and, if found separately, would have been referred to different taxa by some workers. The subocular process of the lacrimal in T. rex, in addition to that of the postorbital, can be used as a landmark to identify the ventral limit of the ocular (eyeball-containing) region of the orbital fenestra.

Acknowledgments

I thank J. O'Connor (Field Museum) for inviting me to contribute an article to this journal. I thank M. Dawson (CM) for providing me with hard copies of the letters exchanged between B. Brown and A. Avinoff. I thank T. Holtz for providing a pdf of Molnar (1991). I thank the three reviewers whose feedback improved the manuscript.

Author contributions

CRediT: **Thomas D. Carr:** Conceptualization, Investigation, Resources, Writing – original draft.

Disclosure statement

No potential conflict of interest was reported by the author(s).

Funding

This project did not rely upon external funding.

ORCID

Thomas D. Carr (b) http://orcid.org/0000-0001-9000-0132

Data availability statement

The descriptive data upon which this description is in part based, can be found in Carr (2020): Supplemental Data 2).

References

- Allain, R., & Chure, D. J. (2002). *Poekilopleuron bucklandii*, the theropod dinosaur from the Middle Jurassic (Bathonian) of Normandy. *Palaeontology*, 45(6), 1107–1121. https://doi.org/10.1111/1475-4983.00277
- Brochu, C. A. (2003). Osteology of *tyrannosaurus rex*: Insights from a nearly complete skeleton and high-resolution computed tomographic analysis of the skull. *Society of Vertebrate Paleontology Memoir*, 7, 1–138. https://doi.org/10. 2307/3889334
- Brusatte, S. L., Carr, T. D., & Norell, M. A. (2012). The osteology of *Alioramus*, a gracile and long-snouted tyrannosaurid (Dinosauria: Theropoda) from the late Cretaceous of Mongolia. *Bulletin of the American Museum of Natural History*, 366, 1–197. https://doi.org/10.1206/770.1
- Campione, N. E., Evans, D. C., Brown, C. M., Carrano, M. T., & Revell, L. (2014). Body mass estimation in on-avian bipeds using a theoretical conversion to quadruped stylopodial proportions. *Methods in Ecology and Evolution*, *5*(9), 913–923. https://doi.org/10.1111/2041-210X.12226
- Carpenter, K. (1990). Variation in *tyrannosaurus rex*. In K. Carpenter & P. J. Currie (Eds.), *Dinosaur systematics: Approaches and perspective* (pp. 141–145). University of Cambridge Press.
- Carr, T. D. (1999). Craniofacial ontogeny in Tyrannosauridae (Dinosauria: Coelurosauria). *Journal of Vertebrate Paleontology*, 19(3), 497–520. https://doi.org/10.1080/02724634.1999.10011161
- Carr, T. D. (2020). A high-resolution growth series of *Tyrannosaurus rex* obtained from multiple lines of evidence. *PeerJ*, 8, e9192. https://doi.org/10.7717/peerj.9192
- Carr, T. D. (2022). A reappraisal of tyrannosauroid fossils from the Iren Dabasu Formation (Coniacian-Campanian), Inner Mongolia, People's Republic of China. *Journal of Vertebrate Paleontology*, 42(5), e2199817. https://doi.org/10.1080/02724634.2023.2199817
- Carr, T. D., Napoli, J. G., Brusatte, S. L., Holtz, T. R., Hone, D. W., Williamson, T. E., & Zanno, L. E. (2022). Insufficient evidence for multiple species of *tyrannosaurus* in the latest Cretaceous of North America: A comment on "The tyrant lizard king, queen and emperor: Multiple lines of morphological and stratigraphic evidence support subtle evolution and probable speciation within the North American genus *tyrannosaurus*". *Evolutionary Biology*, *49*(3), 327–341. https://doi.org/10.1007/s11692-022-09573-1
- Carr, T. D., & Sues, H.-D. (2010). A taxonomic assessment of the type series of Albertosaurus sarcophagus and the identity of Tyrannosauridae (Dinosauria, Coelurosauria) in the Albertosaurus bonebed from the Horseshoe Canyon Formation (Campanian–Maastrichtian, Late Cretaceous) this article is one of a series of papers published in this special issue on the theme Albertosaurus. *Canadian Journal of Earth Sciences*, 47(9), 1213–1226. https://doi.org/10.1139/E10-035
- Claessens, L. P. (2004). Dinosaur gastralia; origin, morphology, and function. *Journal of Vertebrate Paleontology*, 24(1), 89–106. https://doi.org/10.1671/A1116-8
- Currie, P. J. (2003). Allometric growth in tyrannosaurids (Dinosauria: Theropoda) from the upper Cretaceous of North America and Asia. *Canadian Journal of Earth Sciences*, 40(4), 651–665. https://doi.org/10.1139/e02-083
- Dalman, S. G., Loewen, M. A., Pyron, R. A., Jasinski, S. E., Malinzak, D. E., Lucas, S. G., Fiorillo, A. R., Currie, P. J., & Longrich, N. R. (2024). A giant tyrannosaur from the Campanian-Maastrichtian of southern North America and the evolution of tyrannosaurid gigantism. *Scientific Reports*, *14*(1), 22124. https://doi.org/10.1038/s41598-023-47011-0



- Dececchi, T. A., Mloszewska, A. M., Holtz, T. R., Jr., Habib, M. B., Larsson, H. C., & Cuff, A. (2020). The fast and the frugal: Divergent locomotory strategies drive limb lengthening in theropod dinosaurs. *PLOS ONE*, *15*(5), e0223698. https://doi.org/10.1371/journal.pone.0223698
- Dingus, L., & Norell, M. (2010). *Barnum Brown: The man who discovered Tyrannosaurus rex*. University of California Press. Gold, M. E. L., Brusatte, S. L., & Norell, M. A. (2013). The cranial pneumatic sinuses of the tyrannosaurid *Alioramus* (Dinosauria: Theropoda) and the evolution of cranial pneumaticity in theropod dinosaurs. *American Museum Novitates*, 3790(3790), 1–46. https://doi.org/10.1206/3790.1
- Hendrickx, C., Mateus, O., & Evans, A. R. (2014). *Torvosaurus gurneyi* n. sp. the largest terrestrial predator from Europe, and a proposed terminology of the maxilla anatomy in nonavian theropods. *PLOS ONE*, *9*(3), e88905. https://doi.org/10.1371/journal.pone.0088905
- Holtz, T. R., Jr. (1995). The arctometatarsalian pes, an unusual structure of the metatarsus of Cretaceous Theropoda (Dinosauria: Saurischia). *Journal of Vertebrate Paleontology*, *14*(4), 480–519. https://doi.org/10.1080/02724634.1995.10011574
- Hurrell, S. (2019). *Palaeogravity calculations based on weight and mass estimates of four* Tyrannosaurus rex specimens [online]. Hurum, J. H., & Sabath, K. (2003). Giant theropod dinosaurs from Asia and North America: Skulls of *tarbosaurus bataar* and *tyrannosaurus rex* compared. *Acta Palaeontologica Polonica*, 48(2), 161–190.
- Hutchinson, J. R., Bates, K. T., Molnar, J., Allen, V., & Makovicky, P. J. (2011). Correction: A computational analysis of limb and body dimensions in *Tyrannosaurus rex* with implications for locomotion, ontogeny, and growth. *PLOS ONE*, *9*(5), e97055. https://doi.org/10.1371/journal.pone.0097055
- Kawabe, S., & Hattori, S. (2022). Complex neurovascular system in the dentary of *tyrannosaurus*. *Historical Biology*, *34*(7), 1137–1145. https://doi.org/10.1080/08912963.2021.1965137
- Larson, P. (2008). Variation and sexual dimorphism in *Tyrannosaurus rex*. In P. L. Larson & Carpenter, K. C., eds. *Tyrannosaurus rex*, the tyrant king (pp. 103–127). Indiana University Press.
- Molnar, R. E. (1991). The cranial morphology of tyrannosaurus rex. Palaeontographica, Abteilung A, 217, 137–176.
- Osborn, H. F. (1905). *Tyrannosaurus* and other Cretaceous carnivorous dinosaurs. *Bulletin of the American Museum of Natural History*, 21(article 14), 259–265.
- Osborn, H. F. (1906). *Tyrannosaurus*, upper Cretaceous carnivorous dinosaur, (second communication). *Bulletin of the AMNH*, 22(article 16), 281–296.
- Osborn, H. F. (1912). The crania of *Tyrannosaurus* and *Allosaurus*. *Memiors of the American Museum of Natural History*, 1, 1–30. Osborn, H. F. (1916). Skeletal adaptations of *Struthiomimus*, *Ornitholestes*. *Tyrannosaurus Bulletin of the American Museum of Natural History*, 35, 733–771.
- Paul, G. S. (1998). Limb design, function and running performance in ostrich-mimmics and tyrannosaurs. *GAIA: Revista de Geociências*, 15, 257–270.
- Paul, G. S. (2025). A presentation of the current data on the exceptionally diverse non-tyrannosaurid eutyrannosaur and tyrannosaurid genera and species of western North America during the end Cretaceous North American interchange. *Mesozoic*, 2(2), 85–138. https://doi.org/10.11646/mesozoic.2.2.1
- Paul, G. S., Persons, W. S., & Van Raalte, J. (2022). The tyrant lizard king, queen and emperor: Multiple lines of morphological and stratigraphic evidence support subtle evolution and probable speciation within the North American genus *tyrannosaurus*. *Evolutionary Biology*, 49(2), 156–179. https://doi.org/10.1007/s11692-022-09561-5
- Persons, W. S., Currie, P. J., & Erickson, G. M. (2019). An older and exceptionally large adult specimen of *Tyrannosaurus rex. The Anatomical Record*, 303(4), 656–672. https://doi.org/10.1002/ar.24118
- Porter, W. R., & Witmer, L. M. (2020). Vascular patterns in the heads of dinosaurs: Evidence for blood vessels, sites of thermal exchange, and their role in physiological thermoregulatory strategies. *The Anatomical Record*, 303(4), 1075–1103. https://doi.org/10.1002/ar.24234
- Sampson, S. D., & Witmer, L. M. (2007). Craniofacial anatomy of majungasaurus crenatissimus (Theropoda: Abelisauridae) from the late cretaceous of Madagascar. *Journal of Vertebrate Paleontology*, 27(S2), 32–104. https://doi.org/10.1671/0272-4634(2007)27[32:CAOMCT]2.0.CO;2
- Smith, J. B. (2005). Heterodonty in *tyrannosaurus rex*: Implications for the taxonomic and systematic utility of theropod dentitions. *Journal of Vertebrate Paleontology*, *25*(4), 865–887. https://doi.org/10.1671/0272-4634(2005)025[0865: HITRIF]2.0.CO;2
- Tereshchenko, V. S. (2020). Sexual dimorphism in the postcranial skeleton of dinosaurs. *Paleontological Journal*, *54*(12), 1410–1433. https://doi.org/10.1134/S0031030120120047
- Urban, M. A., & Lamanna, M. C. (2006). Evidence of a giant tyrannosaurid (Dinosauria: Theropoda) from the upper Cretaceous (? Campanian) of Montana. *Annals of Carnegie Museum*, *75*(4), 231–235. https://doi.org/10.2992/0097-4463(2006)75[231:EOAGTD]2.0.CO;2
- Usami, Y., & Kinugasa, R. (2017). A possibility of fast running of tyrannosaurus. DEStech Transactions on Engineering and Technology Research, 118(amma), 126. https://doi.org/10.12783/dtetr/amma2017/13347
- Wolff, E. D., Salisbury, S. W., Horner, J. R., Varricchio, D. J., & Hansen, D. M. (2009). Common avian infection plagued the tyrant dinosaurs. *PLOS ONE*, *4*(9), e7288. https://doi.org/10.1371/journal.pone.0007288

Appendix

Appendix 1. Details on transfer of the type specimen from the AMNH to the CM, based on the written correspondence between Barnum Brown and Andrey Avinoff

The type was discovered by Barnum Brown in Montana in 1902; portions of the specimen were collected in 1902 and 1905. While at the AMNH, the fossil initially had the specimen number AMNH 973 and Henry Fairfield Osborn published on it from 1905 to 1916. CM 9380 has an unusual history for a type specimen because it was sold and transferred from one museum to another.

In the archives of the CM, there is a series of letters (1941 to 1942) that were exchanged between Barnum Brown (Curator of Fossil Reptiles, AMNH) and Dr. Andrey Avinoff (Director, CM) that provides the details of the sale of the type from New York to Pittsburgh. Osborn had died on November 6, 1935, and so he was not involved in the agreement. Since the Blitz had started in September 1940, the rationale for the transfer, according to Brown, was to preserve one of two *T. rex* specimens held by the museum (AMNH 973, AMNH 5027) should it be bombed, and the specimens destroyed (Dingus and Norell, 2010). Although this concern is expressed in Brown's memoirs (Dingus and Norell, 2010, p. 309), it does not appear in his communications with Avinoff; to shed some light on the concerns of the day, I provide a summary of that exchange here.

The transfer from the AMNH to the Carnegie Museum was facilitated by Mr. LeRoy Kay and Mr. Sydney Prentice, both of the CM, in December 1940 during a visit to the AMNH to see Barnum Brown (Brown, letter Jan. 9, 1941). In the meantime, the Blitz had ended on May 11, 1941. By June 1941, the AMNH President and Administration gave approval "to sell the type specimen of *Tyrannosaurus*, the money to be used as an endowment for this Department [of Palaeontology]" (Brown, letter June 26, 1941). The skull and hind limbs were previously mounted for exhibit by the AMNH, and those were offered to the CM unaltered (Brown, letter October 22, 1941), which the CM accepted (Avinoff letter November 4, 1941).

By the end of October 1941, the specimen was packed into 15 wooden cases for shipment; the cases had open tops for safety inspection while in transit, by truck, from Manhattan to Pittsburgh; Brown requested that a CM staff member accompany the specimen to ensure its safe travel (Brown, letter October 31, 1941). In 1941, the fossil was sold for \$7,000.00 USD (=\$150, 316.19; CPI inflation calculator); the payment was made in two installments of \$3,000 USD in 1941, and \$4,000 USD by June 1942 (Avinoff letter November 4, 1941). In the end, the entire shipment was brought by truck to the CM for the sum of \$108.00 USD (=\$2,319.16; CPI inflation calculator). Once at the CM, its specimen number was changed from AMNH 973 to CM 9380.